Supplementary for

Giant polyketide synthase enzymes biosynthesize a giant marine polyether biotoxin.

Timothy R. Fallon[1]*, Vikram V. Shende[1], Igor H. Wierzbicki[2], Robert P. Auber[3,4], David J. Gonzalez[2,5], Jennifer H. Wisecaver[3,4], Bradley S. Moore[1,5]*

[1]Center for Marine Biotechnology and Biomedicine, Scripps Institution of Oceanography and University of California, San Diego; 9500 Gilman Dr #0204, La Jolla, CA 92093, USA.
[2]Department of Pharmacology, University of California, San Diego; 9500 Gilman Dr, La Jolla, CA 92093, USA.
[3]Department of Biochemistry, Purdue University; 175 S University St, West Lafayette, IN 47907, USA.
[4]Purdue Center for Plant Biology, Purdue University; 175 S University St, West Lafayette, IN 47907, USA.
[5]Skaggs School of Pharmacy and Pharmaceutical Sciences, University of California, San Diego; 9500 Gilman Dr, La Jolla, CA 92093, USA.

*Corresponding author. Email: tfallon@ucsd.edu (TRF); Email: bsmoore@ucsd.edu (BSM)

Materials and Methods

Cell strains:

The haploid *Prymnesium parvum* strain 12B1 (*48*) was a gift of Dr. William Driscoll (Pennsylvania State University, Harrisburg). Strain 12B1 is available from the UTEX Culture Collection of Algae at UT-Austin under UTEX accession UTEX LB 3227.

Media preparation:

For proteomic mass spectrometry:

L1-Si@25 (25% salinity) algal growth media (*49*) was prepared from 12L of 18.2 Mohm·cm water (ultrapure water) dispensed from a laboratory water purifier [Millipore, Milli-Q Advantage A10, CAT# Z00Q0V0WW], 4L seawater [Scripps Institution of Oceanography seawater system], concentrated stocks for L1 media [National Center for Marine Algae, CAT# MKL150L] and 1.5 mM $NaHCO_3$ to adjust for the lack of carbon from seawater, all within a polycarbonate 20L carboy [Thermo Fisher Scientific, CAT# 2251-0050]. The carboy was then capped with a 3-port closure [Thermo Fisher Scientific, CAT# 2162-0831] plus pre-installed interior 6" and 30" silicone tubing. Two of the three ports were temporarily blocked for autoclaving, while the third port was interfaced with a small piece of silicone tubing and a Whatman HEPA-VENT disk filter [Cytiva, CAT# 6723-5000]. The vented carboy was autoclaved using the "Cycle 3 LIQUID 60 MIN" in a Beta Star Medium Sterilizer Series autoclave.

For rRNA depletion RNA-Seq:

A similar method was used to above, excepting media preparation was scaled down to 8L in a single 9L bottle [Corning, CAT# 1596-9L] & it was autoclaved in a Hirayama HV-50 autoclave at 121˚C for 60 minutes, with the 0% exhaust setting.

Creation of v1.1 P. parvum 12B1 reference genome by targeted reassembly:

Previously published (*20*) Oxford Nanopore Technology (ONT) MinION genomic DNA reads [# of reads: 447907, # of nucleotides: 4005418850, filename:12B1_above_3kb_nanopore_sorted.bam, checksum: seqkit.v0.1_DLS_k0_9c68687a7acb147c412be4b83753e237, SRA:SRR18033808] were aligned against an unpublished intermediate version v0.3 of the 12B1 reference genome assembly [12B1_scaffolds_v0.3.fasta ; checksum: seqkit.v0.1_DLS_k0_6561035ed292bc5039428c769267f70b] using the NGMLR aligner (*50*). A suspicious region [v1.0:12B1-Scaf17:2286312-2287047] of the PKZILLA-1 N-terminus that showed increased coverage, a higher proportion of visible single nucleotide variation (SNV), and a high proportion of a large indel was noted through graphical inspection with Integrated Genomics Viewer v2.14 (*51*). ONT gDNA reads intersecting this suspicious PKZILLA-1 N-terminal region, were extracted using "bedtools intersect" (*52*). The extracted reads [# of reads: 41, # of nucleotides: 475352, filename: suspicious_hotspot1@2500bp_N-term_region.bam, checksum: seqkit.v0.1_DLS_k0_d202591ca9f50940752c50f50395048e], were then assembled using Flye (v2.9.2-b1786), using a parameter scan from 100-10000 for the "--min-overlap" parameter, and inclusion of the "--keep-haplotypes --meta --scaffold" parameters. The source code of Flye had been patched to allow for values of <1000 for the "--min-overlap" parameter. The resulting 29 targeted assemblies all consisted of only a single contig, of which there were only 5 unique sequences across the 29 assemblies. Next, the PKZILLA-1 gene model was partially lifted over to each of the 5 unique targeted reassembly contigs using the flo pipeline (https://github.com/wurmlab/flo) (*53*), which uses the ucsc-kent tools (http://hgdownload.cse.ucsc.edu/admin/exe/), blat (*54*), GNU parallel (*55*), and genometools (*56*) internally. The translated peptide and nucleotide representations of the lifted-over PKZILLA-1 N-terminal 1st exon, were extracted using a custom Nextflow (*57*) workflow (https://github.com/photocyte/PPYR_OGS/blob/master/utility_scripts/extract_gff_features.nf). These peptide and nucleotide representations of the lifted over PKZILLA-1 features were identical across the 5 unique contigs, so a random representative selection was made for downstream analyses. These

representative peptide & nucleotide representations of the lifted 1st exon were next aligned against the analogous extractions of the reference 1st exon using kalign2 (*58*), and these multiple sequence alignments were manually inspected with mview (*59*). This analysis revealed a 609 bp tandem repetitive region that was missing from the reference assembly, but also revealed that the targeted re-assembly was otherwise identical to the reference assembly (excepting a single upstream homopolymer indel, that is not unusual with unpolished Nanopore assemblies & was ignored in further downstream analyses). The v1.1 version of the 12B1 assembly [filename: 12B1_scaffolds_v1.1.fasta ; checksum: seqkit.v0.1_DLS_k0_99243f7852f0aa7f150e6169739e61a0] was then constructed by adding the 609 bp region with the 'replace' subcommand of seqkit, targeting the replacement to its homologous loci on scaffold 12B1-Scaf17 of the v1.0 genome, as determined by kalign2. This 12B1 genome assembly v1.1 is available on Zenodo (doi:10.5281/zenodo.10023322).

***P. parvum* growth and harvesting for rRNA depletion RNA-Seq:**

P. parvum strain 12B1 was grown within 125 mL borosilicate glass Erlenmeyer flasks in 50 mL of L1-Si@25 media. Mouths of the flasks were sealed against contamination using 10 cm x 10 cm squares of air-permeable and sterilizable cellulose-polyester wrapping paper [Cardinal Health, CAT# 4008] that was sealed around the neck of the flask using rubber bands. Before use, the flasks including mouth seal & rubber bands were sterilized and cleaned by autoclaving with 75 mL of ultrapure water. This water was removed before addition of the L1-Si@25 media & seeding of the *P. parvum* culture. Post-autoclave manipulations of the flasks took place in a Type II Biosafety Cabinet. Ongoing culturing of the flasks took place in a 22˚C incubator [Fisher Scientific, CAT# 146E] retrofit with full spectrum LED grow lights [GE Lighting, BR30, CAT# 93101230], corresponding to ~2200 lux from above under a 14:10 light:dark cycle. Routine cell concentration measurements were recorded with a Muse flow cytometer [Luminex, CAT# 0500-3115]. The day phase cells were harvested 3 hours after the light to dark transition and a concentration of ~378e3 cells/mL. The night phase cells were harvested 3 hours after the dark to light transition and a concentration of 559e3 cells/mL. Harvesting occurred by transferring the flask content to a 50 mL polypropylene (PP) centrifuge tube (CFT) and centrifuging with a swinging bucket centrifuge [Beckman, CAT# X-15R], with parameters: 3000×*g*, 10 minutes, 18˚C, accel=MAX, decel=MAX. The supernatant was removed by decanting, and the cell pellet resuspended in the remaining adherent liquid with a P1000 pipette. The cell suspension was transferred to a 2 mL PP microcentrifuge tube (MCT), and 1000 µL plus 400 µL of 4˚C TRIzol Reagent [Invitrogen, CAT# 1559026] were added in quick succession. Post-TRIzol addition, samples were stored at -80˚C for less than a week.

RNA extraction and rRNA depletion RNA-Seq:

TRIzol-stored cell samples (see "P. parvum growth and harvesting for rRNA depletion RNA-Seq" methods) were removed from the -80˚C and 280 µL of 24:1 chloroform:isoamyl alcohol [Acros Organics, CAT#327155000] was added. Samples were manually mixed by inversion for ~1 minute, and then centrifuged in a fixed angle centrifuge at 24,000×*g* for 10 minutes. The upper aqueous layer was transferred to a new 2 mL PP MCT and 1 mL of 100% ethanol (denatured) was added. Total RNA was purified from the resulting mixture using chaotropic silica column nucleic acid purification with a commercial kit [Zymo Research, RNA Clean & Concentrator-25, CAT# R1017], following the manufacturer's instructions (*60*). The day and night phase samples yielded 632 ng and 1177 ng of RNA, respectively. These samples were stored at -80˚C for less than a week. The ppMCTs containing purified RNA were then transported to the UCSD Institute for Genomic Medicine (IGM) genomics core facility on dry ice and stored at -80˚C until use. The samples were prepared into deoxyuridine triphosphate (dUTP)-stranded sequencing libraries by the IGM, using a commercially available kit [Illumina, TruSeq Stranded Total RNA with Ribo-Zero Plant, CAT# 20020610], following the manufacturer's instructions. Libraries were sequenced at IGM on a NovaSeq 6000 sequencer [Illumina] using the paired-end mode. Libraries were sequenced over 4 separate NovaSeq runs to increase

coverage. Libraries were split across an unknown number of physical flowcell lanes. Libraries were multiplexed within lanes with an unknown type and number of other samples. Raw RNA-Seq reads are available on NCBI SRA with Bioproject: PRJNA936443, with SRA accessions SRR23517916 (night) and SRR23517917 (day).

RNA-Seq alignment, reference guided transcriptome assembly, and quantification:
rRNA depletion RNA-Seq reads were trimmed using trimmomatic v0.39 (*61*) with parameters "ILLUMINACLIP:adapters.fa:2:30:10 SLIDINGWINDOW:4:5 LEADING:5 TRAILING:5 MINLEN:25" and aligned to an unpublished intermediate version v0.3 of the 12B1 reference assembly [12B1_scaffolds_v0.3.fasta ; checksum: seqkit.v0.1_DLS_k0_6561035ed292bc5039428c769267f70b] with hisat2 v2.2.1 (*62*) using parameters "--rna-strandness R --fr --no-mixed --no-discordant --max-intronlen 3000". Reads from the day and night phase samples were merged, and the merged reads were then assembled into transcripts using stringtie v2.2.1 with parameters "--rf" (*63*). Poly-A pulldown (SRR1685644)(*23*) and rRNA depletion RNA-Seq reads shown in figures were re-aligned against the 12B1 v1.1 assembly using the same programs (hisat2) and parameters, excepting the changed parameter "--max-intronlen 5000". RNA-Seq was independently quantified against the 12B1 v1.1 gene-model annotation predicted transcripts (doi:10.5281/zenodo.10023330) using the rRNA depletion day phase (SRR23517917) and night phase (SRR23517916) samples with Kallisto v0.50.0 with parameters "--rf-stranded". Kallisto results are available on Zenodo (doi:10.5281/zenodo.10023426).

Definition of PKS hotspots within the 12B1 genome
The *P. parvum* 12B1 PKS hotspots were originally defined off the unpublished intermediate versions v0.3 of the 12B1 reference assembly and gene annotation. First, PKS domain polypeptide sequences from *P. parvum* 12B1 were selected by analyzing the TSV format InterProScan (*25*) results produced from the gene-model derived polypeptides as described in (*20*), and, selecting using bedtools and seqkit, those polypeptide regions that received the InterPro annotation IPR016039, IPR036736, IPR036291, IPR042104 or IPR020807, IPR029063, and IPR020843 matches for the ketosynthase (KS), acyl-carrier-protein (ACP), ketoreductase (KR), dehydratase (DH), SAM methyltransferase (MT), and enoyl-reductase (ER) domains, respectively. The polypeptide sequences of these selected domains were then used as a tblastn query against the v0.3 12B1 genomic assembly, using parameters `-outfmt 5 -evalue 0.001`. The blast XML results were converted to GFF using a custom script (https://github.com/photocyte/general_scripts/blob/master/blastxml2gff.py). Next, overlapping and redundant tblastn hits on the same strand were collapsed using 'bedtools merge -s'. These bed alignments, representing same-strand coding evidence for PKS domains, were clustered into "hotspots" i.e. regions with evidence of PKS coding sequence without explicit hypotheses as to the gene model structures, via merging adjacent alignments through 'bedtools slop -b' and 'bedtools merge'. The bedtools slop -b parameter was iterated over a range of values, and 5000 bp was determined as the most interpretable where each hotspot likely arose from 1 gene. These v0.3 assembly and annotation derived hotspots were lifted over to the v1.1 assembly without issue using seqkit and bedtools, and are available on Zenodo (doi:10.5281/zenodo.10309063).

Construction of PKZILLA gene models:
The construction of the PKZILLA gene models was originally based off an unpublished intermediate version v0.3 of the 12B1 reference assembly. Supervised gene models for the PKZILLAs were constructed by joining or extending predicted exons from the hisat2/stringtie RNA-Seq alignment and reference guided transcriptome assembly (see "RNA-Seq alignment, reference guided transcriptome assembly, and quantification" methods section), with exons from *ab initio* gene models that were generated as previously described (*20*) but based off an unpublished intermediate version v0.3 of the 12B1 reference assembly. For additional guiding evidence, splice-aware protein to genome alignments of PKS protein domains sourced from the *P. parvum* 12B1 gene annotation (*20*) were produced with a

pre-search using tblastn from BLAST+ v2.13.0 (*64*) with the following parameters: "-threshold 13 -word_size 2 -max_intron_length 1000 -outfmt '6 sseqid slen sstart send qseqid qlen qstart qend pident length evalue score' -evalue 0.01", followed by an intron-aware alignment using the prot2genome utility "funannotate-p2g.py", with parameters "--maxintron 500 --exonerate_pident 10" from v1.8.14 of the funannotate genome annotation software (*65*). Funannotate-p2g.py calls exonerate v2.4.0 (*66*) internally. Evidence for potential introns was created using the "hints.BAM.gff" file generated by funannotate v1.8.14 from the hisat2 aligned reads (see "RNA-Seq alignment, reference guided transcriptome assembly, and quantification" methods). Notably, we found that the coding regions of the presumed PKZILLAs were flagged as repeats by the repeatmasking process used to generate the *ab initio* gene models, thus our decision to perform a supervised gene-model construction based on protein-alignments and RNA-seq alignments. This combined evidence was viewed as tracks against the genomic assembly in Integrated Genomics Viewer (IGV) v2.14 (*51*). The PKZILLA gene models (in GFF format) were then iteratively edited with a text editor, with iterative inspection in IGV confirming compatibility with the evidence. As visibility of features in IGV was sensitive to their exact ordering in the GFF file, GFF files were validated for correctness and double sorted with genometools and igvtools before viewing, using a custom Nextflow script (https://github.com/photocyte/PPYR_OGS/blob/master/utility_scripts/doubleSort.nf). After the tracks were validated, features sequences (i.e. gene, mRNA, CDS, polypeptides) were extracted using a custom Nextflow script (https://github.com/photocyte/PPYR_OGS/blob/master/utility_scripts/extract_gff_features.nf).

Integration of PKZILLA gene models into the reference 12B1 v1.1 gene annotation:

As the PKZILLA gene models were originally based off an unpublished intermediate version v0.3 of the 12B1 reference assembly (see "Construction of PKZILLA gene models" methods), it was necessary to integrate the PKZILLA gene models into a reference gene model annotation based off the v1.1 genome assembly (see "Creation of v1.1 P. parvum 12B1 reference genome by targeted reassembly" methods). Only scaffolds 12B1-Scaf8 and 12B1-Scaf32 changed between genome assembly version v0.3 used for PKZILLA model creation (see "Construction of PKZILLA gene models" methods section) and the published genome assembly version v1.0 [12B1_scaffolds_v1.fasta ; seqkit.v0.1_DLS_k0_25524daa93426ca36fa6f688345c06d0] (*20*). As described in the "Creation of v1.1 P. parvum 12B1 reference genome by targeted reassembly" methods section, scaffold 12B1-Scaf17 v1.0 was modified to produce genome assembly v1.1 [12B1_scaffolds_v1.1.fasta ; seqkit.v0.1_DLS_k0_99243f7852f0aa7f150e6169739e61a0]. non-PKZILLA-1 v1.0 gene models on the modified 12B1-Scaf17 were lifted over using the flo pipeline (https://github.com/wurmlab/flo) (*53*), which uses the ucsc-kent tools (http://hgdownload.cse.ucsc.edu/admin/exe/), blat (*54*), GNU parallel (*55*), and genometools (*56*) internally. Comparisons of extracted feature sequences (i.e. gene, mRNA, CDS, polypeptides), produced using a custom Nextflow (*57*) workflow (https://github.com/photocyte/PPYR_OGS/blob/master/utility_scripts/extract_gff_features.nf), from the v1.0 and v1.1 gene models confirmed they were successfully lifted over without fragmentation. Next, PKZILLA-1 was aligned and lifted over from v0.3 to the v1.1 assembly using the flo pipeline as described above. Given the lack of changes on the PKZILLA-2 and -3 containing scaffolds, 12B1-Scaf7 and 12B1-Scaf10 respectively, between genome assembly versions v0.3 and v1.1, PKZILLA-2 and -3 were directly lifted over to the v1.1 assembly via concatenation of the GFF files. Fragmented gene models from the v1.0 annotation which overlapped with the lifted over PKZILLA gene models, were removed using bedtools subtract. The identifiers for the removed gene models are available as 'all.remove.list.sorted.txt' on Zenodo (doi:10.5281/zenodo.10023330). In total, 25 gene models were removed. Successful liftover of the PKZILLA gene models was validated by graphical inspection using Integrated Genomics Viewer v2.16 (*51*) and by comparison of seqkit sum hashes of the extracted sequence features. The resulting GFF file of the v1.1 gene models is available as '12B1_v1.1.gff3' on Zenodo (doi:10.5281/zenodo.10023330). The extracted sequence features (gene, mRNA, translated

polypeptide, individual translated CDSs, individual exons, individual introns, etc.), were extracted using a custom Nextflow script (https://github.com/photocyte/PPYR_OGS/blob/master/utility_scripts/extract_gff_features.nf) that used genometools (*56*) internally. These extracted v1.1 assembly & v1.1 annotation sequence features are available on Zenodo (doi:10.5281/zenodo.10023330).

***P. parvum* growth, harvesting, and lyophilization for proteomic mass spectrometry:**

Prymnesium parvum strain 12B1 were grown in a semi-continuous batch format, i.e. removing a subset of culture at late-exponential to early-stationary phase and diluting the remaining culture with fresh media. *P. parvum* were grown on the laboratory benchtop in a 20L polycarbonate carboy [Thermo Fisher Scientific, CAT# 2251-0050] with media prepared as described in the "Media preparation for proteomic mass spectrometry" methods and under a 14:10 light:dark cycle with ~3200 lux from above (measured at shoulder of carboy) from full spectrum LED grow lights [SpiderFarmer, CAT# SF1000], ambient laboratory temperature control (~18-20˚C), and 6 liters per minute (LPM) of aeration with laboratory pressurized air. Air was delivered below the water surface via the interior 6" silicone tubing attached to a 10 mL glass pipette [Fisher Scientific, CAT# 13-678-27F]. The interior 30" silicone tubing remained coiled below the water surface and was used for daily culture sampling (1 mL) using a pipette controller [Corning, CAT# 4099], large scale culture harvesting (1L+) using a peristaltic pump, and addition of fresh autoclaved media using a peristaltic pump. Daily cell concentration measurements were recorded with a Muse flow cytometer [Luminex, CAT# 0500-3115]. For proteomics, cells were harvested at a concentration of 400,000 cells / mL via two rounds of 500 mL centrifugation with parameters: 3500×g, 10 minutes, accel=5, decel=5, temperature=18˚C, in 500 mL polypropylene centrifuge tubes (CFTs) [Corning, CAT# 431123] using a X-14R swinging bucket centrifuge [Beckman Coulter, CAT# A99465]. The centrifugation also used a blue adapter sleeve [Beckman Coulter, CAT# 349846], a gray conical adaptor base [Beckman Coulter], and a compatible rotor and buckets [Beckman Coulter, CAT# SX4750A]. Cell concentration measurements of the supernatant indicated a 54% harvesting efficiency. The pelleted cell mass was flash frozen with liquid N_2 inside the 500 mL CFTs and lyophilized for >48 hours using a nominally -103˚C, 12 mTorr lyophilizer [SP Industries, CAT# 4KBTZL-105], backed by a rotary vane vacuum pump [Edwards, CAT# RV5]. Four 500 mL CFTs were lyophilized at a time in a single Multi-Tainer container [FTS Systems]. Next, the 500 mL CFTs were placed on dry ice, and the lyophilized cell mass was scraped using a spatula/scoopula into a dry-ice cooled 50 mL polypropylene CFT [Corning, CAT# 352070], and stored long-term at -80˚C.

Sample preparation for proteomic mass spectrometry:

Preparation of proteomic subsample:

A 50 mL CFT containing lyophilized *P. parvum* 12B1 biomass (see "*P. parvum* growth, harvesting and lyophilization for proteomic mass spectrometry" method) was removed from the -80˚C and allowed to equilibrate to room temperature under lyophilizer vacuum. A 4.8 mg sample of lyophilized biomass was removed using a spatula, transferred into a 1.5 mL polypropylene microcentrifuge tube (ppMCT), & had its mass measured using an analytical balance [Sartorius, CAT# CPA124S]. The ppMCT containing sample was then transported to the UCSD Collaborative Center for Multiplexed Proteomics (CCMP) proteomics core facility on dry ice and stored at -80˚C until use.

Cell lysis, reduction, and alkylation:

The sample was next suspended in 500 µL of Lysis buffer (6M urea, 7% SDS, 50 mM tetraethylammonium bicarbonate (TEAB) [Sigma-Aldrich, CAT# T7408-500ML], pH 7.7 adjusted with phosphoric acid) supplemented with 4-(2-aminoethyl)benzenesulfonyl fluoride (AEBSF) and phenylmethylsulfonyl fluoride (PMSF) containing cOmplete ULTRA Mini Tablets, EDTA-free (½ tablet for 10 mL of buffer) [Roche, CAT# 05892791001] protease inhibitors, and PhosSTOP (½ tablet for 10 mL of buffer) [Roche, CAT# 4906845001] phosphatase inhibitors. Greater than typical quantities of

biomass were used as input into the method to maximize sensitivity, thus non-solubilized material was still present in the tube after addition of lysis buffer. Next, sedimented non-solubilized material was removed via pipette aspiration (~50 µL) and the remaining cell suspension transferred to a 2 mL Protein LoBind Tube [Eppendorf, CAT# 022431102] ppMCT. The sample was mixed for 10 minutes in a Vortex Genie 2 vortex mixer [Scientific Industries, CAT# 00-SI-0236] and sonicated using Qsonica Sonicator Q125 [Qsonica, CAT# Q125-110] equipped with a 1.6 mm microtip probe [Qsonica, CAT# 4417] with the following parameters: amplitude 20; 1 second pulse; 5 second break; 5 pulses. The lysate was centrifuged for 5 minutes at 16,000×*g*, room temperature (RT), and 250 µL of the supernatant was transferred into a new 2 mL Protein LoBind Tube. The sample was then chemically reduced by addition of 5 µL 0.5 M dithiothreitol (DTT) (9.8 mM final concentration) [Invitrogen, CAT# 15508-013] (prepared in a HPLC-grade water [Fisher Chemical, CAT# W5-4]), and incubated for 30 minutes at 47˚C. Next, the sample was cooled on ice for 5 minutes and the solubilized proteins were alkylated by addition of 15 µL 0.5 M iodoacetamide (IAA) (27.8 mM final concentration) [Sigma-Aldrich, CAT# I1149] (prepared in a HPLC-grade water) with incubation for 45 minutes at RT in the dark. The alkylation reaction was quenched by addition of 5 µL 0.5 M DTT (9.09 mM final concentration) and incubated for 15 minutes at RT. The sample was centrifuged for 5 minutes at 16,000×*g*, RT, and the resulting supernatant containing solubilized chemically reduced and alkylated proteins was transferred into a new 2 mL Protein LoBind Tube.

Protein digestion:

The protein sample (~275 µL) was next acidified with 27 µL of 12% phosphoric acid (final concentration: ~100 mM) [Sigma-Aldrich, CAT# 49685-500ML] and mixed with 1500 µL of Binding buffer (90% methanol [Fisher Chemicals, CAT# A452-4], 50 mM TEAB, pH 7.1 adjusted with phosphoric acid). The acidified sample was loaded onto an SDS binding S-Trap mini column [ProtiFi, CAT# C02–mini-80] and centrifuged for 1 minute at 1000×*g*, RT. The column was washed 5 times with 500 µL of Binding buffer with 1 minute centrifugation at 1000×*g*, RT, per each wash. The column was centrifuged for an additional 2 minutes at 2000×*g*, RT, to remove residual methanol. Next, the column was transferred into a new ppMCT collection tube (provided with the S-Trap mini columns) and prepared for on-column digestion by addition of 10 µg (20 µL) of Sequencing Grade Modified Trypsin [Promega, CAT# V5113] and 105 µL of 50 mM TEAB. The column was briefly centrifuged (<2000×g), and the resulting flow-through reapplied onto the column. Next, the proteins were on-column trypsin digested for 3 hours at 47˚C. Peptides were eluted from the column with 125 µL of 50 mM TEAB (1 minute centrifugation at 2000×g, RT), 125 µL of 5% formic acid [Fisher Chemicals, CAT# A118P-500] (1 minute centrifugation at 2000×g, RT), and 125 µL of 50% acetonitrile [Fisher Chemicals, CAT# A998-4] (5 minute centrifugation at 2000×g, RT), resulting in a ~500 µL solution of peptides in ~25 mM TEAB, ~1.25% formic acid, ~12.5% acetonitrile.

Peptide desalting:

The peptide solution was frozen at -80˚C and lyophilized using a Savant SPD111V SpeedVac Concentrator [Thermo Scientific, CAT# SPD111V-115], in line with -105˚C Savant RVT5105 Refrigerated Vapor Trap [Thermo Scientific, CAT# RVT5105-115], with vacuum supplied by a Fisher Scientific Maxima D4A Rotary Vane Pump [Thermo Scientific, CAT# 010574A]. The resulting solids were resuspended in 500 µL of 0.1% trifluoroacetic acid (TFA) [Thermo Scientific, CAT# 28901] in HPLC-grade H_2O via vortexing for 20 minutes in a Vortex Genie 2 vortex mixer. A Sep-Pak tC18 1 cc Vac Cartridge (50 mg sorbent) [Waters, CAT# WAT054960] was placed in a NucleoVac 24 Vacuum Manifold [MACHEREY-NAGEL, CAT# 740299] and washed with 1 mL of 100% acetonitrile and 2 mL of 0.1% TFA using laboratory vacuum. The peptide solution was centrifuged for 5 minutes at 16000×*g*, RT, and the supernatant was applied onto the tC18 cartridge. Column-bound peptides were washed with 5 mL of 0.1% TFA and eluted with 750 µL of 40% acetonitrile, 0.5% acetic acid and 750 µL of 80% acetonitrile, 0.5% acetic acid into a 2 mL Protein LoBind Tube.

Peptide quantification:

The resulting desalted peptide sample was frozen at -80˚C, lyophilized (as described above), and the solids resuspended in 500 µL of 50% acetonitrile via vortexing in a Vortex Genie 2 vortex mixer for 20 minutes. Notably, an undissolved precipitate was observed at this step, which is unusual for this protocol. The undissolved precipitate may indicate a high proportion of post-translationally modified peptides with poor solubility in 50% acetonitrile, i.e. glycosylated peptides, or other non-peptide molecules that were carried over in the protocol. The peptide solution was next centrifuged for 5 minutes at 16000×*g*, RT, and the supernatant containing only soluble peptides was transferred into a new 2 mL Protein LoBind Tube. The peptide concentration was determined with the BCA-like Biuret-reaction-based Pierce Quantitative Colorimetric Peptide Assay kit [Thermo Scientific, CAT# 23275].

Sample preparation for mass-spectrometry analysis:

A 20 µg sample of peptides was frozen at -80˚C and lyophilized (as described above), and resuspended in 20 µL of 5% acetonitrile, 5% formic acid, (final concentration 1 µg/µL) and vortexed at room temperature for 20 minutes in a vortex mixer. Samples were transferred to 300 µL Target Polyspring glass Inserts [Thermo Scientific, CAT# C4010-630] within 9 mm glass autosampler vials with pierceable PTFE septa [Thermo Scientific, CAT# C5000-580W].

Proteomic liquid chromatography, mass spectrometry:

1 µL of sample (1 µg of peptides) was injected onto an Easy-Spray PepMap Neo 2 µm C18 75 µm X 150 mm column [Thermo Fisher, CAT# ES75150PN] using an Thermo Easy-nLC 1000 liquid chromatography instrument (HPLC) [Thermo Fisher, CAT# LC120]. Peptides were separated via reverse-phase chromatography at a flow rate of 0.4 µL/minute. Solvent A of the mobile phase consisted of 0.1% formic acid in HPLC-grade water, while solvent B consisted of 0.1% formic acid in acetonitrile. An initial 2-min isocratic gradient flow of 3% B was followed by a linear increase up to 25% B for 85 min, increased to 45% B over 15 min, and a final increase to 95% B over 15 min, whereupon B was held for 6 min and returned to baseline (2 min) and held for 10 min, for a total of 183 min. Sample spectra were collected on an Orbitrap Fusion tribrid mass spectrometer (Thermo Scientific, Wikidata:Q120754733) that collected MS^1 data in positive ion mode within the 375 to 1,500 m/z range, Orbitrap resolution: 120000, data type: centroid**,** precursor ion isolation window (m/z): 0.7**,** and HCD collision energy set at 30%. Data dependent MS^2 fragmentation spectra were recorded in the linear ion trap. A vendor-software exported report on the used MS^1 and MS^2 methods is available on Zenodo (doi:10.5281/zenodo.10023360). 3 separate injections & MS runs, i.e. “technical replicates” were performed off the same resuspended peptide sample.

Proteomic peptide & protein identification:

Peak lists obtained from MS/MS spectra were identified using X!Tandem version X! Tandem Vengeance (2015.12.15.2) (*67*) and Comet version 2023.01 rev. 2 (*68*). The search was conducted using SearchGUI version 4.2.17 (*69*).

Protein identification was conducted against a concatenated target/decoy (*70*) version of the *Prymnesium parvum* 12B1 polypeptides (predicted from gene models) including 24938 (target) or 49876 (target+decoy) sequences. The filename of the used database was: simple_nostops_12B1v1.1.fasta_concatenated_target_decoy.fasta , the seqkit (v2.5.0) (*71*) checksum was: seqkit.v0.1_PLS_k0_1221bf0c34f4b151e5f4d2c96f391bcd , the MD5 checksum was: 688eaf7347ce157ff94322be6c3d29ff . C-terminal stop codons were removed from the predicted polypeptides before decoy creation. The decoy sequences were created by reversing the target sequences in SearchGUI.

The identification settings were as follows: Trypsin, Specific, with a maximum of 2 missed cleavages 15.0 ppm as MS^1 and 0.2 Da (Th) as MS^2 tolerances; fixed modifications:

Carbamidomethylation of C (+57.021464 Da), variable modifications: Oxidation of M (+15.994915 Da), fixed modifications during refinement procedure: Carbamidomethylation of C (+57.021464 Da), variable modifications during refinement procedure: Acetylation of protein N-term (+42.010565 Da), Pyrolidone from E (-18.010565 Da), Pyrolidone from Q (-17.026549 Da), Pyrolidone from carbamidomethylated C (-17.026549 Da). All algorithm specific settings are listed in the Protein Identification Certificate of Analysis available as 'certificate_of_analysis.txt' on Zenodo (doi:10.5281/zenodo.10023441).

Peptides and proteins were inferred from the spectrum identification results using PeptideShaker version 2.2.25 (*72*). Peptide Spectrum Matches (PSMs), peptides and proteins were validated at a 1.0% False Discovery Rate (FDR) estimated using the decoy hit distribution. All validation thresholds are listed in the Certificate of Analysis available as 'certificate_of_analysis.txt' on Zenodo (doi:10.5281/zenodo.10023441). Spectrum counting abundance indexes were estimated using the Normalized Spectrum Abundance Factor (*73*) adapted for better handling of protein inference issues and peptide detectability.

Source data files (.raw, .mzML files) are available via ProteomeXchange with identifier PXD044632 (doi:10.6019/PXD044632), while resulting files from the downstream SearchGUI & PeptideShaker proteomic analysis are available on Zenodo (doi:10.5281/zenodo.10023441).

Analysis of proteomic results:

The 'Default Peptide Report.txt' TSV from the SearchGUI & PeptideShaker analysis was filtered down to those peptides that confidently matched (as scored by SearchGUI & PeptideShaker) against the PKZILLAs using a custom Jupyter notebook. The vast majority (68/70) of confident peptides that matched against the PKZILLAs, cross-matched only to the PKZILLAs, and the remaining 2/70 that also matched non-PKZILLA proteins, were removed from downstream analyses, as their removal minorly decreased the confidence of presented interpretations but also simplified explanations of this analysis. The Jupyter notebook next classified confident peptides as protein-unique (only matched a single PKZILLA protein), or those that were protein-multimatch (matched >= 2 PKZILLA proteins), and further sub-classified those categories down to those peptides that matched/were translated from a single PKZILLA CDS/exon region (exon-unique), or those that arose from multiple PKZILLA CDS/exon regions (exon-multimatch). This Jupyter notebook and spreadsheets of the resulting peptide categorizations are available on Zenodo (doi:10.5281/zenodo.10028959). See also fig. S8, S9.

IntroProScan annotation of PKZILLA domains:

The 3 PKZILLA polypeptides were extracted from all gene model polypeptides of the 12B1 gene annotation, and annotated with InterProScan v5.64-96.0 (*25*) using Singularity/Apptainer v3.5.8 (*74*, *75*) execution of the InterProScan Docker image, via a custom Nextflow wrapper workflow (*76*). In brief, all available InterProScan searches were performed, and post-processing off the GFF annotations was applied to remove certain PKS domain annotations for the KR and ER domains (Table S3) that gave erroneous duplicate annotations from shared homology. The workflow and InterProScan results for the PKZILLA polypeptides are available on Zenodo (doi:10.5281/zenodo.10023460). Specific InterProScan annotations that were deemed to be diagnostic for and representative of particular PKS domains are described in the "run2_filter.tsv" file of the aforementioned Zenodo dataset, and renaming from the InterPro entry identifiers to human readable identifiers are defined in "renaming.tsv" and "renaming2.tsv". Full graphical plots of all domains on the PKZILLAs are available in the "./results/pdf_2_PDF_A_1B/output/*.pdf" files, whereas graphical plots of a length normalized representation of the diagnostic PKS domains are available in the "./results/beads_on_string:pdf_2_PDF_A_1B/output/*.pdf" files. See also (maintext Fig. 2). Non length normalized representations are shown in fig. S6, S7, and the source analysis is available on Zenodo (doi:10.5281/zenodo.10093617). Graphical plots were generated with DNA Features Viewer (*77*). Non-

PKZILLA polypeptides were independently annotated with the same process but with a separate execution and a simplified workflow entry-point of 'do_simple_nonparallel_scan' that did not include graphical plotting. The workflow and InterProScan results for the non-PKZILLA polypeptides are available on Zenodo (doi:10.5281/zenodo.10011739).

Analysis of active site residues within PKZILLA PKS domains:

The presence or absence of expected conserved active site residues (catalytic or prosthetic group attachment sites) within domains of the PKZILLAs, were determined for the polyketide ketosynthase (KS), acyl carrier protein (ACP), dehydratase (DH), and ketoreductase (KR), flavin oxygenase (FLX), and enoyl (ER) domains, using either multiple sequence alignment liftover of the active site location & interpretation using the single- or multi-residue motif as defined by InterProScan annotations, or, locations & motifs as defined from literature sources, namely Fig. S4 of (*17*), Fig. S35 of (*78*), and Fig. S5 of (*79*). Notably active site residues for the ER and FLX domains were not available via InterProScan or literature sources. Essential and universally conserved active site residues for the ERs have not been reported despite determined efforts as of 2015 (*80*). For the FLX domains, which via AlphaFold2 (*81*, *82*) structural predictions and FoldSeek (*83*) structural similarity searches (doi: 10.5281/zenodo.10120640) have significant yet divergent structural homology with flavin-containing monooxygenase (FMO) proteins, catalytic active site residues have been claimed for certain structural homologs (*84*), but are not conserved across the full set of active FMO structural homologs (*85*), and thus the FLXs were not included in the PKZILLA active site analysis.

Annotated PKS domains were sourced from the 'gt_extractfeat' process results of the PKZILLA InterProScan available on Zenodo (doi:10.5281/zenodo.10023460), and renamed according to their increasing order N-terminal to C-terminal on the PKZILLA polypeptides, i.e. KS1, KS2, KS3, etc. A custom bash script using seqkit (*71*), bedtools (*52*), and kalign2 (*58*), was used to create multiple sequence alignments of, and extract the residues at matching active sites, from the PKZILLA PKS domains. All ACP, and DH domains for PKZILLA-1 and -2 had the expected active site residues, while the ER and FLX domains were not included due to a lack of active site information. KS domains were scored as KS^0 aka "non-elongating"/"condensation-incompetent"/"transacylase" KSs based on the deviation of the histidine in the HGTGT active site motif (*29*, *86*, *87*). In contrast, KR domains had two unusual aspects: **(1)** They came in two classes - contiguous or split. The KR domain is made up of two homologous N-terminal structural and C-terminal catalytic subdomains. Typically, these two subdomains are contiguous or nearly so. However certain fatty acid synthase (FAS) or PKS proteins show a split configuration, where the two KR subdomains are intervened and split by another PKS domain. This configuration can be seen with the InterPro domain annotations for the Porcine (*Sus scrofa*) FAS protein (https://www.ebi.ac.uk/interpro/protein/UniProt/I3LCW1/), where the ER domain intervenes between the two KR subdomains. In the literature, the subdomains showing this phenomena have been dubbed as the N-terminal KR^s or KR_S (structural) or C-terminal KR^c or KR_C (catalytic) subdomains (*88–90*). We use the nomenclature KR or KRf (full-length), KRn (N-terminal), and KRc (C-terminal) to distinguish our 3 subclasses of ketoreductase (sub)domains. Notably, some unannotated gaps in the PKZILLA are similar to the KRn subdomains and show a nearby annotated KRc subdomain, suggesting that KRn domains may have diverged away from bioinformatic detection (table S6, S7). **(2)** The catalytic residues of several KRf and KRc domains do not match with expectations for activity, and thus we interpret their source domains as catalytically inactive. Some KR domains showed expected catalytic residues for activity, yet we anticipated they would be inactive based on our biosynthetic model - thus a 2nd tier of analysis was applied where KR domains predicted to phylogenetically cluster with and descend from the last common ancestor for PKZILLA-1__KR31c0 (inactivity assigned based on active side residues) and PKZILLA-1__KR14c (fig. S12, Table S6, S7, S8, S9) were assigned as inactive. This clade was selected based on their relatively long phylogenetic branches (suggesting relaxation of selection from inactivity), and the matching with expectation of inactivity from the biosynthetic model. An alternative hypothesis is they are catalytically active domains but catalyze non-

standard reactions. Throughout the manuscript and figures we dub these putatively inactive or diverged domains as KR^0/KRf^0/KRf0, KRn^0/KRn0, or KRc^0/KRc0. The workflow and results for this analysis, including Excel spreadsheets of the sequences at active site residues, is available on Zenodo (doi:10.5281/zenodo.10028517).

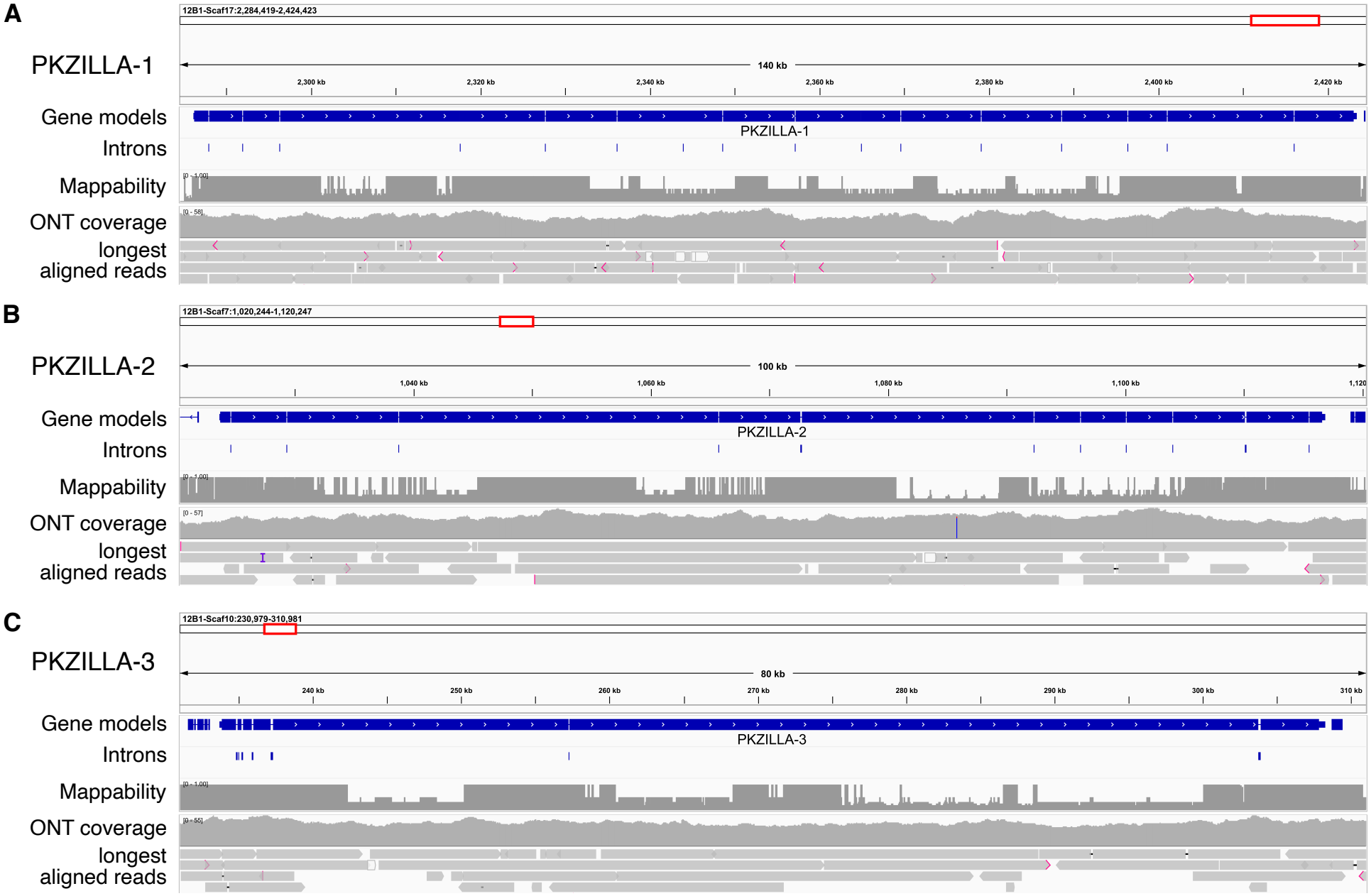
A
PKZILLA-1
12B1-Scaf17:2,284,419-2,424,423
140 kb
2,300 kb
2,320 kb
2,340 kb
2,360 kb
2,380 kb
2,400 kb
2,420 kb
Gene models
PKZILLA-1
Introns
Mappability
[0 - 1.00]
ONT coverage
[0 - 58]
longest aligned reads
B
PKZILLA-2
12B1-Scaf7:1,020,244-1,120,247
100 kb
1,040 kb
1,060 kb
1,080 kb
1,100 kb
1,120
Gene models
PKZILLA-2
Introns
Mappability
[0 - 1.00]
ONT coverage
[0 - 57]
longest aligned reads
C
PKZILLA-3
12B1-Scaf10:230,979-310,981
80 kb
240 kb
250 kb
260 kb
270 kb
280 kb
290 kb
300 kb
310 kb
Gene models
PKZILLA-3
Introns
Mappability
[0 - 1.00]
ONT coverage
[0 - 55]
longest aligned reads

Fig. S1: Expanded genomic detail for PKZILLA gene models. PKZILLA-1,-2,-3 are shown as panel A,B,C. Aligned Oxford Nanopore (ONT) reads (*20*) show no evidence of assembly errors like sharp coverage discontinuities, frequent coincident insertions or deletions, or frequent coincident single nucleotide variations (SNVs), excluding the synonymous SNV T→C (L20550L) in PKZILLA-2. Graphical key: Pink arrows=read soft-clips. Vertical purple bar=read insertions. Black horizontal line=read deletions. IGV parameters: Allele Frequency Threshold=0.70, Hide Small Indels=Yes, Sort Alignments by=aligned read length. Show mismatched bases=Off. Mappability was calculated with genmap v1.3.0 (*91*), with parameters K=100 and E=2. Drops from maximum of the mappability track represent low short read mappability due to repetitive sequences. Figure produced with Integrated Genomics Viewer (IGV) v2.16.2 (*51*).

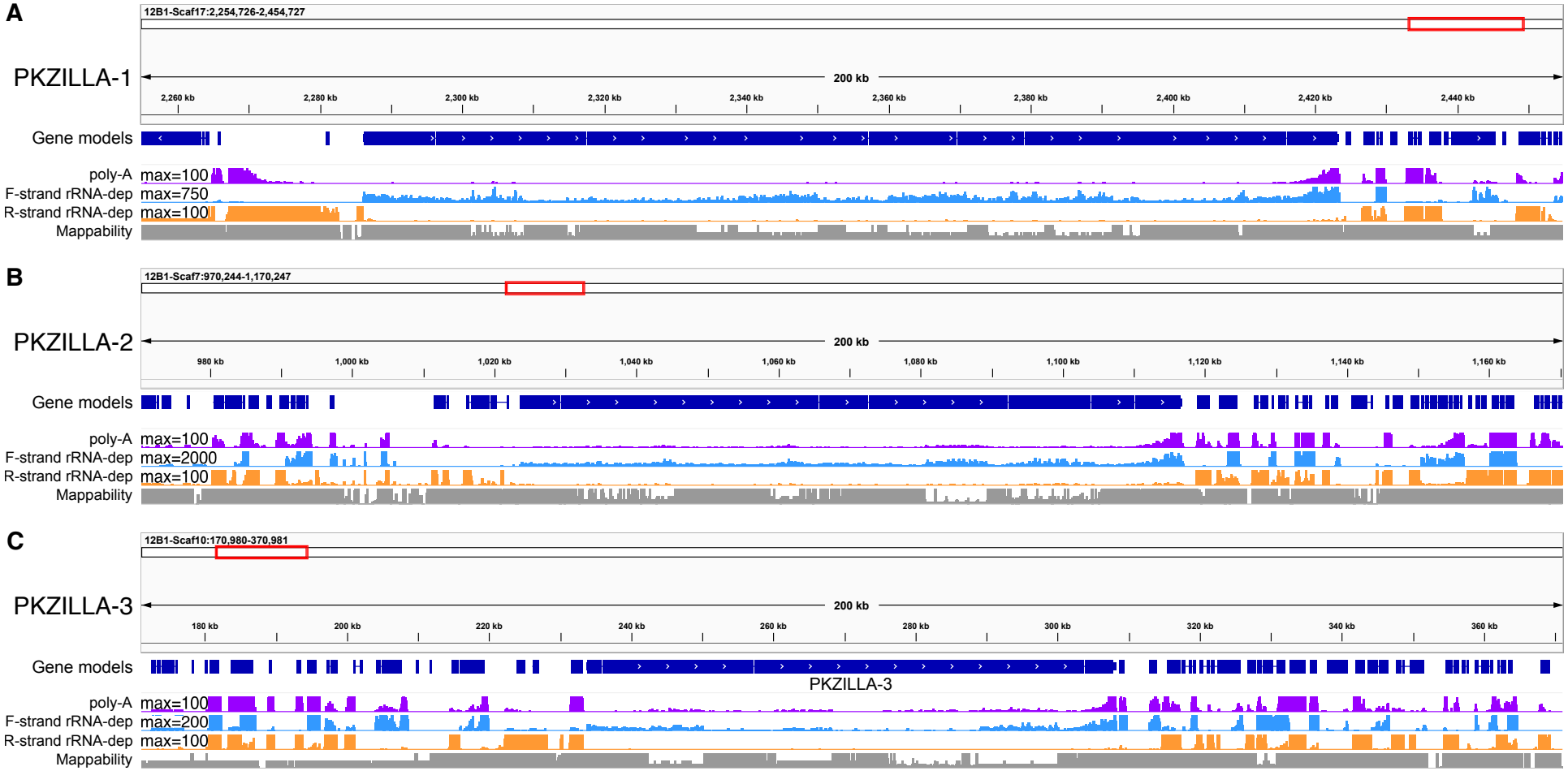

Fig. S2: Expanded transcriptomic detail for PKZILLA gene models. PKZILLA-1,-2,-3 are shown as panel A,B,C. poly-A=Coverage of hisat2 aligned poly-A pulldown RNA-Seq reads. F-strand rRNA-dep=Coverage of extracted forward-stranded reads for hisat2 aligned rRNA depletion RNA-Seq reads. R-strand rRNA-dep=Coverage of extracted reverse-stranded reads for hisat2 aligned rRNA depletion RNA-Seq reads. RNA-Seq coverage tracks have a linear scale, scaled to the maximum values annotated on the tracks. Note that the poly-A and R-strand tracks are scaled to a lower maximum to enhance sensitivity. Note that the antisense strand has negligible coverage, supporting one transcriptional start site (TSS) per hotspot. Mappability was calculated with genmap v1.3.0 (*91*), with parameters K=100 and E=2. Drops from maximum of the mappability track represent low short read mappability due to repetitive sequences. Figure produced with Integrated Genomics Viewer (IGV) v2.16.2 (*51*).

A - PKZILLA-1 Intron #1

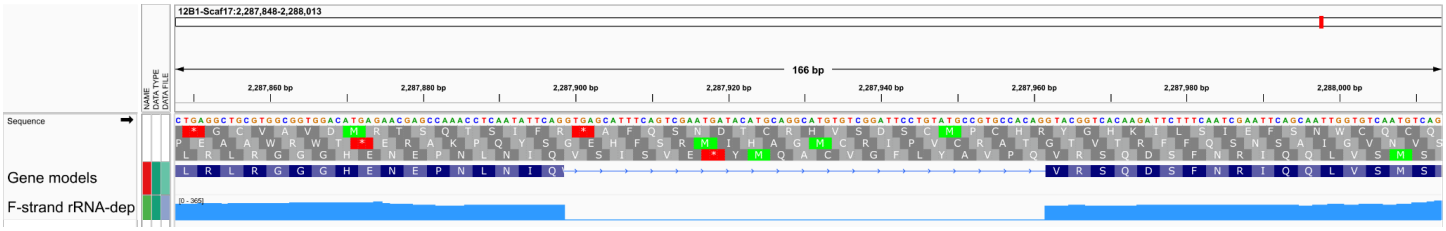

B - PKZILLA-1 Intron #2

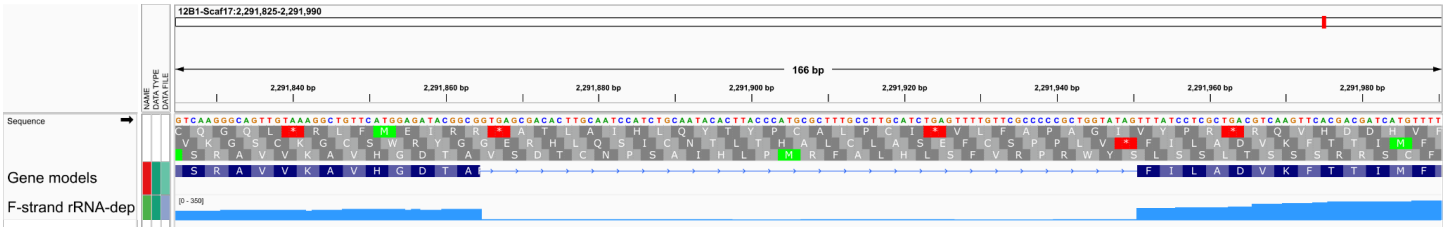

C - PKZILLA-1 Intron #3

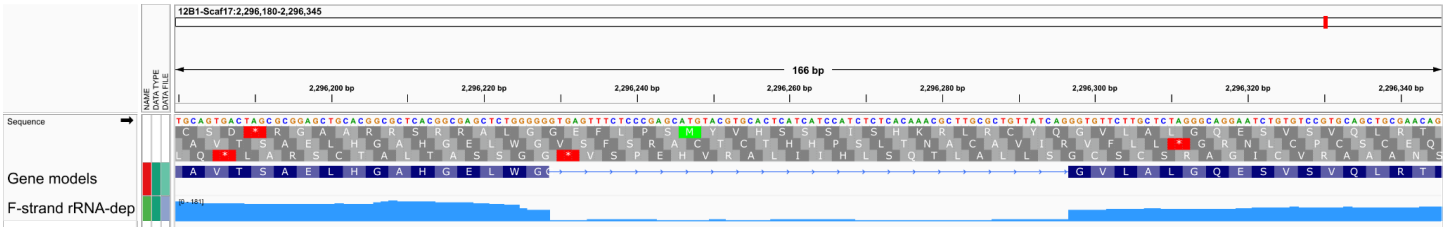

D - PKZILLA-1 Intron #4

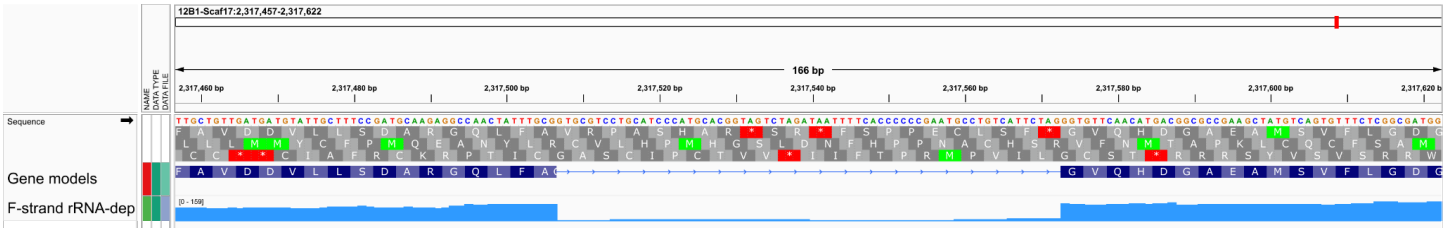

E - PKZILLA-1 Intron #5

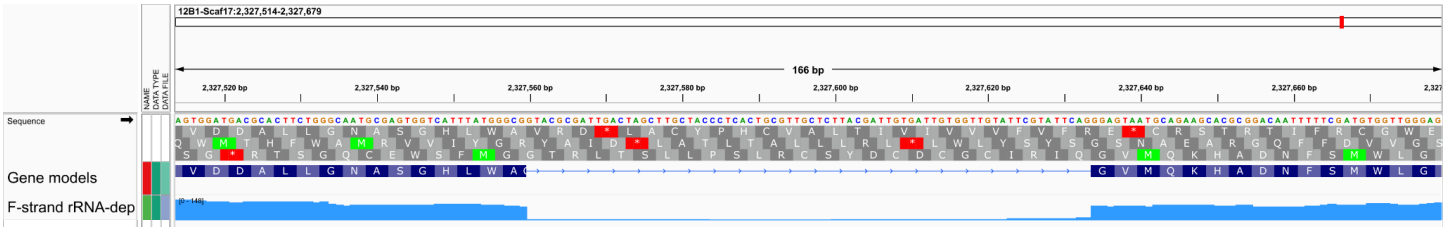

F - PKZILLA-1 Intron #6

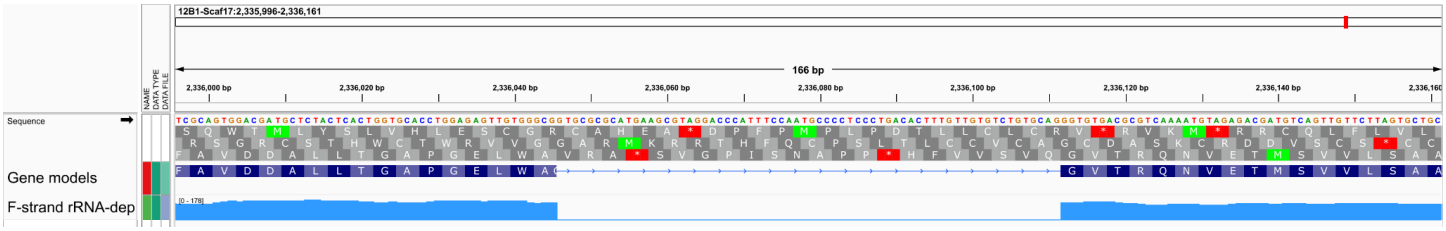

G - PKZILLA-1 Intron #7

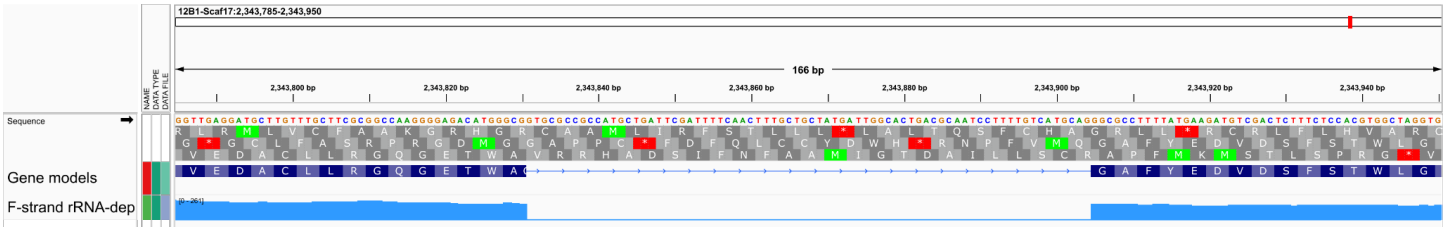

H - PKZILLA-1 Intron #8

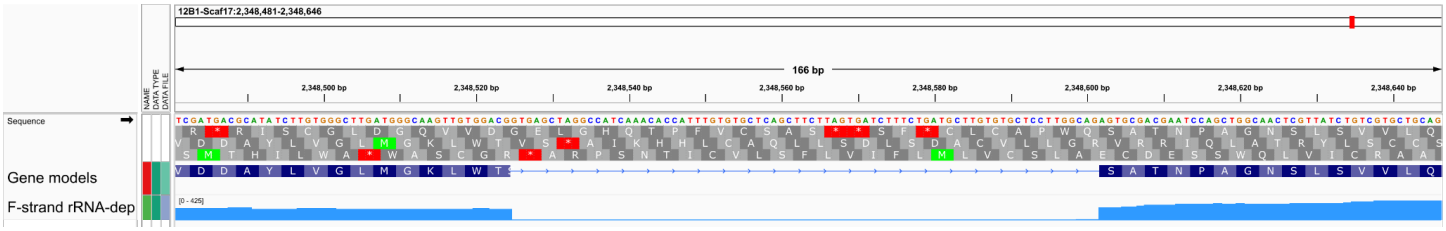

I - PKZILLA-1 Intron #9

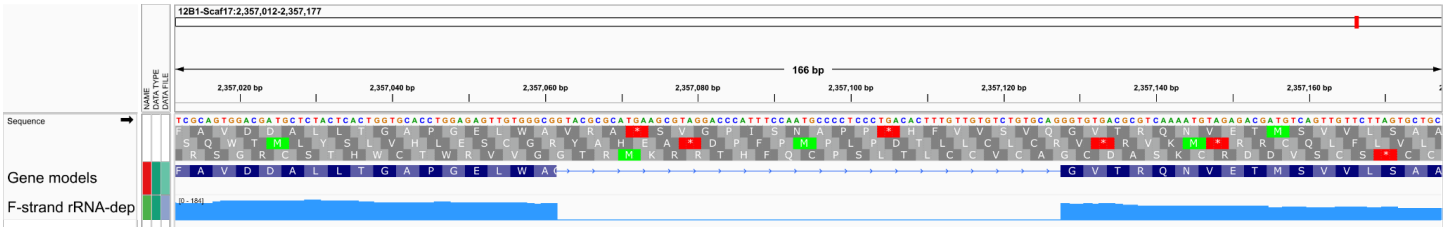

J - PKZILLA-1 Intron #10

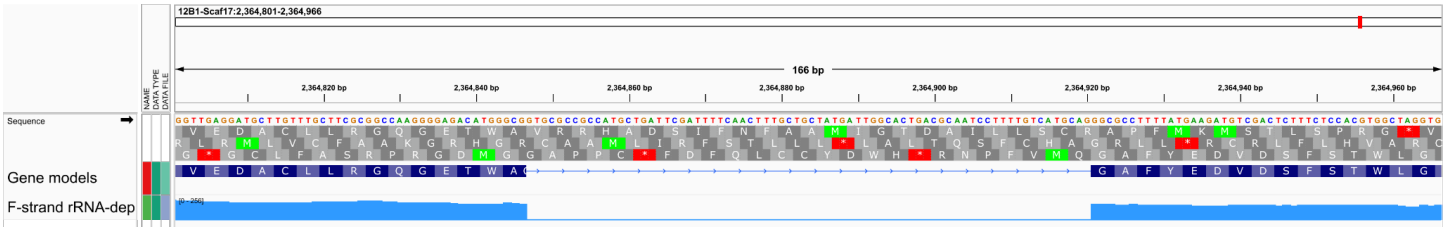

K - PKZILLA-1 Intron #11

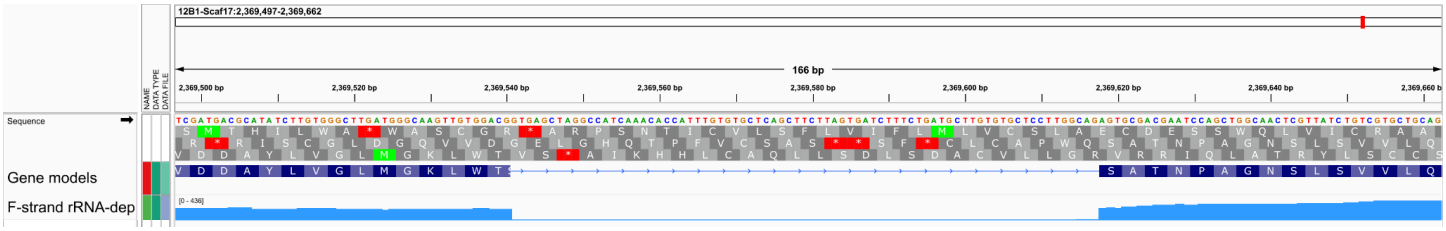

L - PKZILLA-1 Intron #12

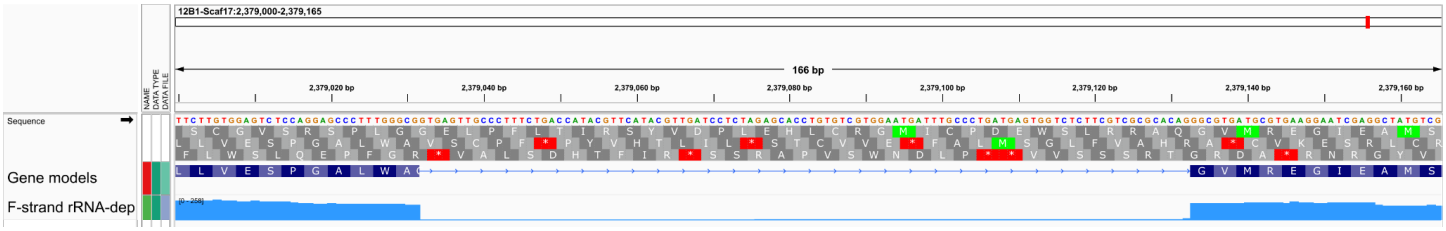

M - PKZILLA-1 Intron #13

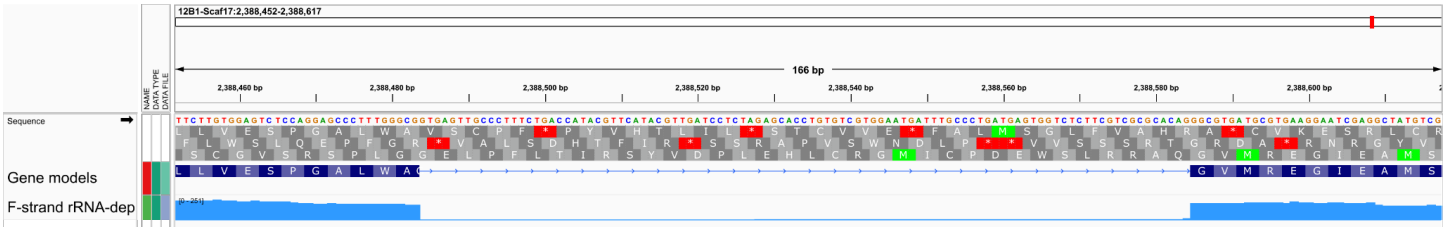

N - PKZILLA-1 Intron #14

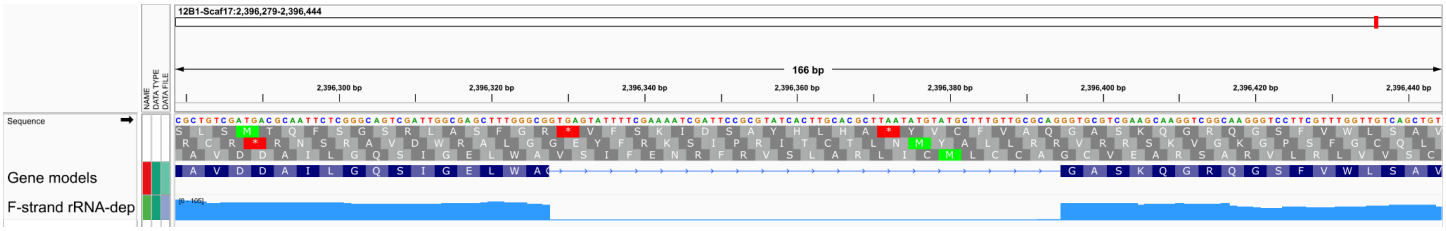

O - PKZILLA-1 Intron #15

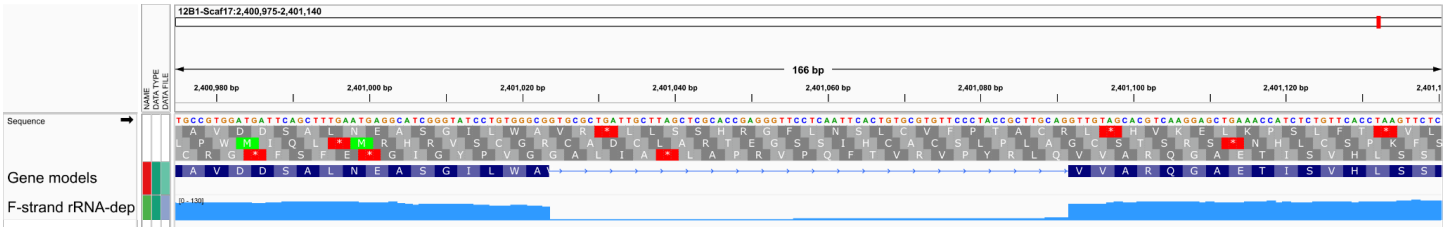

P - PKZILLA-1 Intron #16

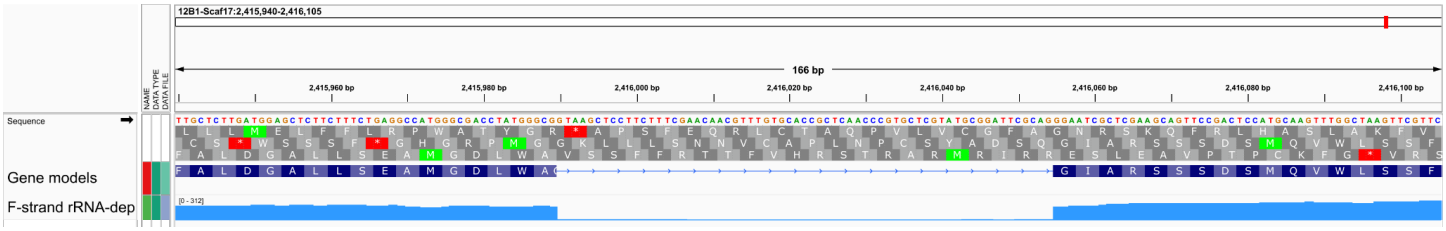

Fig. S3: Detail view of PKZILLA-1 introns. Note the drop in aligned rRNA depletion RNA-Seq coverage, and presence of canonical GT-AG splice donor and acceptor sites. Figure produced with Integrated Genomics Viewer (IGV) v2.16.2 (*51*).

A - PKZILLA-2 Intron #1

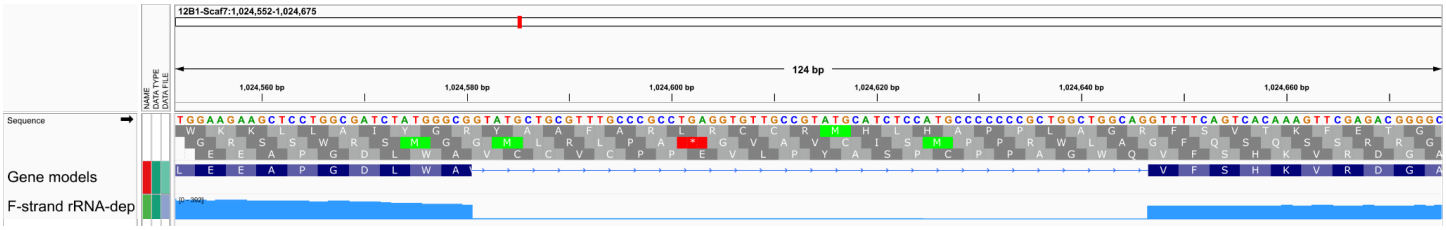

B - PKZILLA-2 Intron #2

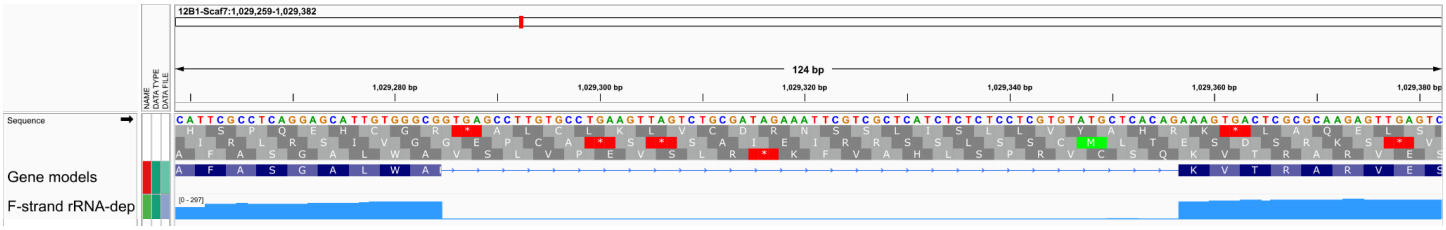

C - PKZILLA-2 Intron #3

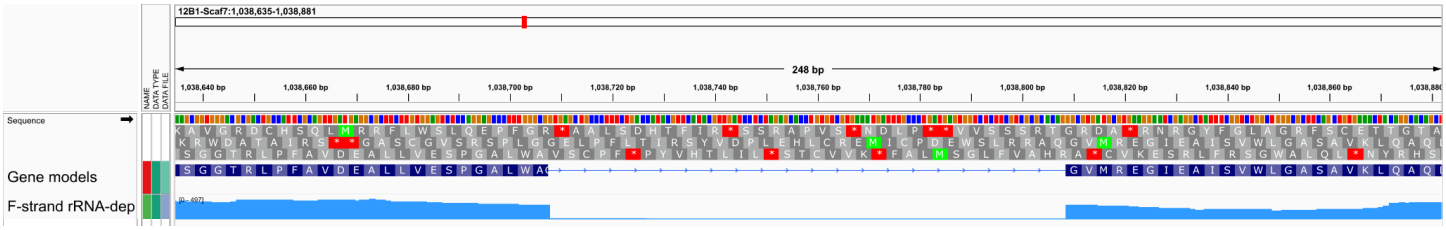

D - PKZILLA-2 Intron #4

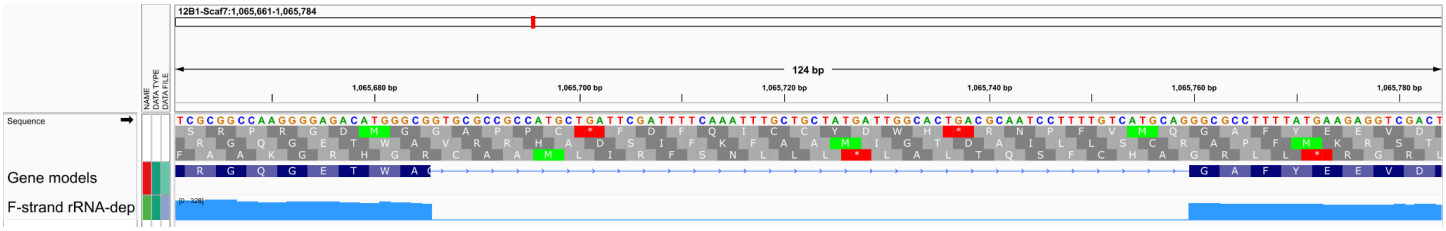

E - PKZILLA-2 Intron #5

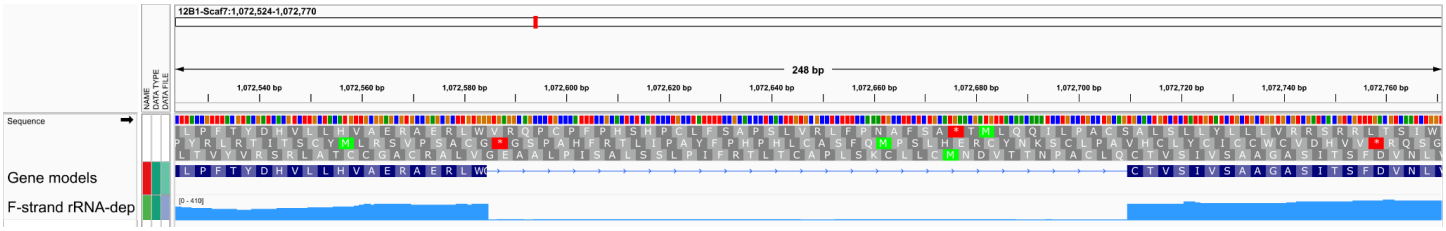

F - PKZILLA-2 Intron #6

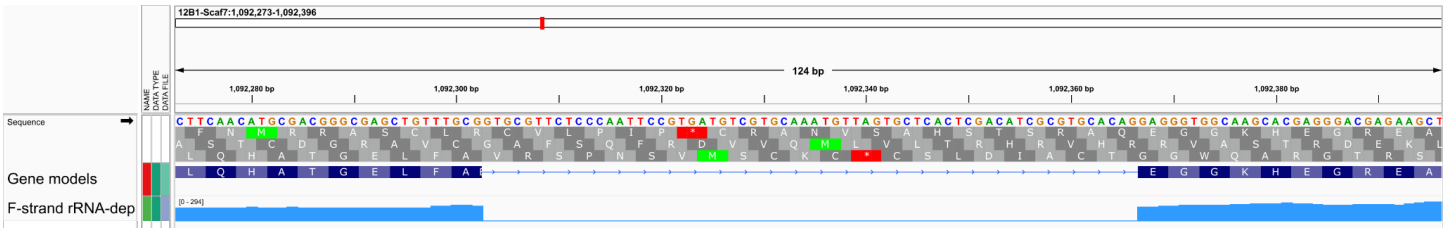

G - PKZILLA-2 Intron #7

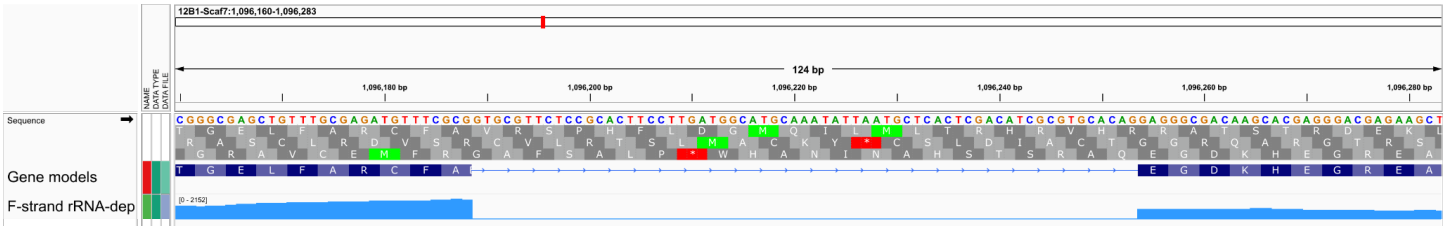

H - PKZILLA-2 Intron #8

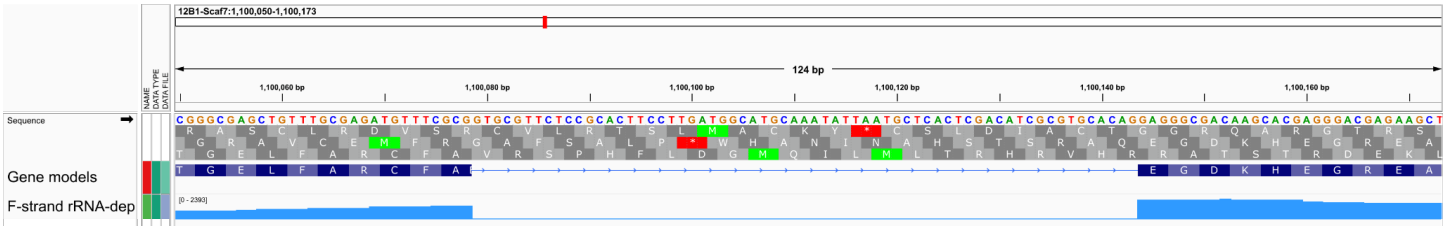

I - PKZILLA-2 Intron #9

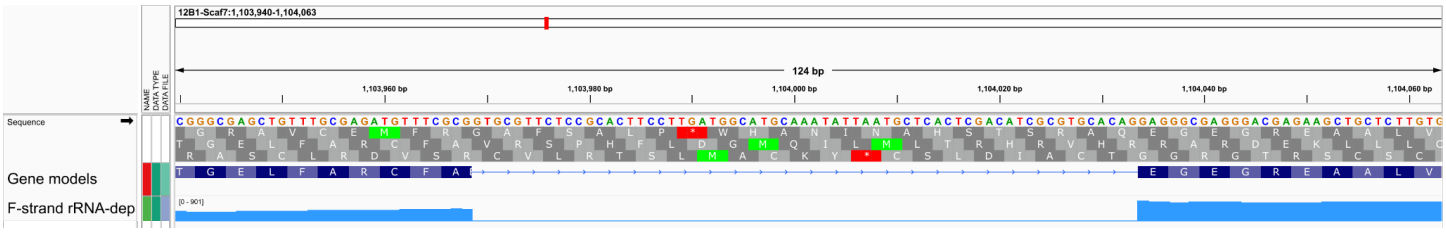

J - PKZILLA-2 Intron #10

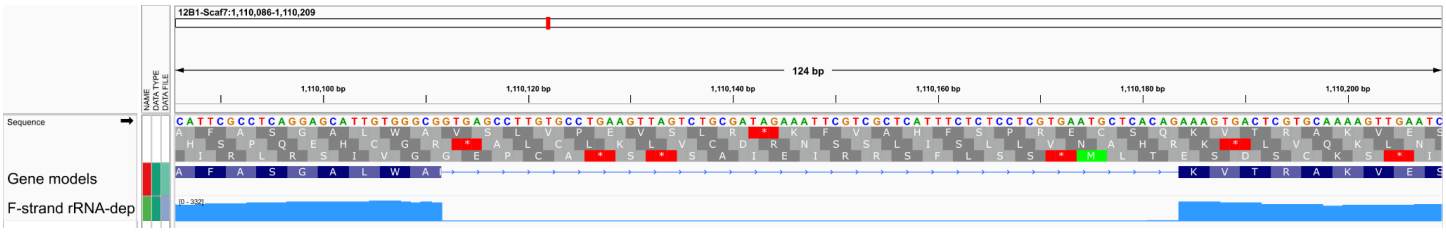

K - PKZILLA-2 Intron #11

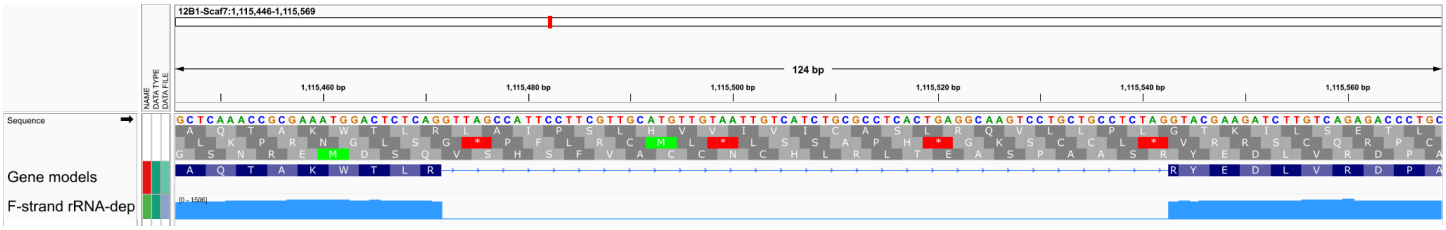

Fig. S4: Detail view of PKZILLA-2 introns. Note the drop in aligned rRNA depletion RNA-Seq coverage, and presence of canonical GT-AG splice donor and acceptor sites. Figure produced with Integrated Genomics Viewer (IGV) v2.16.2 (*51*).

A - PKZILLA-3 Intron #1

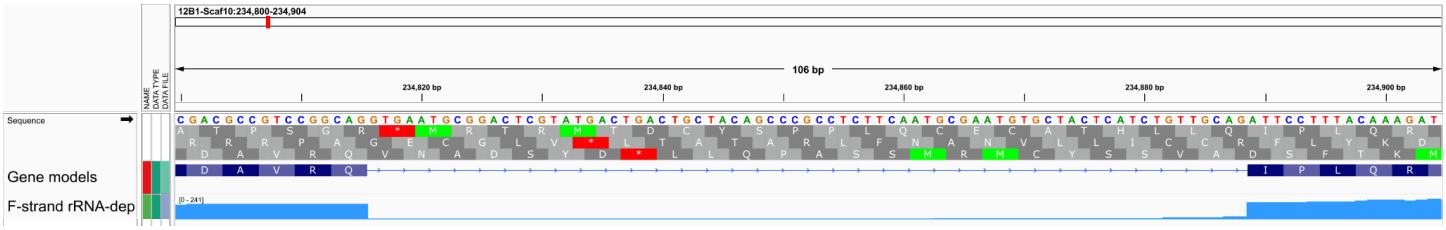

B - PKZILLA-3 Intron #2

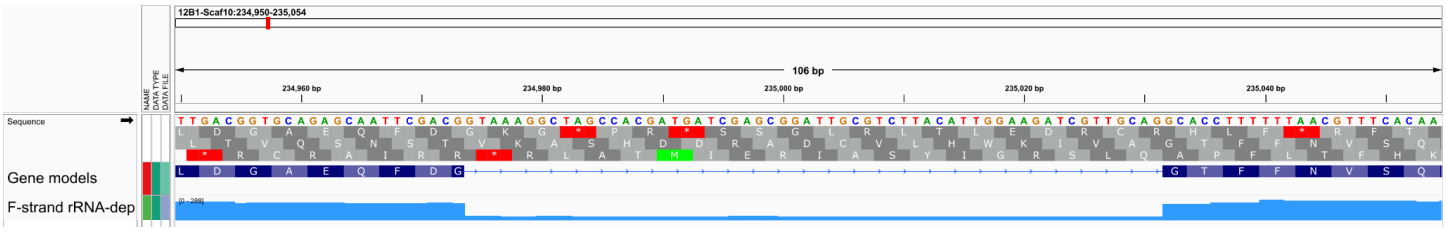

C - PKZILLA-3 Intron #3

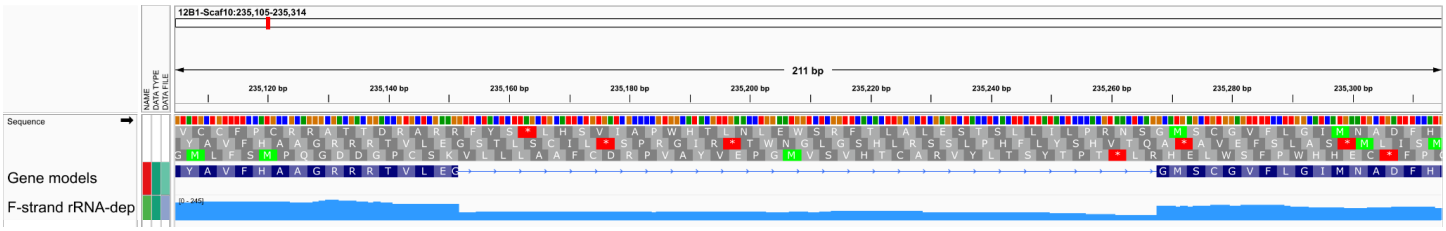

D - PKZILLA-3 Intron #4

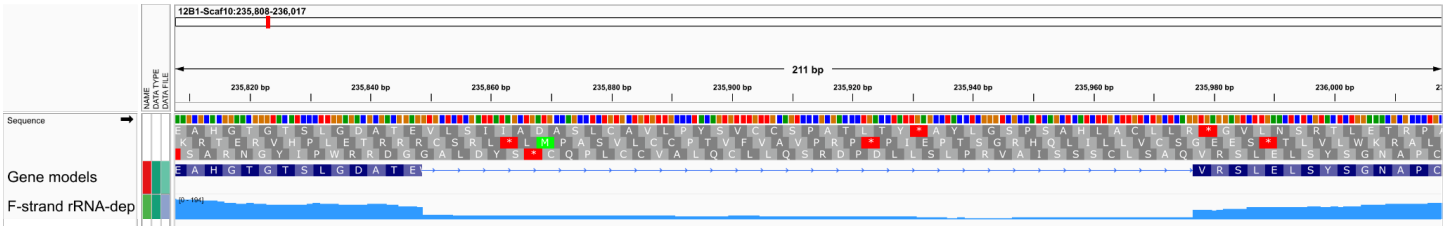

E - PKZILLA-3 Intron #5

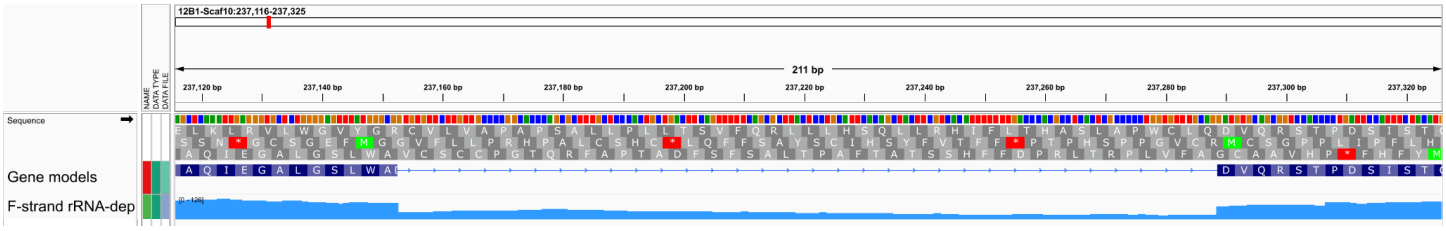

F - PKZILLA-3 Intron #6

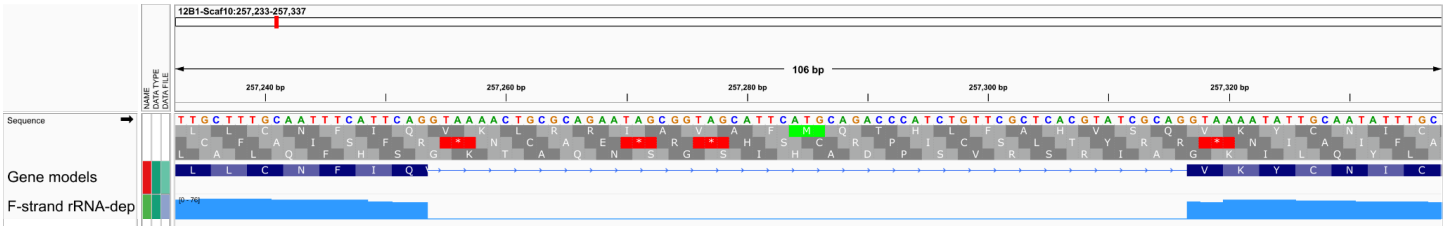

G - PKZILLA-3 Intron #7

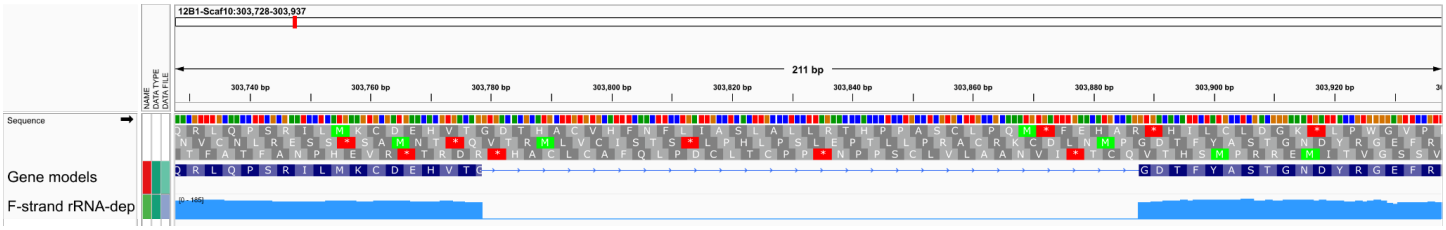

Fig. S5: Detail view of PKZILLA-3 introns. Note the drop in aligned rRNA depletion RNA-Seq coverage, and presence of canonical GT-AG splice donor and acceptor sites. Figure produced with Integrated Genomics Viewer (IGV) v2.16.2 (*51*).

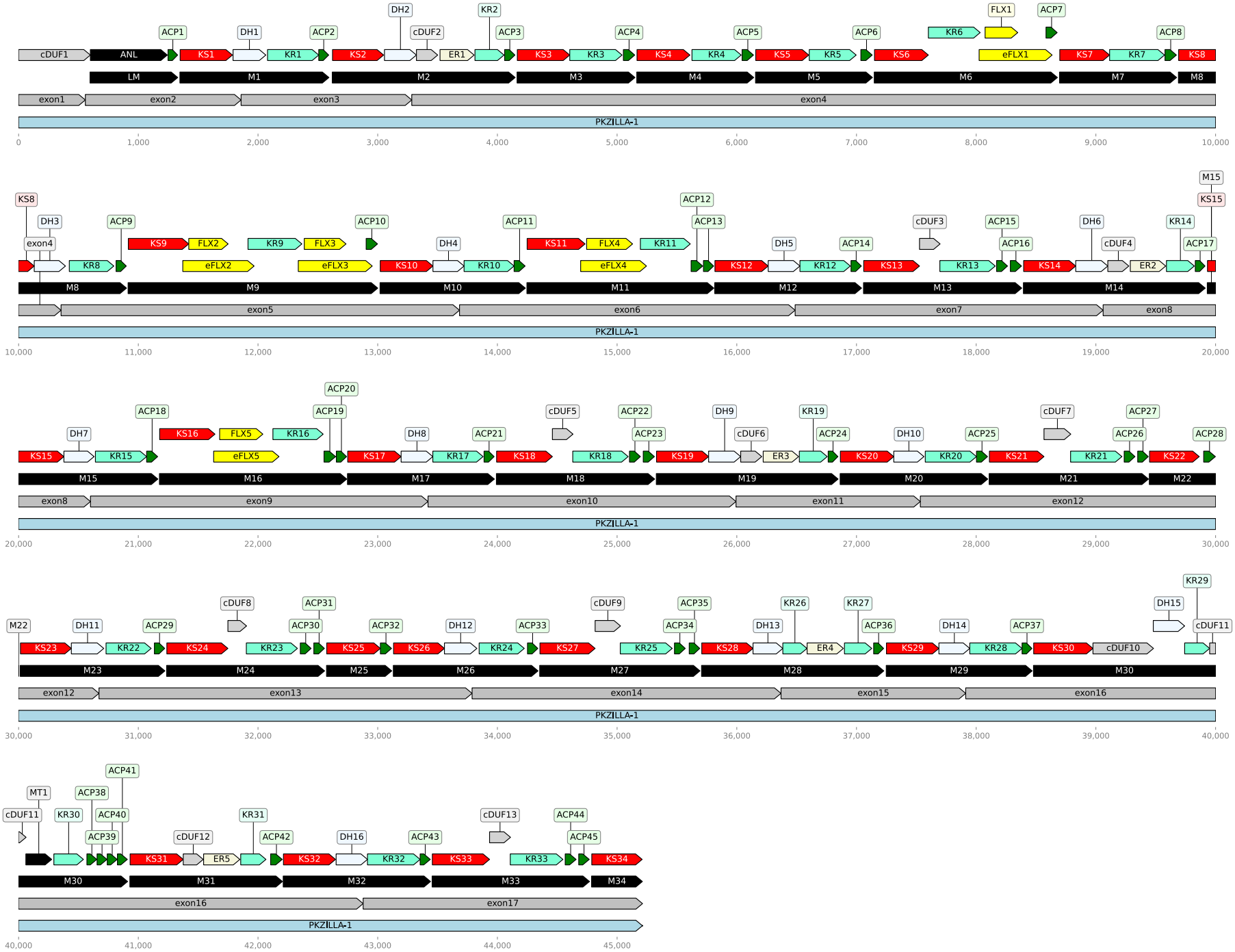
cDUF1
ANL
ACP1
KS1
DH1
KR1
ACP2
KS2
DH2
cDUF2
ER1
KR2
ACP3
KS3
KR3
ACP4
KS4
KR4
ACP5
KS5
KR5
ACP6
KS6
KR6
FLX1
eFLX1
ACP7
KS7
KR7
ACP8
KS8
LM
M1
M2
M3
M4
M5
M6
M7
M8
exon1
exon2
exon3
exon4
PKZILLA-1
0
1,000
2,000
3,000
4,000
5,000
6,000
7,000
8,000
9,000
10,000
KS8
DH3
exon4
KR8
ACP9
KS9
FLX2
eFLX2
KR9
FLX3
eFLX3
ACP10
KS10
DH4
KR10
ACP11
KS11
FLX4
eFLX4
KR11
ACP12
ACP13
KS12
DH5
KR12
ACP14
KS13
cDUF3
KR13
ACP15
ACP16
KS14
DH6
cDUF4
ER2
KR14
ACP17
KS15
M15
M8
M9
M10
M11
M12
M13
M14
exon5
exon6
exon7
exon8
PKZILLA-1
10,000
11,000
12,000
13,000
14,000
15,000
16,000
17,000
18,000
19,000
20,000
DH7
KS15
KR15
ACP18
KS16
FLX5
eFLX5
KR16
ACP19
ACP20
KS17
DH8
KR17
ACP21
KS18
cDUF5
KR18
ACP22
ACP23
KS19
DH9
cDUF6
ER3
KR19
ACP24
KS20
DH10
KR20
ACP25
KS21
cDUF7
KR21
ACP26
ACP27
KS22
ACP28
M15
M16
M17
M18
M19
M20
M21
M22
exon8
exon9
exon10
exon11
exon12
PKZILLA-1
20,000
21,000
22,000
23,000
24,000
25,000
26,000
27,000
28,000
29,000
30,000
M22
DH11
KS23
KR22
ACP29
KS24
cDUF8
KR23
ACP30
ACP31
KS25
ACP32
KS26
DH12
KR24
ACP33
KS27
cDUF9
KR25
ACP34
ACP35
KS28
DH13
ER4
KR26
KR27
ACP36
KS29
DH14
KR28
ACP37
KS30
cDUF10
DH15
cDUF11
KR29
M23
M24
M25
M26
M27
M28
M29
M30
exon12
exon13
exon14
exon15
exon16
PKZILLA-1
30,000
31,000
32,000
33,000
34,000
35,000
36,000
37,000
38,000
39,000
40,000
cDUF11
MT1
KR30
ACP38
ACP39
ACP40
ACP41
cDUF12
ER5
KR31
KS31
ACP42
KS32
DH16
KR32
ACP43
KS33
cDUF13
KR33
ACP44
ACP45
KS34
M30
M31
M32
M33
M34
exon16
exon17
PKZILLA-1
40,000
41,000
42,000
43,000
44,000
45,000

Fig. S6: Graphical plot of non-length-normalized PKZILLA-1 polypeptide (light blue), PKS modules (black), domains (varied colors), and unannotated cDUFs (light gray), and the relationship of shown regions with their source exons (dark gray). Plot generated with DNA Features Viewer (*77*). Source files, scripts, and resulting plots available on Zenodo (doi:10.5281/zenodo.10093617).

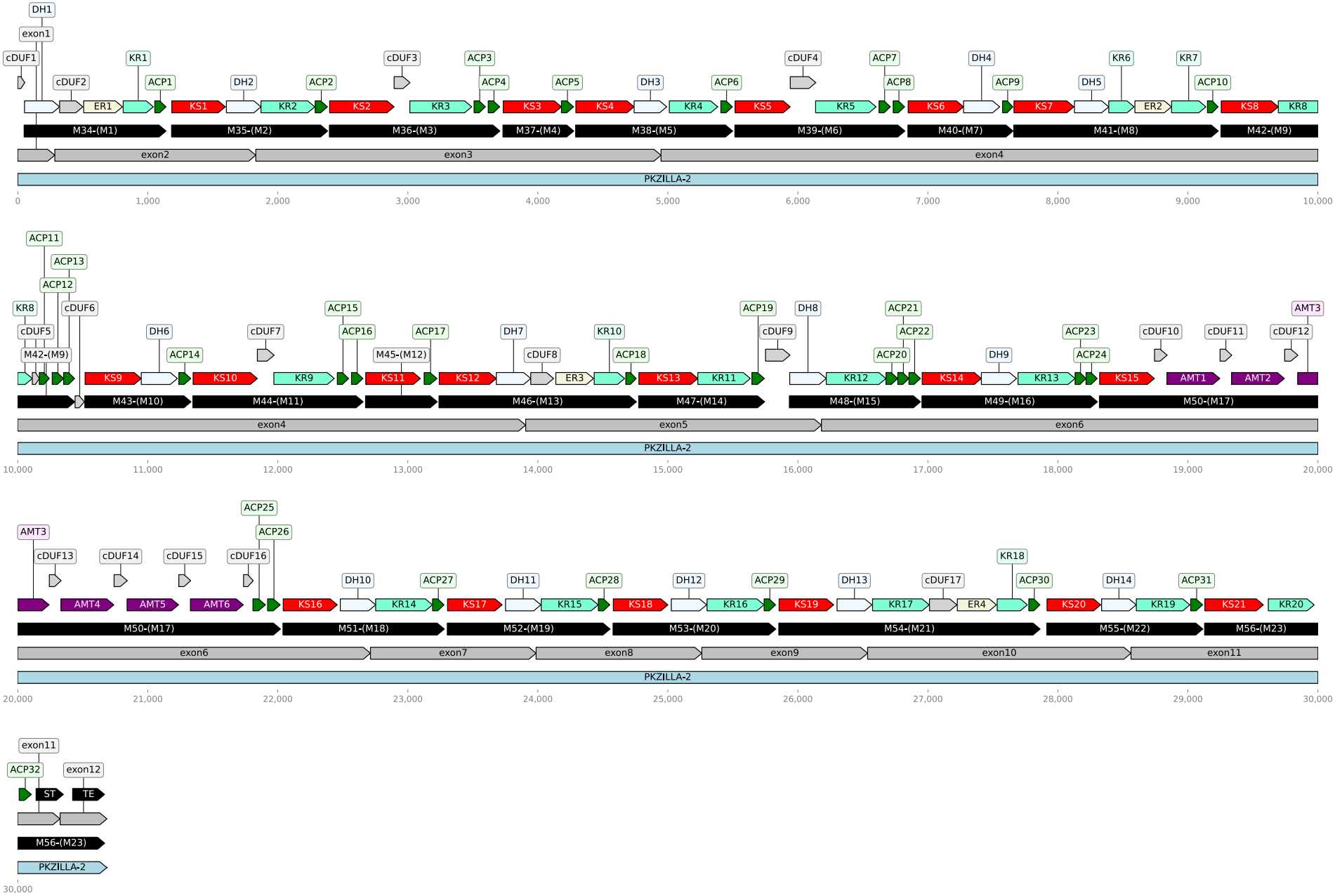
DH1
exon1
cDUF1
KR1
cDUF3
ACP3
cDUF4
ACP7
DH4
KR6
KR7
cDUF2
ACP1
DH2
ACP2
ACP4
ACP5
DH3
ACP6
ACP8
ACP9
DH5
ACP10
ER1
KS1
KR2
KS2
KR3
KS3
KS4
KR4
KS5
KR5
KS6
KS7
ER2
KS8
KR8
M34-(M1)
M35-(M2)
M36-(M3)
M37-(M4)
M38-(M5)
M39-(M6)
M40-(M7)
M41-(M8)
M42-(M9)
exon2
exon3
exon4
PKZILLA-2
0
1,000
2,000
3,000
4,000
5,000
6,000
7,000
8,000
9,000
10,000
ACP11
ACP13
ACP12
KR8
cDUF6
ACP15
ACP19
DH8
ACP21
AMT3
cDUF5
DH6
cDUF7
ACP16
ACP17
DH7
KR10
cDUF9
ACP22
ACP23
cDUF10
cDUF11
cDUF12
M42-(M9)
ACP14
M45-(M12)
cDUF8
ACP18
ACP20
DH9
ACP24
KS9
KS10
KR9
KS11
KS12
ER3
KS13
KR11
KR12
KS14
KR13
KS15
AMT1
AMT2
M43-(M10)
M44-(M11)
M46-(M13)
M47-(M14)
M48-(M15)
M49-(M16)
M50-(M17)
exon4
exon5
exon6
PKZILLA-2
10,000
11,000
12,000
13,000
14,000
15,000
16,000
17,000
18,000
19,000
20,000
ACP25
AMT3
ACP26
cDUF13
cDUF14
cDUF15
cDUF16
DH10
ACP27
DH11
ACP28
DH12
ACP29
DH13
cDUF17
KR18
ACP30
DH14
ACP31
AMT4
AMT5
AMT6
KS16
KR14
KS17
KR15
KS18
KR16
KS19
KR17
ER4
KS20
KR19
KS21
KR20
M50-(M17)
M51-(M18)
M52-(M19)
M53-(M20)
M54-(M21)
M55-(M22)
M56-(M23)
exon6
exon7
exon8
exon9
exon10
exon11
PKZILLA-2
20,000
21,000
22,000
23,000
24,000
25,000
26,000
27,000
28,000
29,000
30,000
exon11
ACP32
exon12
ST
TE
M56-(M23)
PKZILLA-2
30,000

Fig. S7: Graphical plot of non-length-normalized PKZILLA-2 polypeptide (light blue), PKS modules (black), domains (varied colors), and unannotated cDUFs (light gray), and the relationship of shown regions with their source exons (dark gray). Plot generated with DNA Features Viewer (*77*). Source files, scripts, and resulting plots available on Zenodo (doi:10.5281/zenodo.10093617).

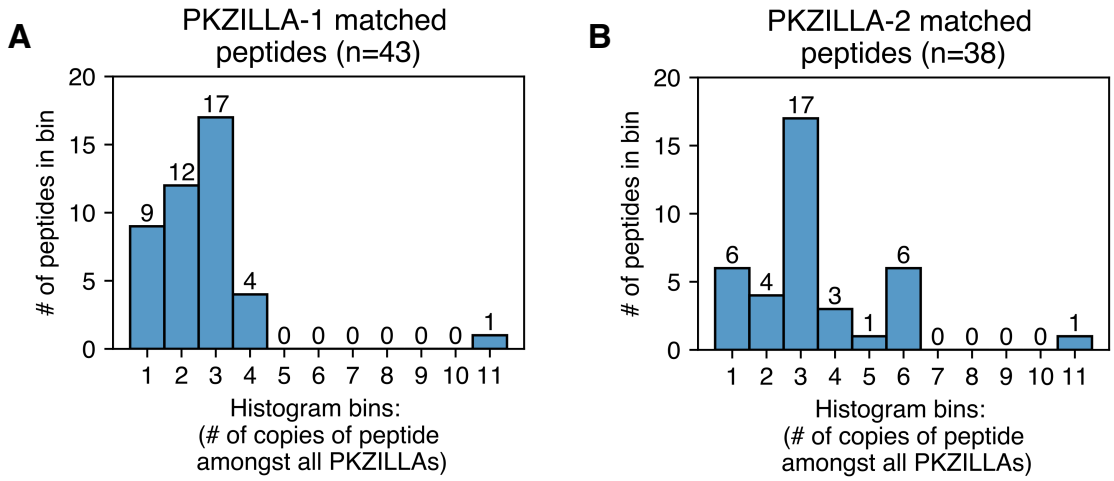

Fig. S8: Histogram of proteomics detected peptides binned by the number of times the specific peptide occurs within the PKZILLA polypeptides of the *Prymnesium parvum* 12B1 proteome. The majority of detected peptides from the PKZILLAs are present >=2 times. These peptides were only present in the PKZILLA gene models and were not found anywhere else in 6-frame translations of the 12B1 genome (doi:10.5281/zenodo.10028959). Source data, workflow, and plots available on Zenodo (doi:10.5281/zenodo.10028959).

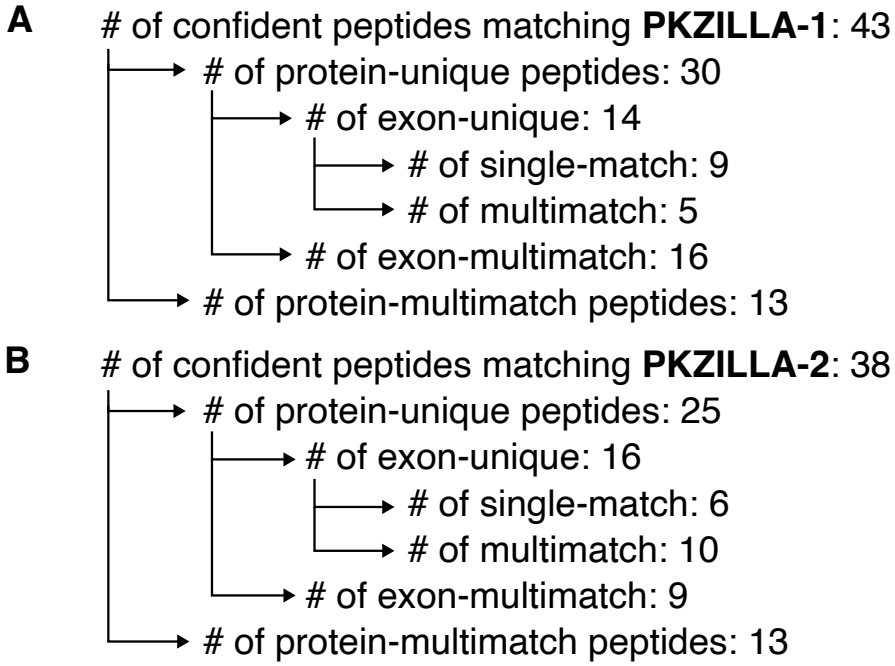

Fig. S9: Hierarchical classification of proteomics detected peptides. **(A)** PKZILLA-1, source values from Zenodo file 'PKZILLA-1_classify_peptides.txt' and **(B)** PKZILLA-2, source values from Zenodo file 'PKZILLA-2_classify_peptides.txt'. Source data, workflow, and these derived data available on Zenodo (doi:10.5281/zenodo.10028959).

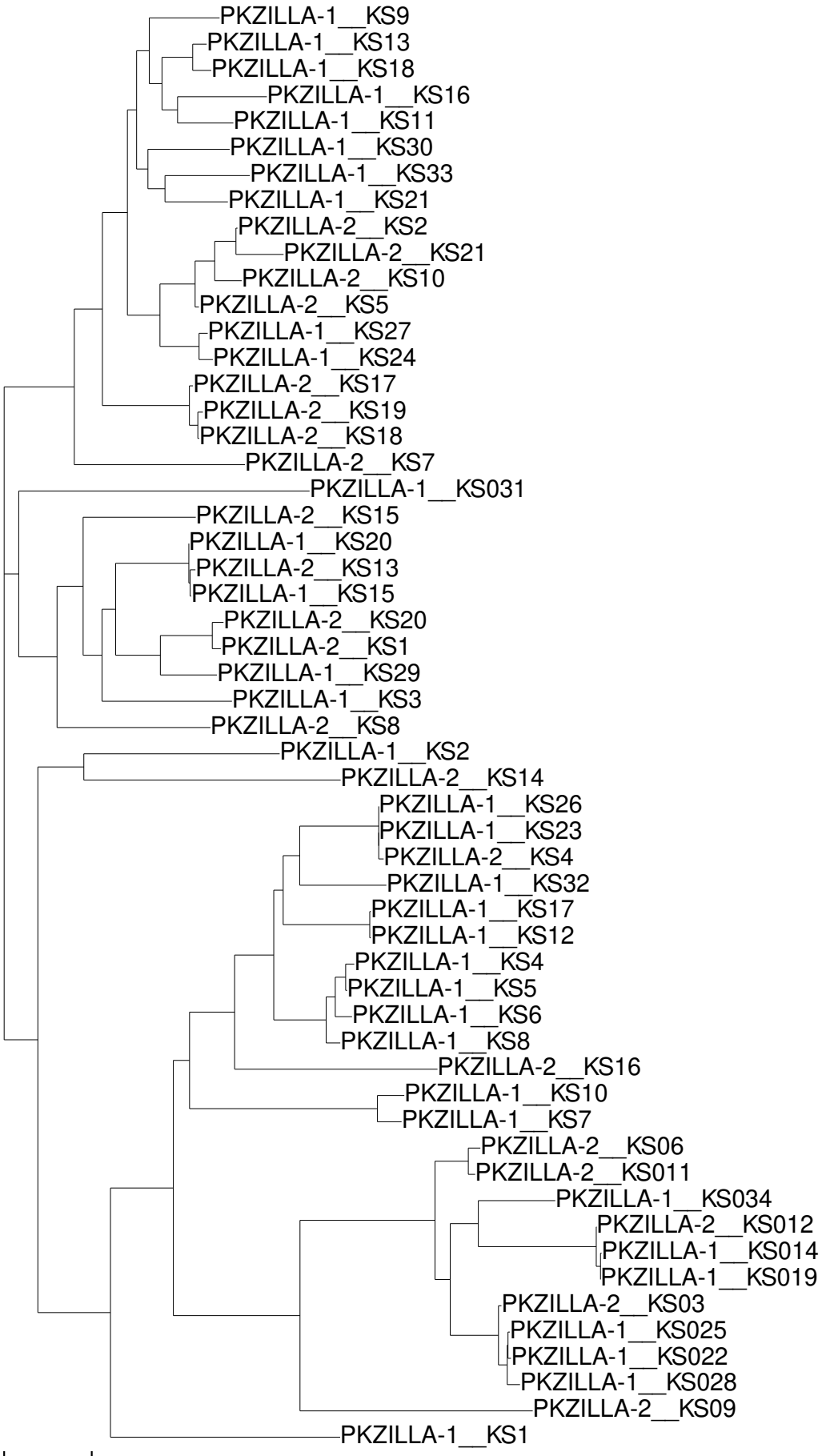
PKZILLA-1__KS9
PKZILLA-1__KS13
PKZILLA-1__KS18
PKZILLA-1__KS16
PKZILLA-1__KS11
PKZILLA-1__KS30
PKZILLA-1__KS33
PKZILLA-1__KS21
PKZILLA-2__KS2
PKZILLA-2__KS21
PKZILLA-2__KS10
PKZILLA-2__KS5
PKZILLA-1__KS27
PKZILLA-1__KS24
PKZILLA-2__KS17
PKZILLA-2__KS19
PKZILLA-2__KS18
PKZILLA-2__KS7
PKZILLA-1__KS031
PKZILLA-2__KS15
PKZILLA-1__KS20
PKZILLA-2__KS13
PKZILLA-1__KS15
PKZILLA-2__KS20
PKZILLA-2__KS1
PKZILLA-1__KS29
PKZILLA-1__KS3
PKZILLA-2__KS8
PKZILLA-1__KS2
PKZILLA-2__KS14
PKZILLA-1__KS26
PKZILLA-1__KS23
PKZILLA-2__KS4
PKZILLA-1__KS32
PKZILLA-1__KS17
PKZILLA-1__KS12
PKZILLA-1__KS4
PKZILLA-1__KS5
PKZILLA-1__KS6
PKZILLA-1__KS8
PKZILLA-2__KS16
PKZILLA-1__KS10
PKZILLA-1__KS7
PKZILLA-2__KS06
PKZILLA-2__KS011
PKZILLA-1__KS034
PKZILLA-2__KS012
PKZILLA-1__KS014
PKZILLA-1__KS019
PKZILLA-2__KS03
PKZILLA-1__KS025
PKZILLA-1__KS022
PKZILLA-1__KS028
PKZILLA-2__KS09
PKZILLA-1__KS1
0.500191

Fig. S10: Phylogenetic analysis of PKZILLA ketosynthase (KS) and non-elongating KS (KS0) domains. Sequences were multiple sequence aligned with kalign2 (*58*) and the unrooted phylogeny calculated with raxml-ng (*92*) using model LG+G4m without bootstraps. Plots generated with ete3 (*93*). Branch lengths are drawn to scale and indicate the number of substitutions per site. Source data, workflow, results, and plots available on Zenodo (doi:10.5281/zenodo.10152638).

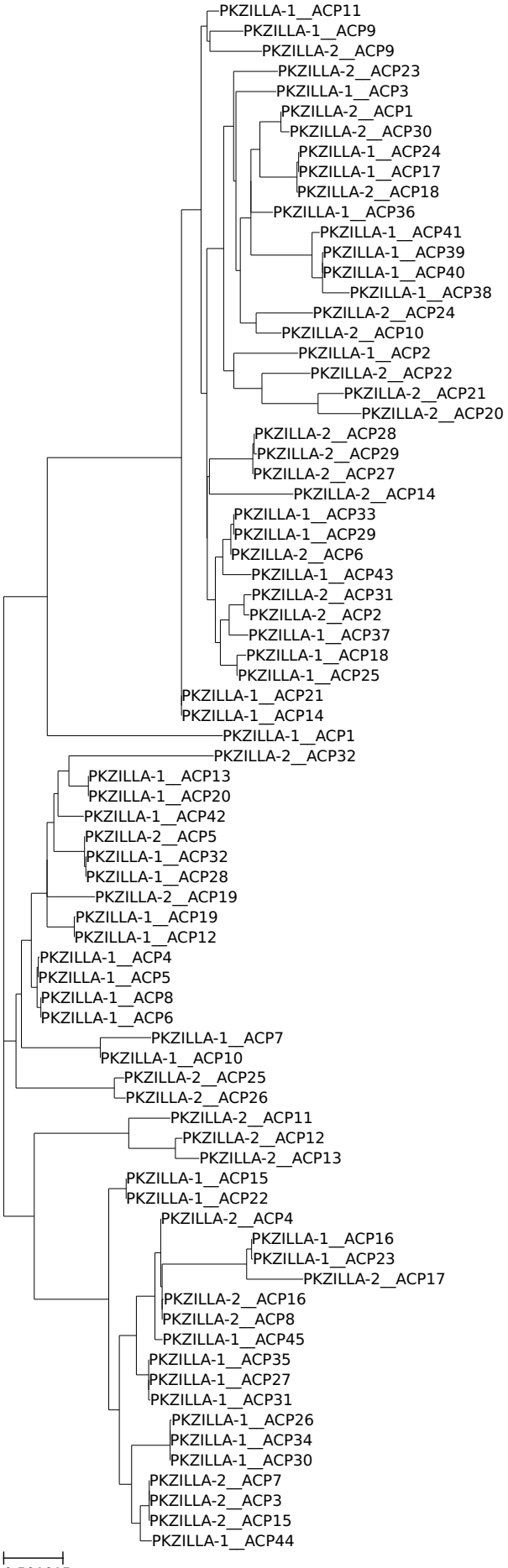
PKZILLA-1__ACP11
PKZILLA-1__ACP9
PKZILLA-2__ACP9
PKZILLA-2__ACP23
PKZILLA-1__ACP3
PKZILLA-2__ACP1
PKZILLA-2__ACP30
PKZILLA-1__ACP24
PKZILLA-1__ACP17
PKZILLA-2__ACP18
PKZILLA-1__ACP36
PKZILLA-1__ACP41
PKZILLA-1__ACP39
PKZILLA-1__ACP40
PKZILLA-1__ACP38
PKZILLA-2__ACP24
PKZILLA-2__ACP10
PKZILLA-1__ACP2
PKZILLA-2__ACP22
PKZILLA-2__ACP21
PKZILLA-2__ACP20
PKZILLA-2__ACP28
PKZILLA-2__ACP29
PKZILLA-2__ACP27
PKZILLA-2__ACP14
PKZILLA-1__ACP33
PKZILLA-1__ACP29
PKZILLA-2__ACP6
PKZILLA-1__ACP43
PKZILLA-2__ACP31
PKZILLA-2__ACP2
PKZILLA-1__ACP37
PKZILLA-1__ACP18
PKZILLA-1__ACP25
PKZILLA-1__ACP21
PKZILLA-1__ACP14
PKZILLA-1__ACP1
PKZILLA-2__ACP32
PKZILLA-1__ACP13
PKZILLA-1__ACP20
PKZILLA-1__ACP42
PKZILLA-2__ACP5
PKZILLA-1__ACP32
PKZILLA-1__ACP28
PKZILLA-2__ACP19
PKZILLA-1__ACP19
PKZILLA-1__ACP12
PKZILLA-1__ACP4
PKZILLA-1__ACP5
PKZILLA-1__ACP8
PKZILLA-1__ACP6
PKZILLA-1__ACP7
PKZILLA-1__ACP10
PKZILLA-2__ACP25
PKZILLA-2__ACP26
PKZILLA-2__ACP11
PKZILLA-2__ACP12
PKZILLA-2__ACP13
PKZILLA-1__ACP15
PKZILLA-1__ACP22
PKZILLA-2__ACP4
PKZILLA-1__ACP16
PKZILLA-1__ACP23
PKZILLA-2__ACP17
PKZILLA-2__ACP16
PKZILLA-2__ACP8
PKZILLA-1__ACP45
PKZILLA-1__ACP35
PKZILLA-1__ACP27
PKZILLA-1__ACP31
PKZILLA-1__ACP26
PKZILLA-1__ACP34
PKZILLA-1__ACP30
PKZILLA-2__ACP7
PKZILLA-2__ACP3
PKZILLA-2__ACP15
PKZILLA-1__ACP44
0.501015

Fig. S11: Phylogenetic analysis of PKZILLA acyl carrier protein (ACP) domains. Sequences were multiple sequence aligned with kalign2 (*58*) and the unrooted phylogeny calculated with raxml-ng (*92*) using model LG+G4m without bootstraps. Plots generated with ete3 (*93*). Branch lengths are drawn to scale and indicate the number of substitutions per site. Source data, workflow, results, and plots available on Zenodo (doi:10.5281/zenodo.10152638).

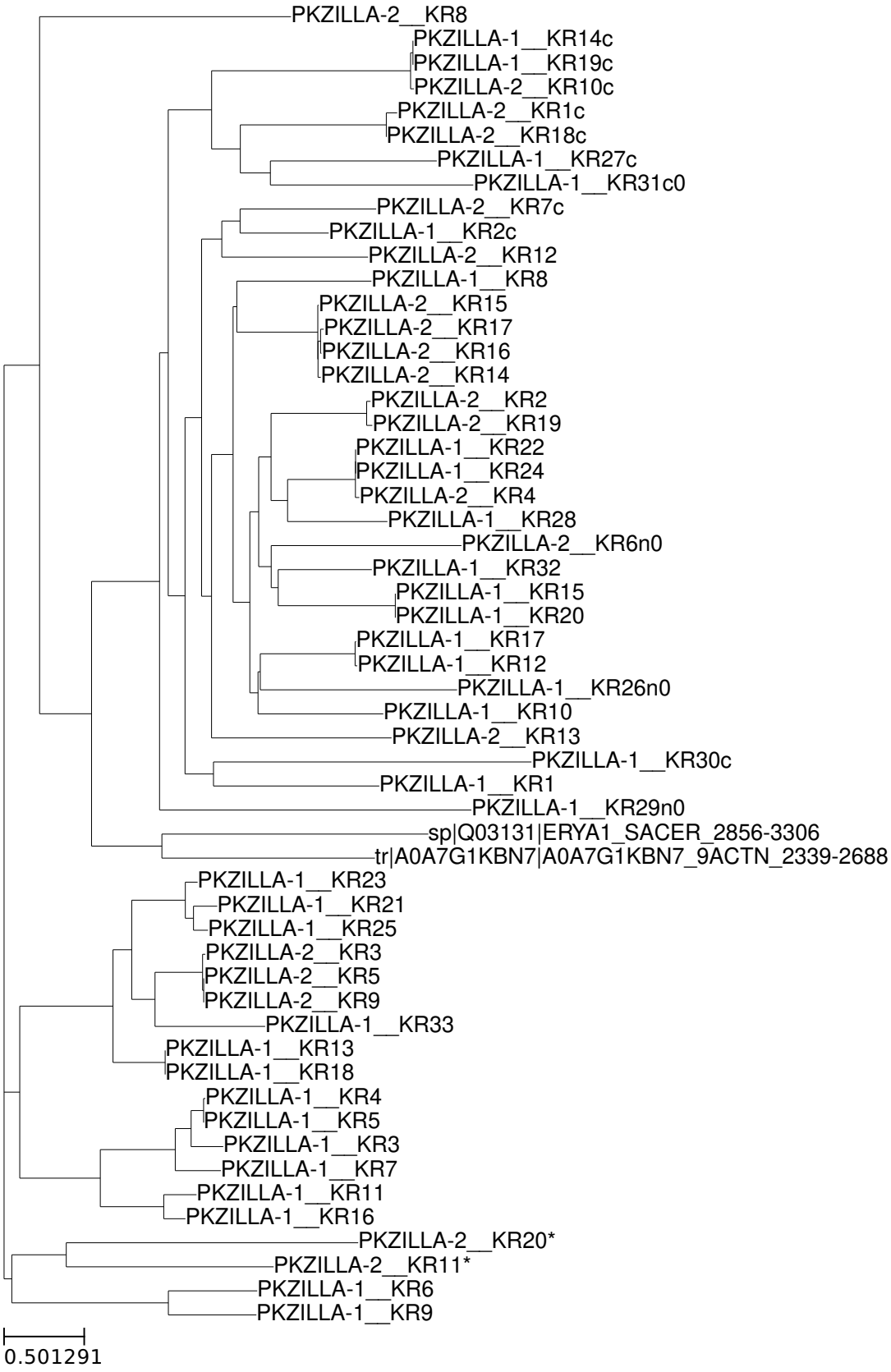
PKZILLA-2__KR8
PKZILLA-1__KR14c
PKZILLA-1__KR19c
PKZILLA-2__KR10c
PKZILLA-2__KR1c
PKZILLA-2__KR18c
PKZILLA-1__KR27c
PKZILLA-1__KR31c0
PKZILLA-2__KR7c
PKZILLA-1__KR2c
PKZILLA-2__KR12
PKZILLA-1__KR8
PKZILLA-2__KR15
PKZILLA-2__KR17
PKZILLA-2__KR16
PKZILLA-2__KR14
PKZILLA-2__KR2
PKZILLA-2__KR19
PKZILLA-1__KR22
PKZILLA-1__KR24
PKZILLA-2__KR4
PKZILLA-1__KR28
PKZILLA-2__KR6n0
PKZILLA-1__KR32
PKZILLA-1__KR15
PKZILLA-1__KR20
PKZILLA-1__KR17
PKZILLA-1__KR12
PKZILLA-1__KR26n0
PKZILLA-1__KR10
PKZILLA-2__KR13
PKZILLA-1__KR30c
PKZILLA-1__KR1
PKZILLA-1__KR29n0
sp|Q03131|ERYA1_SACER_2856-3306
tr|A0A7G1KBN7|A0A7G1KBN7_9ACTN_2339-2688
PKZILLA-1__KR23
PKZILLA-1__KR21
PKZILLA-1__KR25
PKZILLA-2__KR3
PKZILLA-2__KR5
PKZILLA-2__KR9
PKZILLA-1__KR33
PKZILLA-1__KR13
PKZILLA-1__KR18
PKZILLA-1__KR4
PKZILLA-1__KR5
PKZILLA-1__KR3
PKZILLA-1__KR7
PKZILLA-1__KR11
PKZILLA-1__KR16
PKZILLA-2__KR20*
PKZILLA-2__KR11*
PKZILLA-1__KR6
PKZILLA-1__KR9
0.501291

Fig. S12: Phylogenetic analysis of PKZILLA ketoreductase (KR) domains and select representative KR domains from Uniprot. Sequences were multiple sequence aligned with kalign2 (*58*) and the unrooted phylogeny calculated with raxml-ng (*92*) using model LG+G4m without bootstraps. Plots generated with ete3 (*93*). Branch lengths are drawn to scale and indicate the number of substitutions per site. KR domains are annotated as KR/KRf, KRn, KRc depending on their respective classification as a full length non-split KR, a split KR N-terminal subdomain, or a split KR C-terminal subdomain, and "0" is appended to the domain name if the active site residues suggest the domain is catalytically inactive. KR* domains would be expected to be active based on the biosynthetic model, but are bioinformatically predicted to be inactive (table S9), and thus may be false positive predictions of inactivity caused by divergent catalytic properties. For further details on catalytic activity determination via active site analysis, see "Analysis of active site residues within PKZILLA PKS domains" in the Materials and Methods and the associated Zenodo item (doi:10.5281/zenodo.10028517). Source data, workflow, results, and plots available on Zenodo (doi:10.5281/zenodo.10152638).

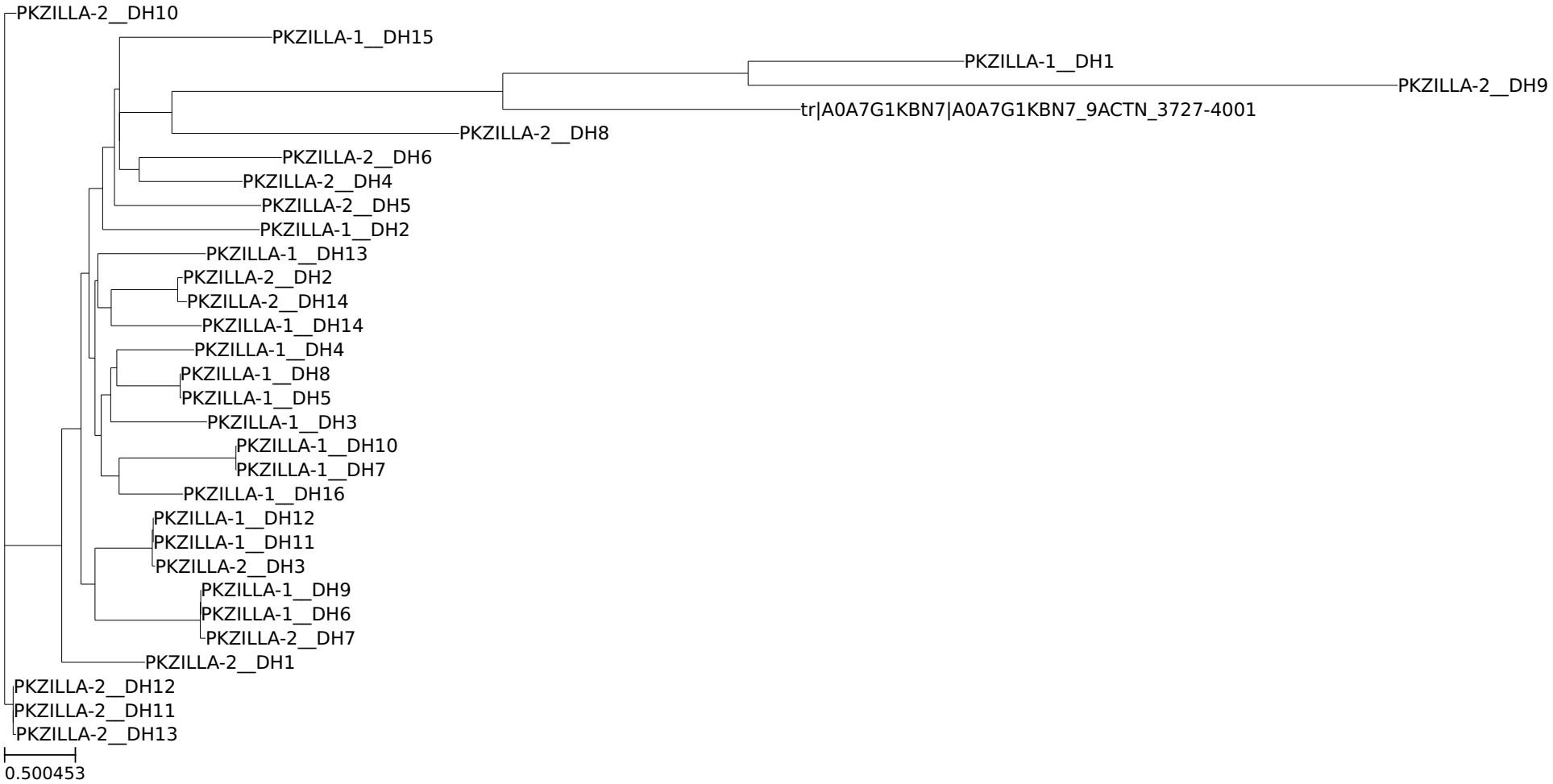

Fig. S13: Phylogenetic analysis of PKZILLA dehydratase (DH) domains and select representative DH domains from Uniprot. Sequences were multiple sequence aligned with kalign2 (*58*) and the unrooted phylogeny calculated with raxml-ng (*92*) using model LG+G4m without bootstraps. Plots generated with ete3 (*93*). Branch lengths are drawn to scale and indicate the number of substitutions per site. Source data, workflow, results, and plots available on Zenodo (doi:10.5281/zenodo.10152638)

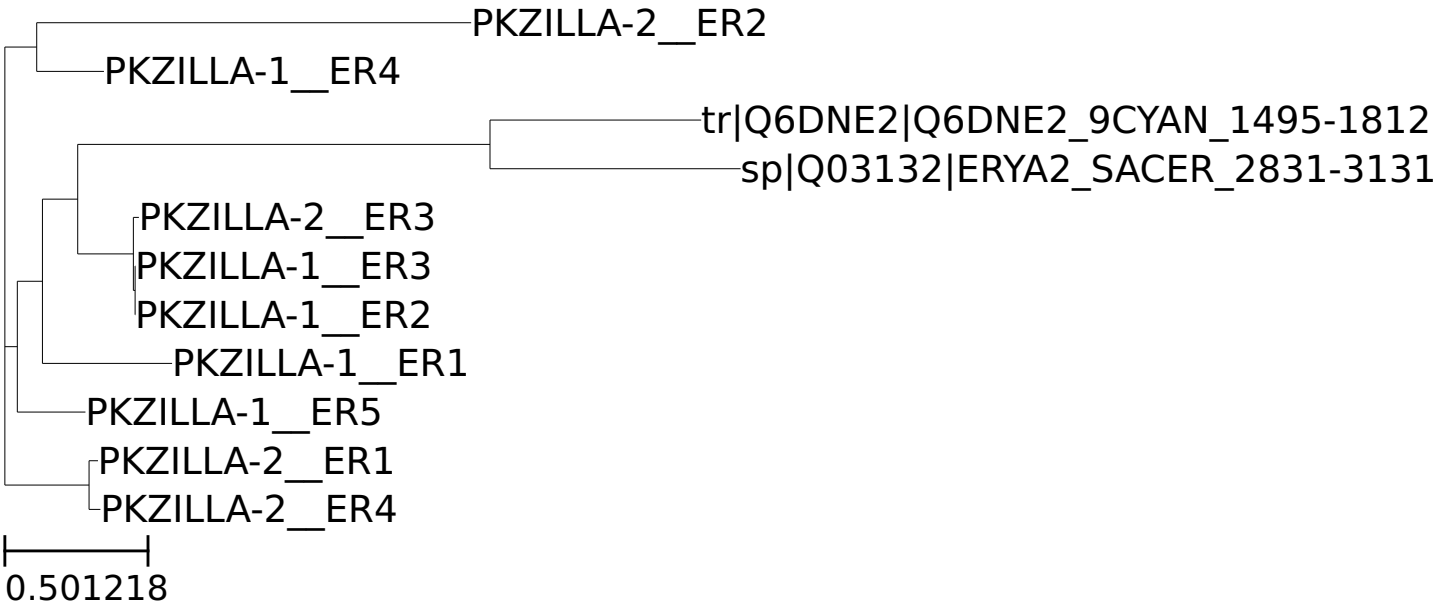

Fig. S14: Phylogenetic analysis of PKZILLA enoyl reductase (ER) domains and select representative ER domains from Uniprot. Sequences were multiple sequence aligned with kalign2 (*58*) and the unrooted phylogeny calculated with raxml-ng (*92*) using model LG+G4m without bootstraps. Plots generated with ete3 (*93*). Branch lengths are drawn to scale and indicate the number of substitutions per site. Source data, workflow, results, and plots available on Zenodo (doi:10.5281/zenodo.10152638).

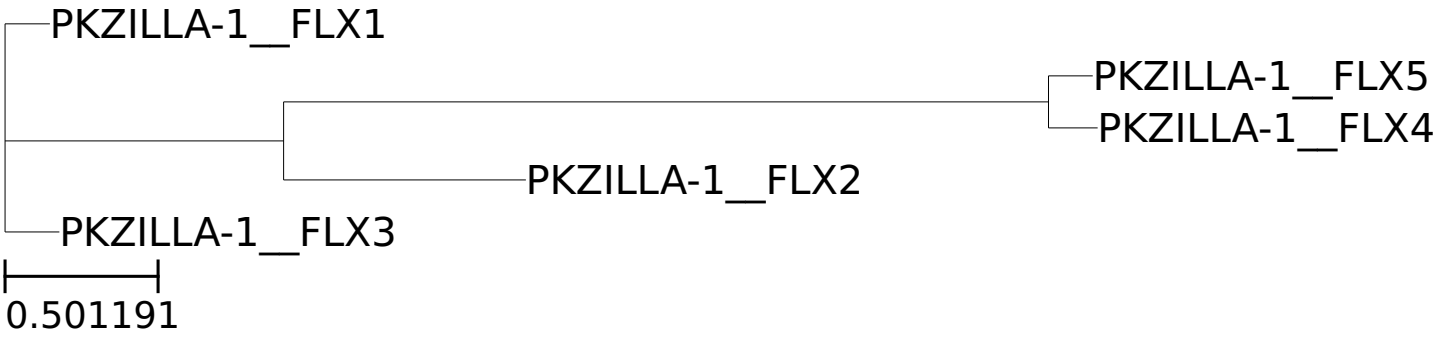

Fig. S15: Phylogenetic analysis of PKZILLA flavin oxygenase (FLX) domains. Sequences were multiple sequence aligned with kalign2 (*58*) and the unrooted phylogeny calculated with raxml-ng (*92*) using model LG+G4m without bootstraps. Plots generated with ete3 (*93*). Branch lengths are drawn to scale and indicate the number of substitutions per site. Source data, workflow, results, and plots available on Zenodo (doi:10.5281/zenodo.10152638).

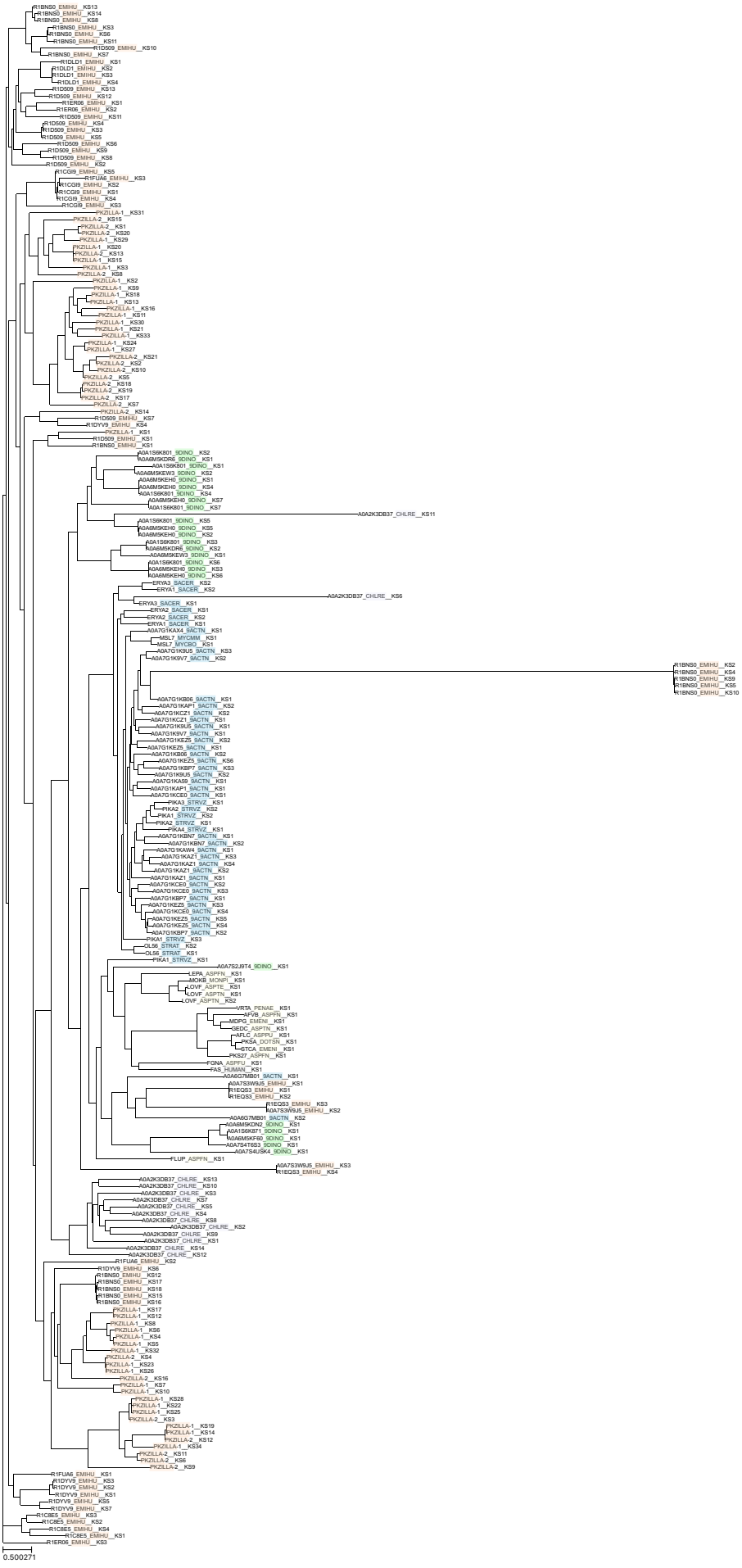
R1BNS0_EMIHU__KS13
R1BNS0_EMIHU__KS14
R1BNS0_EMIHU__KS8
R1BNS0_EMIHU__KS3
R1BNS0_EMIHU__KS6
R1BNS0_EMIHU__KS11
R1D509_EMIHU__KS10
R1BNS0_EMIHU__KS7
R1DLD1_EMIHU__KS1
R1DLD1_EMIHU__KS2
R1DLD1_EMIHU__KS3
R1DLD1_EMIHU__KS4
R1D509_EMIHU__KS13
R1D509_EMIHU__KS12
R1ER06_EMIHU__KS1
R1ER06_EMIHU__KS2
R1D509_EMIHU__KS11
R1D509_EMIHU__KS4
R1D509_EMIHU__KS3
R1D509_EMIHU__KS5
R1D509_EMIHU__KS6
R1D509_EMIHU__KS9
R1D509_EMIHU__KS8
R1D509_EMIHU__KS2
R1CGI9_EMIHU__KS5
R1FUA6_EMIHU__KS3
R1CGI9_EMIHU__KS2
R1CGI9_EMIHU__KS1
R1CGI9_EMIHU__KS4
R1CGI9_EMIHU__KS3
PKZILLA-1__KS31
PKZILLA-2__KS15
PKZILLA-2__KS1
PKZILLA-2__KS20
PKZILLA-1__KS29
PKZILLA-1__KS20
PKZILLA-2__KS13
PKZILLA-1__KS15
PKZILLA-1__KS3
PKZILLA-2__KS8
PKZILLA-1__KS2
PKZILLA-1__KS9
PKZILLA-1__KS18
PKZILLA-1__KS13
PKZILLA-1__KS16
PKZILLA-1__KS11
PKZILLA-1__KS30
PKZILLA-1__KS21
PKZILLA-1__KS33
PKZILLA-1__KS24
PKZILLA-1__KS27
PKZILLA-2__KS21
PKZILLA-2__KS2
PKZILLA-2__KS10
PKZILLA-2__KS5
PKZILLA-2__KS18
PKZILLA-2__KS19
PKZILLA-2__KS17
PKZILLA-2__KS7
PKZILLA-2__KS14
R1D509_EMIHU__KS7
R1DYV9_EMIHU__KS4
PKZILLA-1__KS1
R1D509_EMIHU__KS1
R1BNS0_EMIHU__KS1
A0A1S9K801_9DINO__KS2
A0A6M5KDR6_9DINO__KS1
A0A1S9K801_9DINO__KS1
A0A6M5KEW3_9DINO__KS2
A0A6M5KEH0_9DINO__KS1
A0A6M5KEH0_9DINO__KS4
A0A1S9K801_9DINO__KS4
A0A6M5KEH0_9DINO__KS7
A0A1S9K801_9DINO__KS7
A0A2K3DB37_CHLRE__KS11
A0A1S9K801_9DINO__KS5
A0A6M5KEH0_9DINO__KS5
A0A6M5KEH0_9DINO__KS2
A0A1S9K801_9DINO__KS3
A0A6M5KDR6_9DINO__KS2
A0A6M5KEW3_9DINO__KS1
A0A1S9K801_9DINO__KS6
A0A6M5KEH0_9DINO__KS3
A0A6M5KEH0_9DINO__KS6
A0A2K3DB37_CHLRE__KS6
ERYA3_SACER__KS2
ERYA1_SACER__KS2
ERYA3_SACER__KS1
ERYA2_SACER__KS1
ERYA2_SACER__KS2
ERYA1_SACER__KS1
A0A7G1KAX4_9ACTN__KS1
MSL7_MYCMM__KS1
MSL7_MYCBO__KS1
A0A7G1K9U5_9ACTN__KS3
A0A7G1K9V7_9ACTN__KS2
R1BNS0_EMIHU__KS2
R1BNS0_EMIHU__KS4
R1BNS0_EMIHU__KS9
R1BNS0_EMIHU__KS5
R1BNS0_EMIHU__KS10
A0A7G1KB06_9ACTN__KS1
A0A7G1KAP1_9ACTN__KS2
A0A7G1KCZ1_9ACTN__KS2
A0A7G1KCZ1_9ACTN__KS1
A0A7G1K9U5_9ACTN__KS1
A0A7G1K9V7_9ACTN__KS1
A0A7G1KEZ5_9ACTN__KS2
A0A7G1KEZ5_9ACTN__KS1
A0A7G1KB06_9ACTN__KS2
A0A7G1KEZ5_9ACTN__KS6
A0A7G1KBP7_9ACTN__KS3
A0A7G1K9U5_9ACTN__KS2
A0A7G1KA59_9ACTN__KS1
A0A7G1KAP1_9ACTN__KS1
A0A7G1KCE0_9ACTN__KS1
PIKA3_STRVZ__KS1
PIKA2_STRVZ__KS2
PIKA1_STRVZ__KS2
PIKA2_STRVZ__KS1
PIKA4_STRVZ__KS1
A0A7G1KBN7_9ACTN__KS1
A0A7G1KBN7_9ACTN__KS2
A0A7G1KAW4_9ACTN__KS1
A0A7G1KAZ1_9ACTN__KS3
A0A7G1KAZ1_9ACTN__KS4
A0A7G1KAZ1_9ACTN__KS2
A0A7G1KAZ1_9ACTN__KS1
A0A7G1KCE0_9ACTN__KS2
A0A7G1KCE0_9ACTN__KS3
A0A7G1KBP7_9ACTN__KS1
A0A7G1KEZ5_9ACTN__KS3
A0A7G1KCE0_9ACTN__KS4
A0A7G1KEZ5_9ACTN__KS5
A0A7G1KEZ5_9ACTN__KS4
A0A7G1KBP7_9ACTN__KS2
PIKA1_STRVZ__KS3
OLS6_STRAT__KS2
OLS6_STRAT__KS1
PIKA1_STRVZ__KS1
A0A7S2J9T4_9DINO__KS1
LEPA_ASPFN__KS1
MOKB_MONPI__KS1
LOVF_ASPTE__KS1
LOVF_ASPTN__KS1
LOVF_ASPTN__KS2
ARTA_PENAE__KS1
AFVB_ASPFN__KS1
MDPG_EMENI__KS1
GEDC_ASPTN__KS1
AFLC_ASPPU__KS1
PKSA_DOTSN__KS1
STCA_EMENI__KS1
PKS27_ASPFN__KS1
FGNA_ASPFU__KS1
FAS_HUMAN__KS1
A0A6G7MB01_9ACTN__KS1
A0A7S3W9J5_EMIHU__KS1
R1EQS3_EMIHU__KS1
R1EQS3_EMIHU__KS2
R1EQS3_EMIHU__KS3
A0A7S3W9J5_EMIHU__KS2
A0A6G7MB01_9ACTN__KS2
A0A6M5KDN2_9DINO__KS1
A0A1S9K8P1_9DINO__KS1
A0A6M5KF60_9DINO__KS1
A0A7S4T6E3_9DINO__KS1
A0A7S4USK4_9DINO__KS1
FLUP_ASPFN__KS1
A0A7S3W9J5_EMIHU__KS3
R1EQS3_EMIHU__KS4
A0A2K3DB37_CHLRE__KS13
A0A2K3DB37_CHLRE__KS10
A0A2K3DB37_CHLRE__KS3
A0A2K3DB37_CHLRE__KS7
A0A2K3DB37_CHLRE__KS5
A0A2K3DB37_CHLRE__KS4
A0A2K3DB37_CHLRE__KS8
A0A2K3DB37_CHLRE__KS2
A0A2K3DB37_CHLRE__KS9
A0A2K3DB37_CHLRE__KS1
A0A2K3DB37_CHLRE__KS14
A0A2K3DB37_CHLRE__KS12
R1FUA6_EMIHU__KS2
R1DYV9_EMIHU__KS6
R1BNS0_EMIHU__KS12
R1BNS0_EMIHU__KS17
R1BNS0_EMIHU__KS18
R1BNS0_EMIHU__KS15
R1BNS0_EMIHU__KS16
PKZILLA-1__KS17
PKZILLA-1__KS12
PKZILLA-1__KS8
PKZILLA-1__KS6
PKZILLA-1__KS4
PKZILLA-1__KS5
PKZILLA-1__KS32
PKZILLA-2__KS4
PKZILLA-1__KS23
PKZILLA-1__KS26
PKZILLA-2__KS16
PKZILLA-1__KS7
PKZILLA-1__KS10
PKZILLA-1__KS28
PKZILLA-1__KS22
PKZILLA-1__KS25
PKZILLA-2__KS3
PKZILLA-1__KS19
PKZILLA-1__KS14
PKZILLA-2__KS12
PKZILLA-1__KS34
PKZILLA-2__KS11
PKZILLA-2__KS6
PKZILLA-2__KS9
R1FUA6_EMIHU__KS1
R1DYV9_EMIHU__KS3
R1DYV9_EMIHU__KS2
R1DYV9_EMIHU__KS1
R1DYV9_EMIHU__KS5
R1DYV9_EMIHU__KS7
R1C8E5_EMIHU__KS3
R1C8E5_EMIHU__KS2
R1C8E5_EMIHU__KS4
R1C8E5_EMIHU__KS1
R1ER06_EMIHU__KS3
0.500271

Fig. S16: Phylogenetic analysis of PKZILLA ketosynthase (KS) domains with an expansive set of comparable PKS domain sequences from Uniprot representing bacteria, fungi, green algae, dinoflagellates, haptophytes, and human fatty acid synthase (FAS). See table S10 for key for taxonomic interpretation. Remainder of sequence ID is the uniprot ID and N-terminal to C-terminal ascending domain number. Source data, workflow, and resulting plots available on Zenodo (doi:10.5281/zenodo.10247217).

Fig. S17: Phylogenetic analysis of PKZILLA ketoreductase (KR) domains with an expansive set of comparable PKS domain sequences from Uniprot representing bacteria, fungi, green algae, dinoflagellates, haptophytes, and human fatty acid synthase (FAS). See table S10 for key for taxonomic interpretation. Remainder of sequence ID is the uniprot ID and N-terminal to C-terminal ascending domain number. Source data, workflow, and resulting plots available on Zenodo (doi:10.5281/zenodo.10247217).

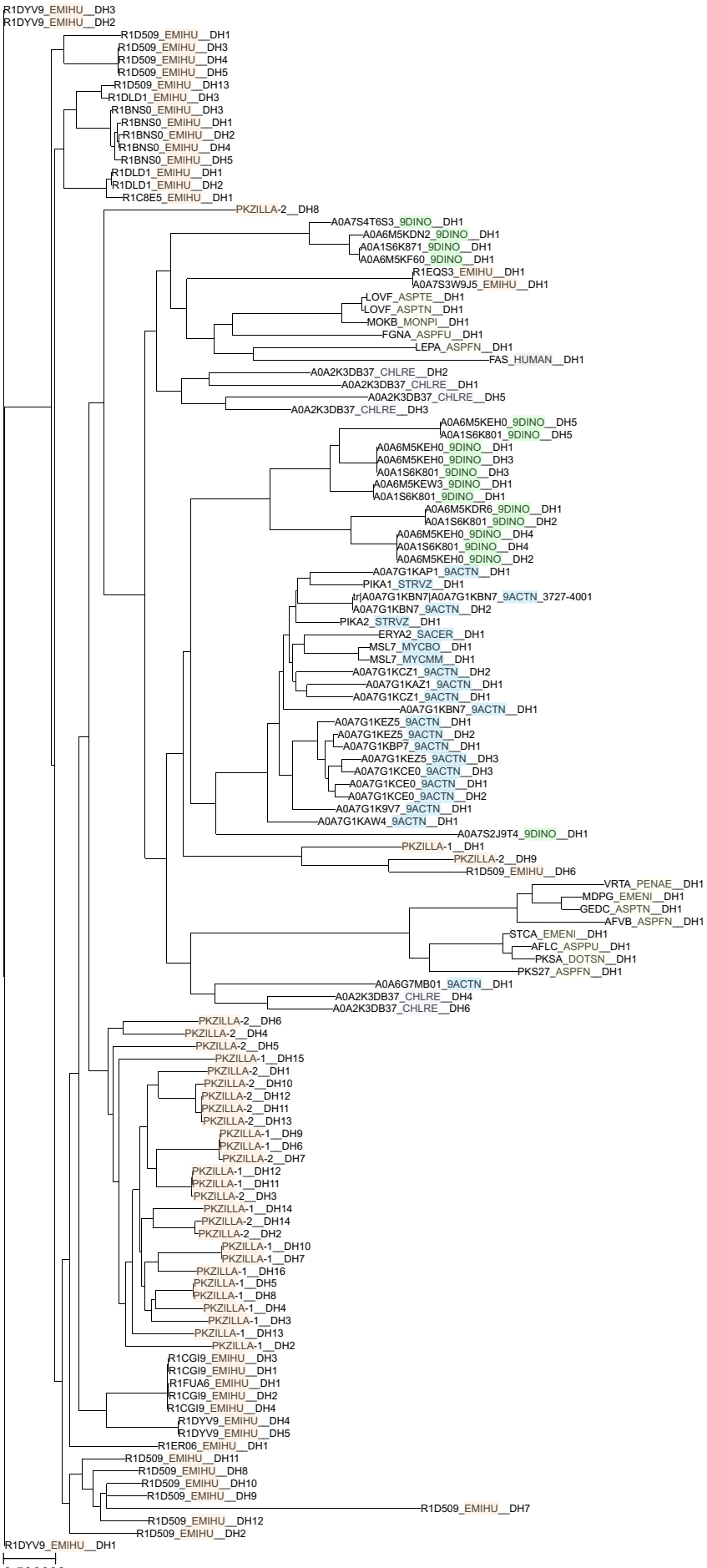
R1DYV9_EMIHU__DH3
R1DYV9_EMIHU__DH2
R1D509_EMIHU__DH1
R1D509_EMIHU__DH3
R1D509_EMIHU__DH4
R1D509_EMIHU__DH5
R1D509_EMIHU__DH13
R1DLD1_EMIHU__DH3
R1BNS0_EMIHU__DH3
R1BNS0_EMIHU__DH1
R1BNS0_EMIHU__DH2
R1BNS0_EMIHU__DH4
R1BNS0_EMIHU__DH5
R1DLD1_EMIHU__DH1
R1DLD1_EMIHU__DH2
R1C8E5_EMIHU__DH1
PKZILLA-2__DH8
A0A7S4T6S3_9DINO__DH1
A0A6M5KDN2_9DINO__DH1
A0A1S6K871_9DINO__DH1
A0A6M5KF60_9DINO__DH1
R1EQS3_EMIHU__DH1
A0A7S3W9J5_EMIHU__DH1
LOVF_ASPTE__DH1
LOVF_ASPTN__DH1
MOKB_MONPI__DH1
FGNA_ASPFU__DH1
LEPA_ASPFN__DH1
FAS_HUMAN__DH1
A0A2K3DB37_CHLRE__DH2
A0A2K3DB37_CHLRE__DH1
A0A2K3DB37_CHLRE__DH5
A0A2K3DB37_CHLRE__DH3
A0A6M5KEH0_9DINO__DH5
A0A1S6K801_9DINO__DH5
A0A6M5KEH0_9DINO__DH1
A0A6M5KEH0_9DINO__DH3
A0A1S6K801_9DINO__DH3
A0A6M5KEW3_9DINO__DH1
A0A1S6K801_9DINO__DH1
A0A6M5KDR6_9DINO__DH1
A0A1S6K801_9DINO__DH2
A0A6M5KEH0_9DINO__DH4
A0A1S6K801_9DINO__DH4
A0A6M5KEH0_9DINO__DH2
A0A7G1KAP1_9ACTN__DH1
PIKA1_STRVZ__DH1
tr|A0A7G1KBN7|A0A7G1KBN7_9ACTN_3727-4001
A0A7G1KBN7_9ACTN__DH2
PIKA2_STRVZ__DH1
ERYA2_SACER__DH1
MSL7_MYCBO__DH1
MSL7_MYCMM__DH1
A0A7G1KCZ1_9ACTN__DH2
A0A7G1KAZ1_9ACTN__DH1
A0A7G1KCZ1_9ACTN__DH1
A0A7G1KBN7_9ACTN__DH1
A0A7G1KEZ5_9ACTN__DH1
A0A7G1KEZ5_9ACTN__DH2
A0A7G1KBP7_9ACTN__DH1
A0A7G1KEZ5_9ACTN__DH3
A0A7G1KCE0_9ACTN__DH3
A0A7G1KCE0_9ACTN__DH1
A0A7G1KCE0_9ACTN__DH2
A0A7G1K9V7_9ACTN__DH1
A0A7G1KAW4_9ACTN__DH1
A0A7S2J9T4_9DINO__DH1
PKZILLA-1__DH1
PKZILLA-2__DH9
R1D509_EMIHU__DH6
VRTA_PENAE__DH1
MDPG_EMENI__DH1
GEDC_ASPTN__DH1
AFVB_ASPFN__DH1
STCA_EMENI__DH1
AFLC_ASPPU__DH1
PKSA_DOTSN__DH1
PKS27_ASPFN__DH1
A0A6G7MB01_9ACTN__DH1
A0A2K3DB37_CHLRE__DH4
A0A2K3DB37_CHLRE__DH6
PKZILLA-2__DH6
PKZILLA-2__DH4
PKZILLA-2__DH5
PKZILLA-1__DH15
PKZILLA-2__DH1
PKZILLA-2__DH10
PKZILLA-2__DH12
PKZILLA-2__DH11
PKZILLA-2__DH13
PKZILLA-1__DH9
PKZILLA-1__DH6
PKZILLA-2__DH7
PKZILLA-1__DH12
PKZILLA-1__DH11
PKZILLA-2__DH3
PKZILLA-1__DH14
PKZILLA-2__DH14
PKZILLA-2__DH2
PKZILLA-1__DH10
PKZILLA-1__DH7
PKZILLA-1__DH16
PKZILLA-1__DH5
PKZILLA-1__DH8
PKZILLA-1__DH4
PKZILLA-1__DH3
PKZILLA-1__DH13
PKZILLA-1__DH2
R1CGI9_EMIHU__DH3
R1CGI9_EMIHU__DH1
R1FUA6_EMIHU__DH1
R1CGI9_EMIHU__DH2
R1CGI9_EMIHU__DH4
R1DYV9_EMIHU__DH4
R1DYV9_EMIHU__DH5
R1ER06_EMIHU__DH1
R1D509_EMIHU__DH11
R1D509_EMIHU__DH8
R1D509_EMIHU__DH10
R1D509_EMIHU__DH9
R1D509_EMIHU__DH7
R1D509_EMIHU__DH12
R1D509_EMIHU__DH2
R1DYV9_EMIHU__DH1
0.500022

Fig. S18: Phylogenetic analysis of PKZILLA dehydratase (DH) domains with an expansive set of comparable PKS domain sequences from Uniprot representing bacteria, fungi, green algae, dinoflagellates, haptophytes, and human fatty acid synthase (FAS). See table S10 for key for taxonomic interpretation. Remainder of sequence ID is the uniprot ID and N-terminal to C-terminal ascending domain number. Source data, workflow, and resulting plots available on Zenodo (doi:10.5281/zenodo.10247217).

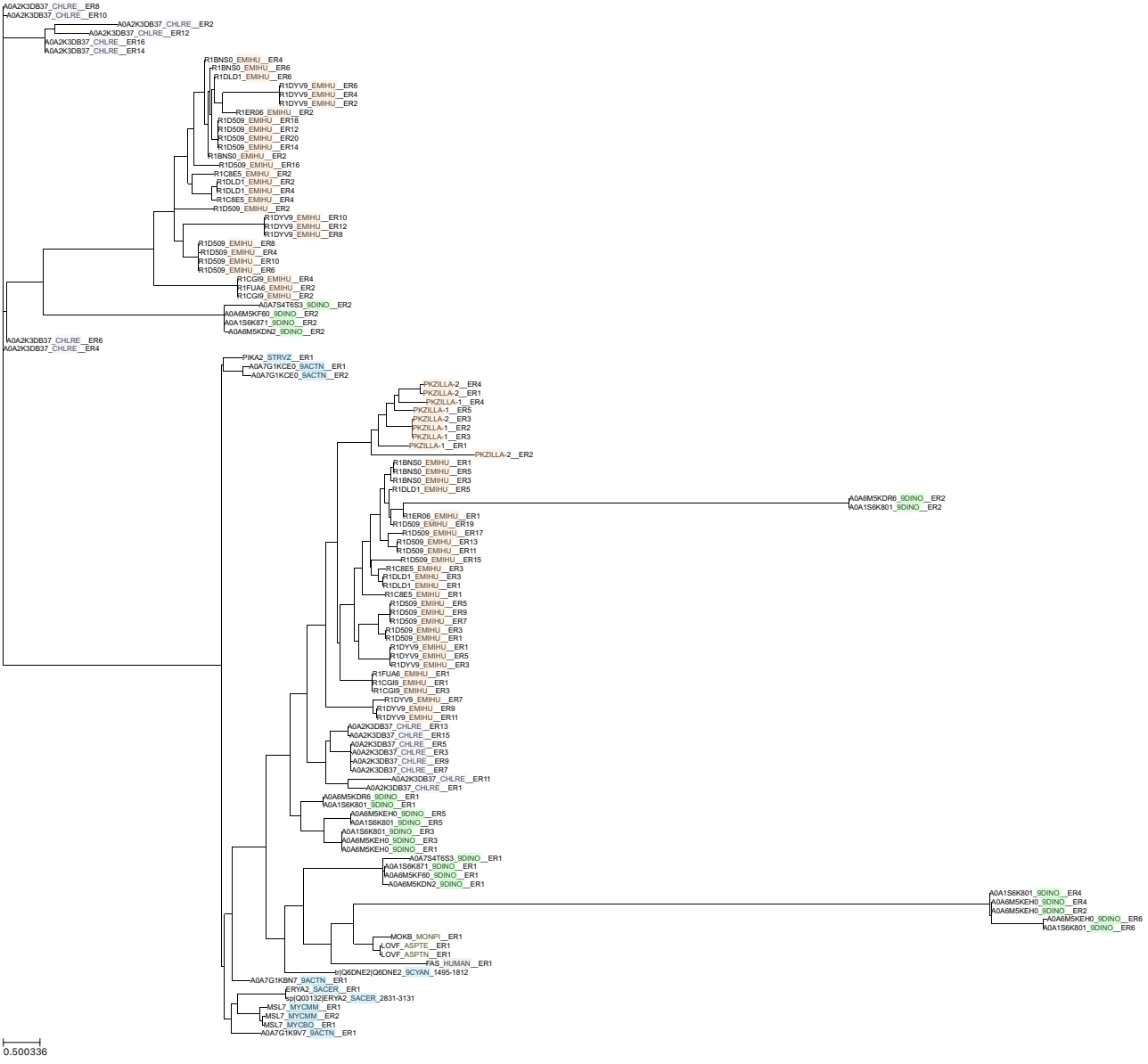

Fig. S19: Phylogenetic analysis of PKZILLA enoyl reductase (ER) domains with an expansive set of comparable PKS domain sequences sequences from Uniprot representing bacteria, fungi, green algae, dinoflagellates, haptophytes, and human fatty acid synthase (FAS). See table S10 for key for taxonomic interpretation. Remainder of sequence ID is the uniprot ID and N-terminal to C-terminal ascending domain number. Source data, workflow, and resulting plots available on Zenodo (doi:10.5281/zenodo.10247217).

PKZILLA-1

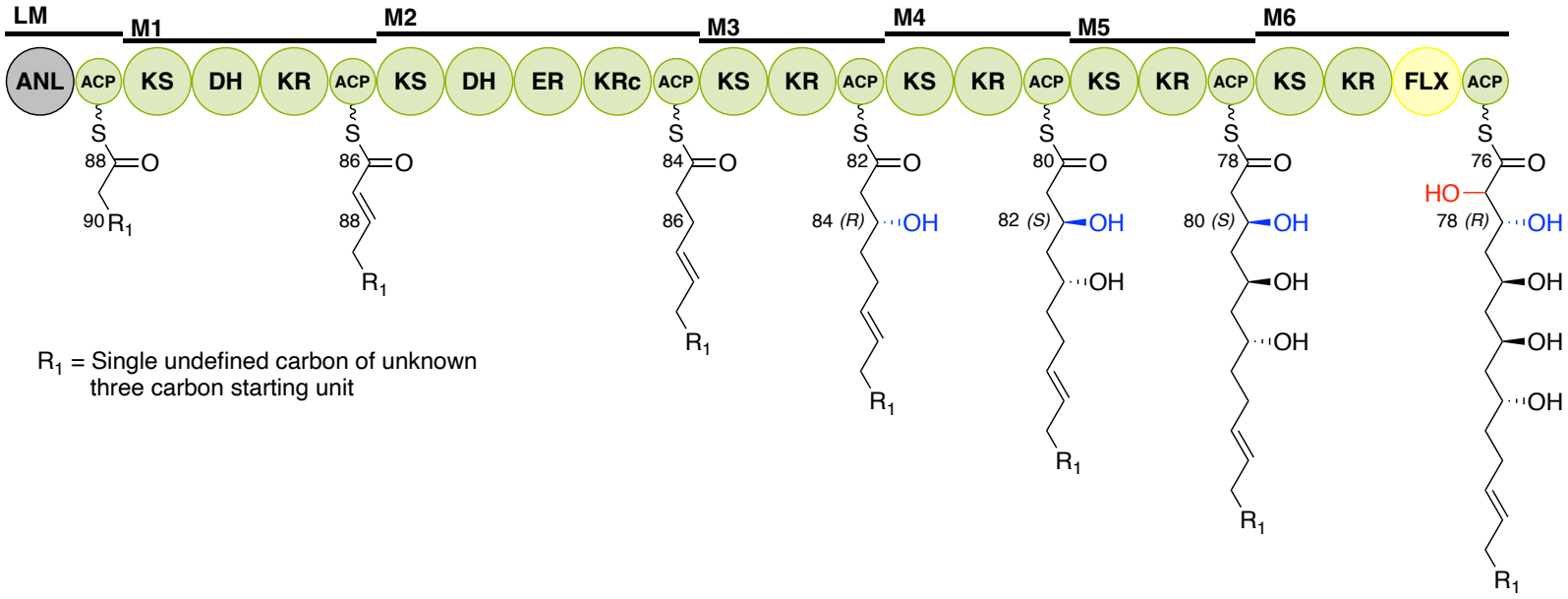

R_1 = Single undefined carbon of unknown three carbon starting unit

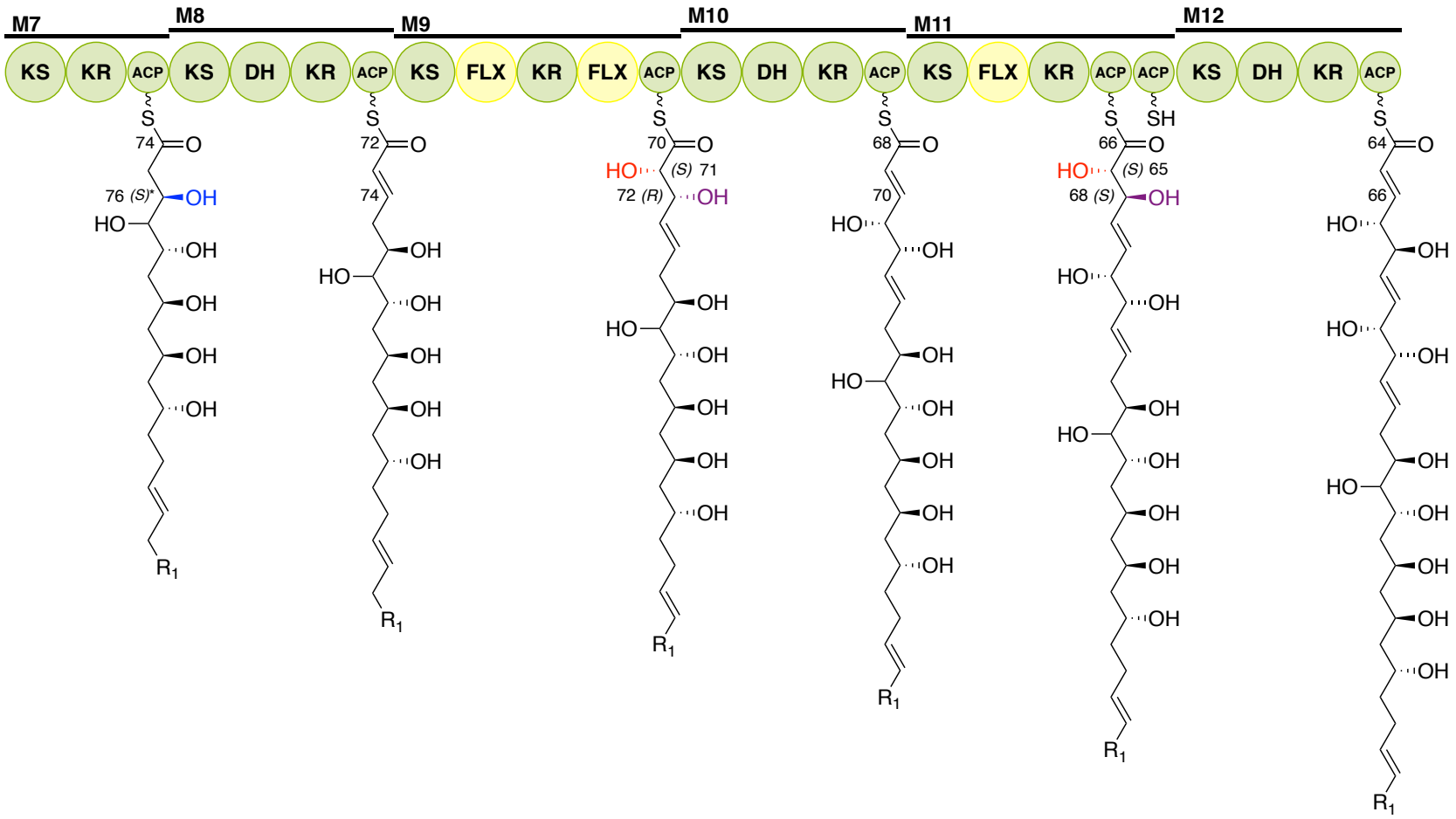
M7
M8
M9
M10
M11
M12
KS
KR
ACP
KS
DH
KR
ACP
KS
FLX
KR
FLX
ACP
KS
DH
KR
ACP
KS
FLX
KR
ACP
ACP
KS
DH
KR
ACP
S
SH
74
72
70
68
66
64
O
76 (S)*
74
72 (R)
70
68
66 (S)
(S) 71
(S) 65
HO
OH
R1

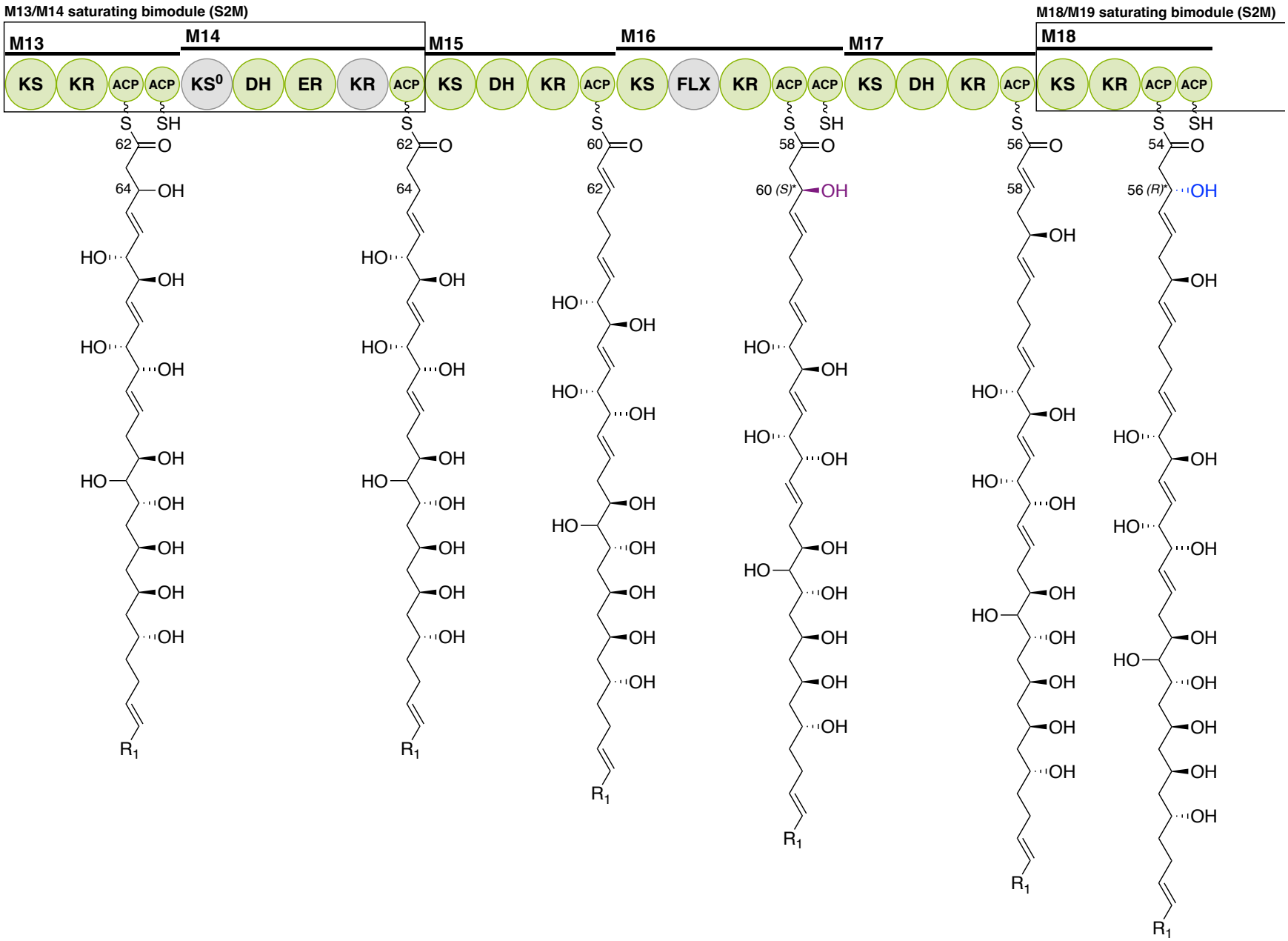
M13/M14 saturating bimodule (S2M)
M18/M19 saturating bimodule (S2M)
M13
M14
M15
M16
M17
M18
KS
KR
ACP
KS0
DH
ER
FLX
S
SH
O
OH
HO
R1
62
64
60
58
56
54
60 (S)*
56 (R)*

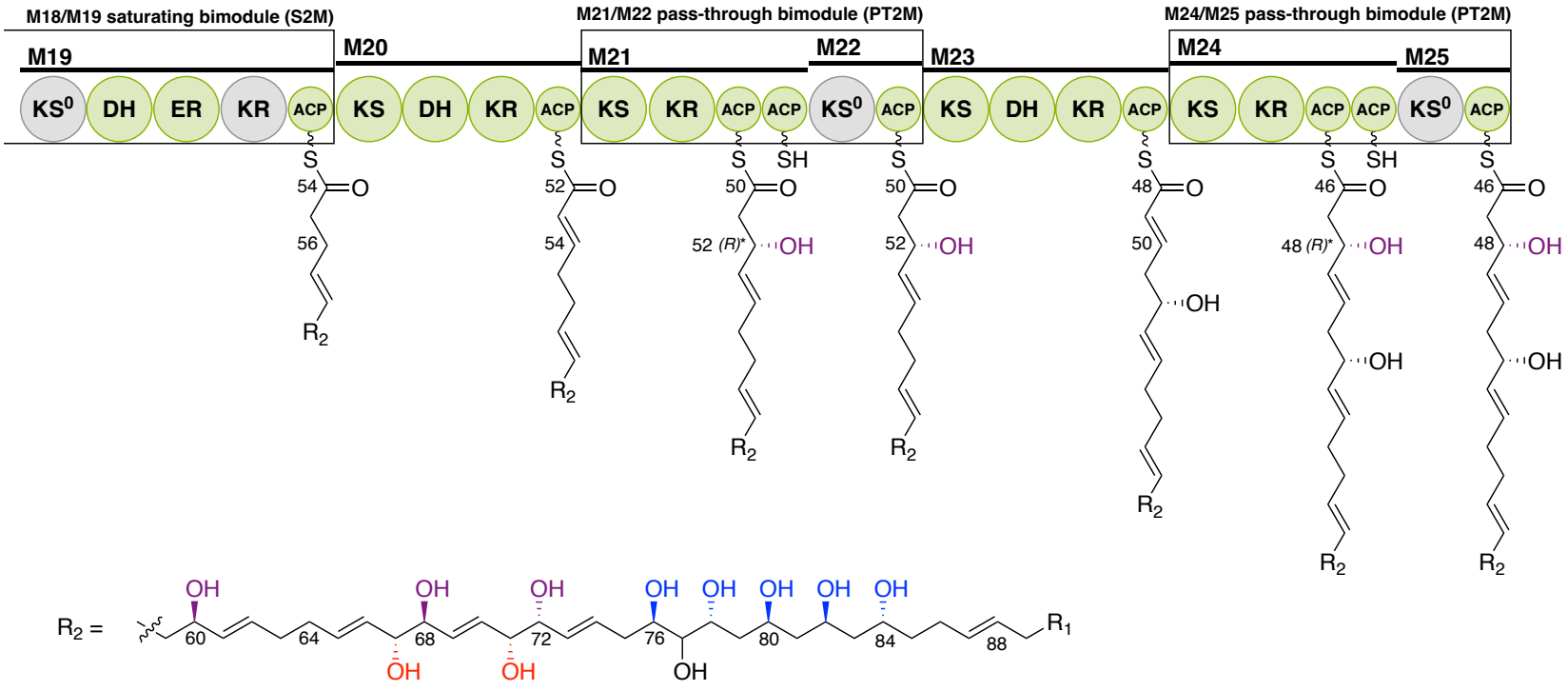
M18/M19 saturating bimodule (S2M)
M21/M22 pass-through bimodule (PT2M)
M24/M25 pass-through bimodule (PT2M)
M19
M20
M21
M22
M23
M24
M25
KS0
DH
ER
KR
ACP
KS
R2 =
R1
OH

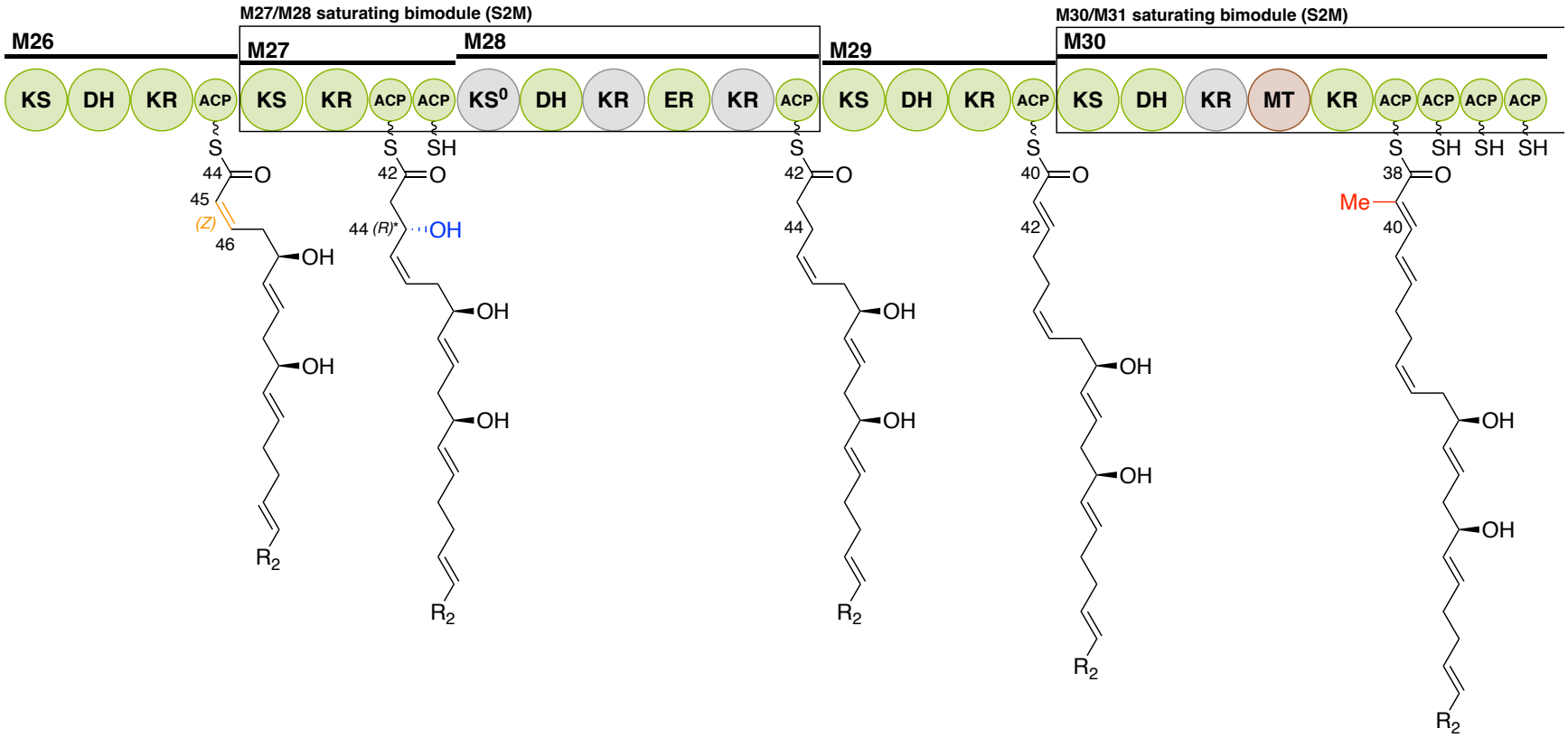
M27/M28 saturating bimodule (S2M)
M30/M31 saturating bimodule (S2M)
M26
M27
M28
M29
M30
KS DH KR ACP KS KR ACP ACP KS0 DH KR ER KR ACP KS DH KR ACP KS DH KR MT KR ACP ACP ACP ACP
S 44 O 45 (Z) 46 OH OH R2
S 42 O 44 (R)* OH OH OH R2
S 42 O 44 OH OH R2
S 40 O 42 OH OH R2
S 38 O Me 40 OH OH R2
SH SH SH

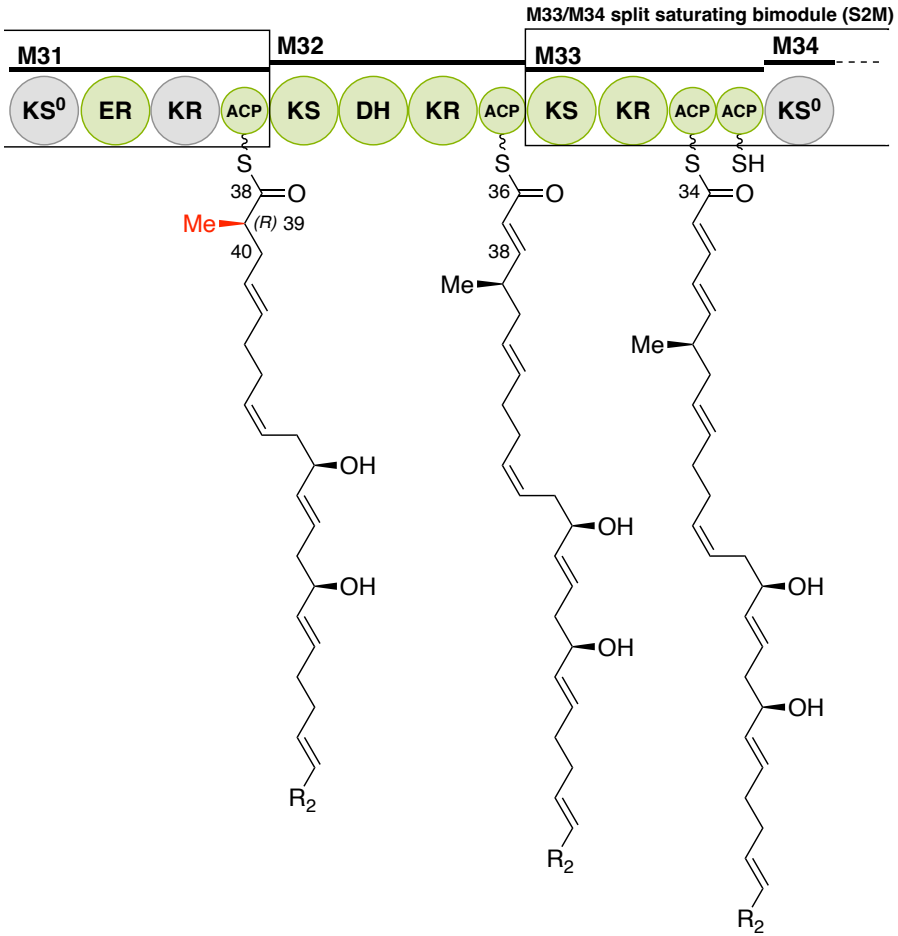

Continues below with PKZILLA-2

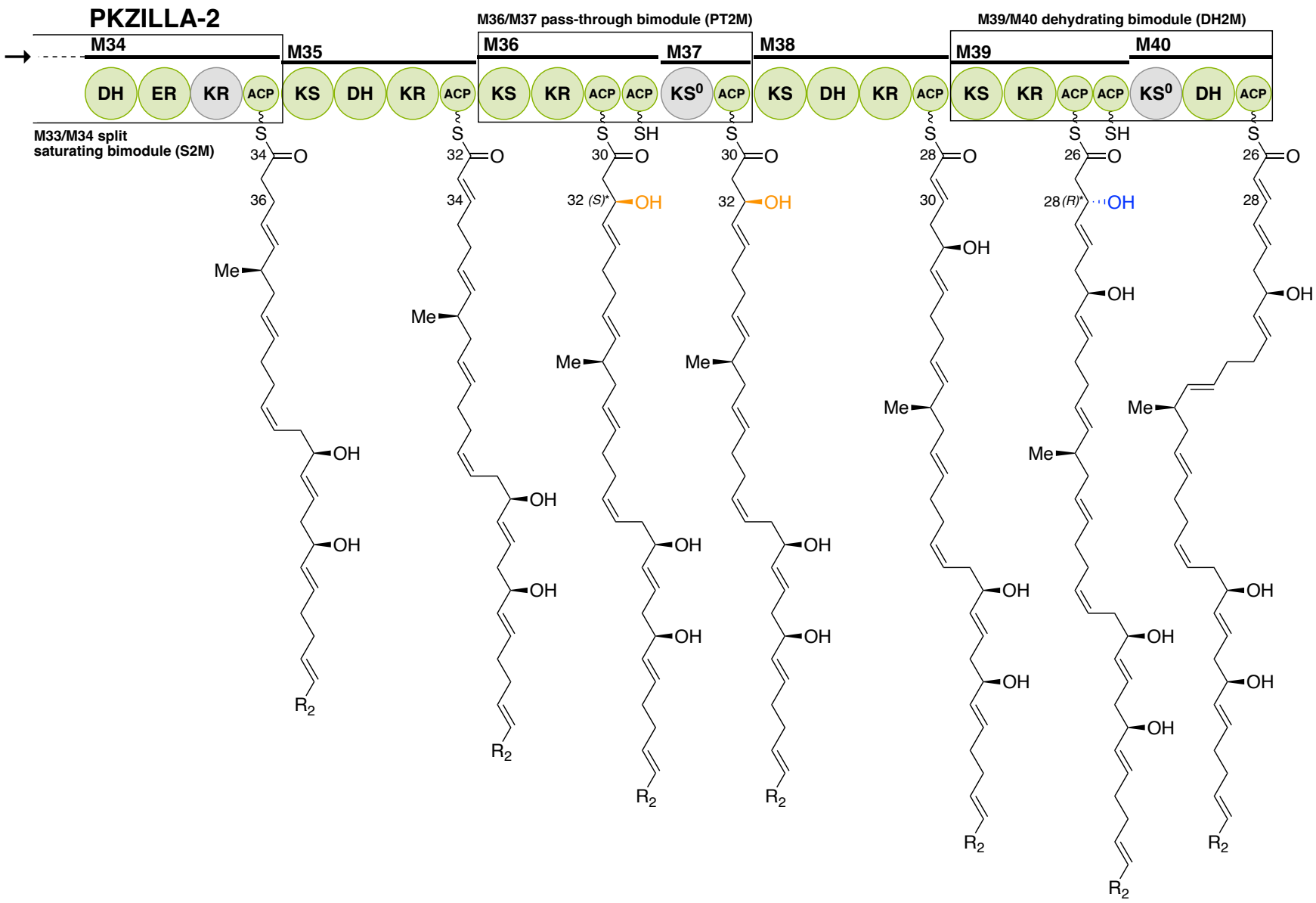
PKZILLA-2
M34
M35
M36
M37
M38
M39
M40
M36/M37 pass-through bimodule (PT2M)
M39/M40 dehydrating bimodule (DH2M)
M33/M34 split
saturating bimodule (S2M)
DH
ER
KR
ACP
KS
KS0
SH
OH
Me
R2

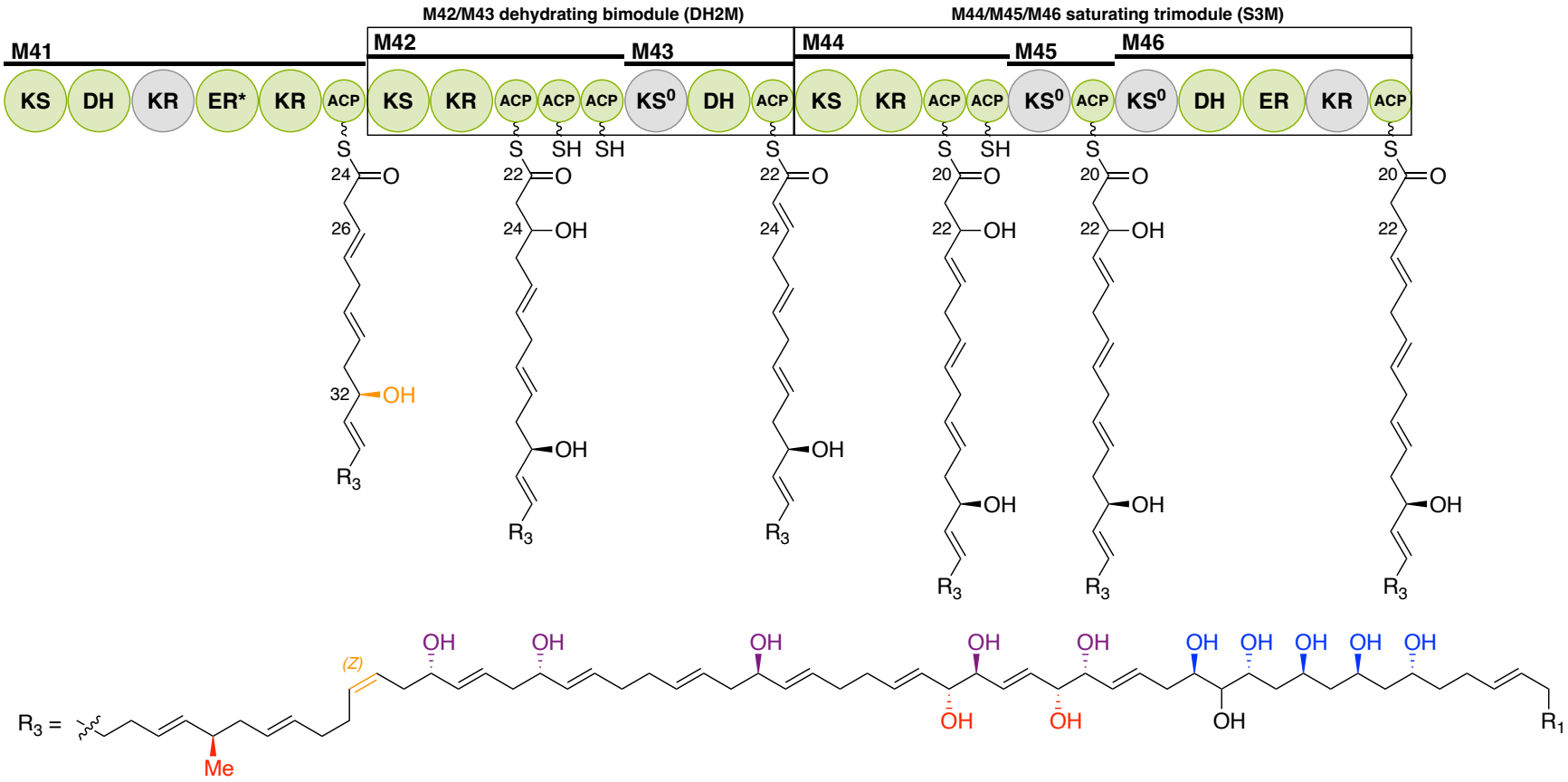
M42/M43 dehydrating bimodule (DH2M)
M44/M45/M46 saturating trimodule (S3M)
M41
M42
M43
M44
M45
M46
KS
DH
KR
ER*
KR
ACP
KS
KR
ACP
ACP
ACP
KS0
DH
ACP
KS
KR
ACP
ACP
KS0
ACP
KS0
DH
ER
KR
ACP
R3 =
Me
(Z)
R1

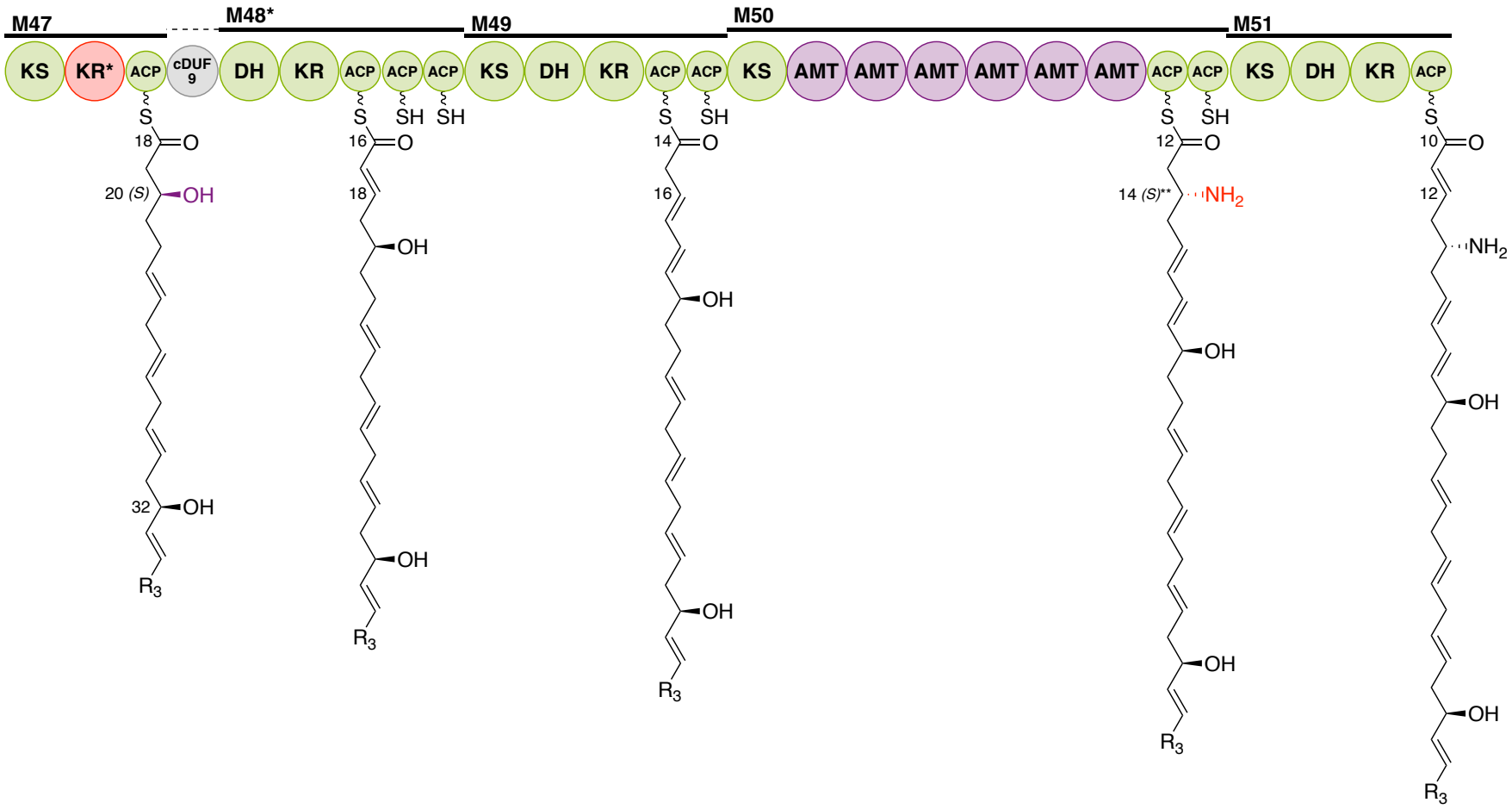
M47
M48*
M49
M50
M51
KS
KR*
ACP
cDUF 9
DH
KR
ACP
ACP
ACP
KS
DH
KR
ACP
ACP
KS
AMT
AMT
AMT
AMT
AMT
AMT
ACP
ACP
KS
DH
KR
ACP
S
18
O
20 (S)
OH
32
OH
R3
S
SH
SH
16
O
18
OH
OH
R3
S
SH
14
O
16
OH
OH
R3
S
SH
12
O
14 (S)**
NH2
OH
OH
R3
S
10
O
12
NH2
OH
OH
R3

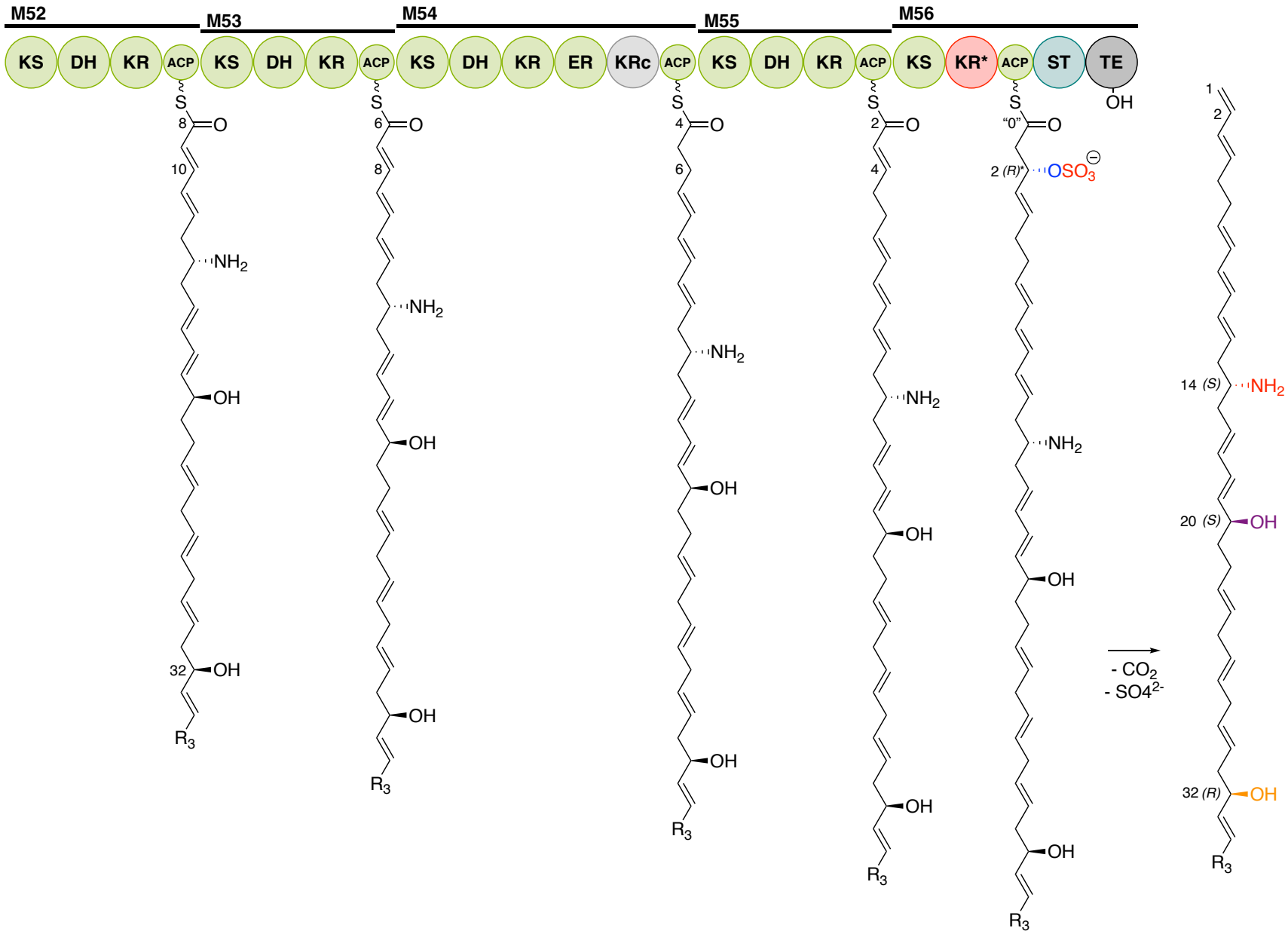
M52
M53
M54
M55
M56
KS
DH
KR
ACP
KS
DH
KR
ACP
KS
DH
KR
ER
KRc
ACP
KS
DH
KR
ACP
KS
KR*
ACP
ST
TE
OH
S
8
O
10
NH2
OH
32
OH
R3
S
6
O
8
NH2
OH
OH
R3
S
4
O
6
NH2
OH
OH
R3
S
2
O
4
NH2
OH
OH
R3
S
"0"
O
2 (R)*
OSO3
NH2
OH
OH
R3
1
2
14 (S)
NH2
20 (S)
OH
32 (R)
OH
R3
- CO2
- SO4 2-

Fig. S20: Polyketide synthase assembly line model for PKZILLA-1/2. Domain abbreviations and color coding follows those used in Fig. 2, excepting that all KS, ACP, KR, DH, ER domains are shown as green. Light-gray colored domains are either predicted to be catalytically inactive from bioinformatic analysis (KRs), or trans-acylating rather than fully condensating (KS^0s), or did not have an apparent attributable catalytic activity (i.e. M16 FLX) despite bioinformatic expectations of catalytic capability. Red domains (KR*s) in M47 and M56, would be expected to be active based on the biosynthetic model, but are bioinformatically predicted to be inactive (table S9), and thus may be false positive predictions of inactivity caused by divergent catalytic properties. Red bond and atom coloration indicates functional groups installed by FLX, MT, AMT, and ST domains, or installed functional groups whose stereochemistry is known only from inferences from empirically reported or retrobiosynthetically inferred stereochemistry (Fig. 3) and does not have a bioinformatic prediction of stereochemistry (Table S12). Blue coloration indicates stereochemistry is only proposed from bioinformatics (Table S12). Purple coloration indicates a match between empirically reported or inferred stereochemical configurations and bioinformatic stereochemical predictions (Table S12). Orange coloration indicates a mis-match between empirically reported or inferred stereochemical/isomeric configurations and bioinformatic predictions (Table S12). *=Due to inversion of Cahn–Ingold–Prelog priority when γ,δ bond is an alkene vs saturated, or if the γ carbon has a hydroxyl, γ,δ carbons were drawn as always saturated and without hydroxyls for the purposes of stereochemical assignment. **=Stereochemical assignment inverted to match configuration on prymnesin, in both cases it is the same configuration barring an inversion of Cahn–Ingold–Prelog priority.

Transcript ID	Gene ID	Scaffold ID	Gene coord. start	Gene coord. end	Gene length (bp)	mRNA length (nt)	Exon count	Closest PKS gene ID	Closest PKS gene distance (kbp)	tpm_day	tpm_night
PKZILLA-1	12B1gPKZILLA-1	12B1-Scaf17	2286087	2423367	137280	136088	17			1.11135	0.713157
PKZILLA-2	12B1gPKZILLA-2	12B1-Scaf7	1023621	1116873	93252	92413	12	12B1g21318	-680.4	2.42293	1.67459
PKZILLA-3	12B1gPKZILLA-3	12B1-Scaf10	233715	308247	74532	73850	8			0.0327181	0.907688
12B1g6935.t1	12B1g6935	12B1-Scaf30	1090474	1117079	26605	24501	7			0.0122754	0.102986
12B1g20558.t1	12B1g20558	12B1-Scaf24	1258375	1280190	21815	19167	25			13.5373	5.5826
12B1g8858.t2	12B1g8858	12B1-Scaf14	381850	402639	20789	20367	6	12B1g8877	90.7	0.297101	0.496385
12B1g8858.t1	12B1g8858	12B1-Scaf14	381850	402639	20789	20448	5	12B1g8877	90.7	0.00288062	0.0022481
12B1g21318.t2	12B1g21318	12B1-Scaf7	323056	343225	20169	19878	2	12B1gPKZILLA-2	680.4	0.306636	0.169165
12B1g21318.t1	12B1g21318	12B1-Scaf7	323056	343225	20169	3753	3	12B1gPKZILLA-2	680.4	0	0
12B1g8877.t1	12B1g8877	12B1-Scaf14	493291	508389	15098	13578	7	12B1g8858	-90.7	1.90592	1.52636
12B1g521.t1	12B1g521	12B1-Scaf9	1906255	1920566	14311	11718	19			6.72458	8.85982
12B1g5199.t1	12B1g5199	12B1-Scaf22	974085	988095	14010	13545	3			0.359611	0.358954
12B1g8961.t1	12B1g8961	12B1-Scaf14	799146	811847	12701	11613	9	12B1g8877	-290.8	0.12426	0.542579
12B1g16712.t1	12B1g16712	12B1-Scaf1	2251945	2264026	12081	11883	2			1.17317	0.828558
12B1g5573.t1	12B1g5573	12B1-Scaf21	668309	680198	11889	11493	6			1.2576	1.35399
12B1g22763.t1	12B1g22763	12B1-Scaf16	1956638	1967275	10637	7761	12			11.6529	5.12936
12B1g3947.t1	12B1g3947	12B1-Scaf5	908335	918651	10316	6363	7	12B1g3948	0.5	0.751993	1.59325
12B1g4698.t1	12B1g4698	12B1-Scaf5	3795505	3804614	9109	8130	5	12B1g4700	3	2.1088	1.27798
12B1g14437.t1	12B1g14437	12B1-Scaf3	1062558	1071078	8520	8127	4			0.725751	0.42423
12B1g3948.t1	12B1g3948	12B1-Scaf5	919101	927118	8017	5415	10	12B1g3947	-0.5	0.37918	1.12212
12B1g23642.t1	12B1g23642	12B1-Scaf26	980919	987804	6885	6585	4			15.6463	9.60298
12B1g4700.t1	12B1g4700	12B1-Scaf5	3807648	3814260	6612	4836	6	12B1g4698	-3	12.1958	3.27771
12B1g8154.t1	12B1g8154	12B1-Scaf13	326108	332557	6449	6225	3			1.38845	0.879017
12B1g18060.t1	12B1g18060	12B1-Scaf33	408311	411415	3105	3105	1			5.65643	2.4474

Table S1: Genomic characteristics of *Prymnesium parvum* 12B1 PKS genes. coord.=coordinate. tpm_day and tpm_night = expression values in transcripts per million (TPM) for day and night rRNA depletion RNA-seq libraries, calculated with Kallisto (doi:10.5281/zenodo.10023425).

seqid	scaffold	start	end	intron length	Upstream reading frame	Downstream reading frame	Reading frame shift from splicing?	Stop codon in intron & upstream reading frame?
PKZILLA-1_intron1	12B1-Scaf17	2287899	2287961	62	3	3	no	yes
PKZILLA-1_intron2	12B1-Scaf17	2291865	2291950	85	3	2	yes	no
PKZILLA-1_intron3	12B1-Scaf17	2296229	2296296	67	2	1	yes	no
PKZILLA-1_intron4	12B1-Scaf17	2317507	2317572	65	1	1	no	yes
PKZILLA-1_intron5	12B1-Scaf17	2327560	2327633	73	1	3	yes	yes
PKZILLA-1_intron6	12B1-Scaf17	2336046	2336111	65	3	3	no	yes
PKZILLA-1_intron7	12B1-Scaf17	2343831	2343904	73	3	2	yes	no
PKZILLA-1_intron8	12B1-Scaf17	2348525	2348601	76	2	1	yes	yes
PKZILLA-1_intron9	12B1-Scaf17	2357062	2357127	65	1	1	no	yes
PKZILLA-1_intron10	12B1-Scaf17	2364847	2364920	73	1	3	yes	no
PKZILLA-1_intron11	12B1-Scaf17	2369541	2369617	76	3	2	yes	yes
PKZILLA-1_intron12	12B1-Scaf17	2379032	2379132	100	2	1	yes	yes
PKZILLA-1_intron13	12B1-Scaf17	2388484	2388584	100	1	3	yes	yes
PKZILLA-1_intron14	12B1-Scaf17	2396328	2396394	66	3	1	yes	no
PKZILLA-1_intron15	12B1-Scaf17	2401024	2401091	67	1	3	yes	yes
PKZILLA-1_intron16	12B1-Scaf17	2415990	2416054	64	3	2	yes	no
PKZILLA-2_intron1	12B1-Scaf7	1024581	1024646	65	3	3	no	no
PKZILLA-2_intron2	12B1-Scaf7	1029285	1029356	71	3	3	no	yes
PKZILLA-2_intron3	12B1-Scaf7	1038708	1038808	100	3	2	yes	yes
PKZILLA-2_intron4	12B1-Scaf7	1065686	1065759	73	2	1	yes	yes
PKZILLA-2_intron5	12B1-Scaf7	1072585	1072709	124	1	3	yes	yes
PKZILLA-2_intron6	12B1-Scaf7	1092303	1092366	63	3	1	yes	yes
PKZILLA-2_intron7	12B1-Scaf7	1096189	1096253	64	1	3	yes	no
PKZILLA-2_intron8	12B1-Scaf7	1100079	1100143	64	3	2	yes	no
PKZILLA-2_intron9	12B1-Scaf7	1103969	1104033	64	2	1	yes	no
PKZILLA-2_intron10	12B1-Scaf7	1110112	1110183	71	1	1	no	yes
PKZILLA-2_intron11	12B1-Scaf7	1115472	1115542	70	1	3	yes	no
PKZILLA-3_intron1	12B1-Scaf10	234816	234888	72	3	1	yes	yes
PKZILLA-3_intron2	12B1-Scaf10	234974	235031	57	1	2	yes	yes
PKZILLA-3_intron3	12B1-Scaf10	235152	235267	115	2	1	yes	yes
PKZILLA-3_intron4	12B1-Scaf10	235849	235976	127	1	3	yes	yes
PKZILLA-3_intron5	12B1-Scaf10	237153	237288	135	3	1	yes	no
PKZILLA-3_intron6	12B1-Scaf10	257254	257316	62	1	1	no	no
PKZILLA-3_intron7	12B1-Scaf10	303779	303887	108	1	2	yes	yes

Table S2: Intron characteristics of PKZILLA genes. See Fig. S3, S4, S5 for detailed graphical views of each intron.

InterProScan annotated region	Short PKS nomenclature	Comments
SSF56801	ANL	Unintegrated into InterPro, but, covers both the "N" and "C" terminal subdomains of an ANL enzyme, unlike other matchers. Alternatively, IPR042099 matches the N-terminal (sub)domain, IPR025110 matches the C-terminal (sub)domain.
G3DSA:1.10.1200.10	ACP	Integrated into InterPro:IPR036736
G3DSA:3.40.47.10	KS	Integrated into InterPro:IPR016039
G3DSA:3.10.129.110	DH	Integrated into InterPro:IPR042104
G3DSA:3.40.50.720	KR	Unintegrated into InterPro. Confirmed cross-match: Ends up nested underneath G3DSA:3.90.180.10 (ER). But, the longest available matcher for the KR.
G3DSA:3.90.180.10	ER	Unintegrated into InterPro. Possible cross-match: Ends up nested underneath G3DSA:3.40.50.720 (KR)?. But, the longest available matcher for the ER. IPR020843 is a possible alternative.
G3DSA:3.50.50.60	FLX	Integrated into InterPro:IPR036188
G3DSA:3.40.50.150	MT	Integrated into InterPro:IPR029063
G3DSA:3.90.1150.10	AMT	Integrated into InterPro:IPR015422
SSF53474	TE	Integrated into InterPro:IPR029058
PF13469	ST	Integrated into InterPro:IPR027417. Formerly annotated with G3DSA:3.40.50.300, but PF13469/sulfotransferase is a more informative annotation.
PF00668	C	Integrated into InterPro:IPR001242. NRPS-like condensation domain. In PKZILLA-3
G3DSA:3.30.1610.10	S59	Integrated into InterPro:IPR036903. This is a weak hit on PKZILLA-3. Autoproteolytic C-terminal nucleoporin thing.

Table S3: Specific InterProScan annotations that were deemed to be diagnostic for and representative of particular PKS domains within the PKZILLA polypeptides, and used to select these domains for downstream analyses and figures. The table includes all non-trivially small and/or weak matches and non-intrinsically disordered region matches that were found in the PKZLLAs. Table is derived from "run2_filter.tsv" used in Zenodo workflows for InterProScan annotations of the PKZILLAs (doi:10.5281/zenodo.10023460), and non-PKZILLAs (doi:10.5281/zenodo.10011739).

seqid	domain sequence
PKZILLA-1	ANL-ACP-KS-DH-KR-ACP-KS-DH-ER-KR-ACP-KS-KR-ACP-KS-KR-ACP-KS-KR-ACP-KS-KR-FLX-ACP-KS-KR-ACP-KS-DH-KR-ACP-KS-FLX-KR-FLX-ACP-KS-DH-KR-ACP-KS-FLX-KR-ACP-ACP-KS-DH-KR-ACP-KS-KR-ACP-ACP-KS-DH-ER-KR-ACP-KS-DH-KR-ACP-KS-FLX-KR-ACP-ACP-KS-DH-KR-ACP-KS-KR-ACP-ACP-KS-DH-ER-KR-ACP-KS-DH-KR-ACP-KS-KR-ACP-ACP-KS-ACP-KS-DH-KR-ACP-KS-KR-ACP-ACP-KS-ACP-KS-DH-KR-ACP-KS-KR-ACP-ACP-KS-DH-KR-ER-KR-ACP-KS-DH-KR-ACP-KS-DH-KR-MT-KR-ACP-ACP-ACP-ACP-KS-ER-KR-ACP-KS-DH-KR-ACP-KS-KR-ACP-ACP-KS
PKZILLA-2	DH-ER-KR-ACP-KS-DH-KR-ACP-KS-KR-ACP-ACP-KS-ACP-KS-DH-KR-ACP-KS-KR-ACP-ACP-KS-DH-ACP-KS-DH-KR-ER-KR-ACP-KS-KR-ACP-ACP-ACP-KS-DH-ACP-KS-KR-ACP-ACP-KS-ACP-KS-DH-ER-KR-ACP-KS-KR-ACP-DH-KR-ACP-ACP-ACP-KS-DH-KR-ACP-ACP-KS-AMT-AMT-AMT-AMT-AMT-AMT-ACP-ACP-KS-DH-KR-ACP-KS-DH-KR-ACP-KS-DH-KR-ACP-KS-DH-KR-ER-KR-ACP-KS-DH-KR-ACP-KS-KR-ACP-ST-TE
PKZILLA-3	KS-DH-ER-KR-ACP-KS-KR-ACP-KS-KR-ACP-KS-KR-ACP-KS-DH-MT-KR-ACP-ACP-KS-KR-ER-KR-ACP-KS-DH-KR-ACP-KS-DH-KR-ACP-KS-DH-ER-KR-ACP-KS-KR-FLX-ACP-KS-KR-ACP-KS-KR-ACP-KS-KR-ACP-KS-KR-ACP-KS-DH-KR-ACP-KS-DH-KR-ACP-KS-DH-KR-ACP-KS-KR-ACP-KS-DH-KR-ACP-ACP-S59-C

Table S4: Linear sequence of polyketide synthase (PKS) domains within the PKZILLA polypeptides of *Prymnesium parvum* 12B1. Analogous rows for non-PKZILLA PKS polypeptides are not shown for brevity, but are available on Zenodo (doi:10.5281/zenodo.10028239).

seqid	# of AA residues	M.W. (MDa)	# of modules	# of domains	# of ANLs	# of KSs	# of ACPs	# of KRs	# of DHs	# of ERs	# of FLXs	# of MTs	# of AMTs	# of STs	# of TEs	# of S59s	# of Cs
PKZILLA-1	45,212	4.73	35	140	1	34	45	33	16	5	5	1	0	0	0	0	0
PKZILLA-2	30,685	3.23	23	99	0	21	32	20	14	4	0	0	6	1	1	0	0
PKZILLA-3	24,439	2.59	19	76	0	19	21	20	9	3	1	1	0	0	0	1	1

Table S5: Counts of polyketide synthase (PKS) residues, domains, and modules within the PKZILLA polypeptides of *Prymnesium parvum* 12B1. AA=amino acid. M.W.=Molecular weight, calculated with ProtParam (https://web.expasy.org/protparam/). Analogous rows for non-PKZILLA PKS sequences are not shown for brevity, but are available on Zenodo (doi:10.5281/zenodo.10028239).

cDUF ID	PKZILLA coordinates	Length	In module	Comments
PKZILLA-1__cDUF1	PKZILLA-1:0-598	598	N/A	At N-terminus of PKZILLA-1. InterProScan annotates as an intrinsically disordered region.
PKZILLA-1__cDUF10	PKZILLA-1:38976-39480	504	M30	Sequence and structurally similar to FLX domains. Unclear if functional or vestigial. Dubbed cveFLX6 (cve=candidate, vestigial, extended)
PKZILLA-1__cDUF7	PKZILLA-1:28567-28789	222	M21	Sequence similarity to FLX domains. Short, probably vestigial.
PKZILLA-1__cDUF9	PKZILLA-1:34817-35027	210	M27	Sequence similarity to FLX domains. Short, probably vestigial.
PKZILLA-1__cDUF2	PKZILLA-1:3324-3500	176	M2	Sequence similarity to KR domains. Nearby KRc. Likely an unannotated KRn structural subdomain.
PKZILLA-1__cDUF4	PKZILLA-1:19100-19274	174	M14	Sequence similarity to KR domains. Nearby KRc. Likely an unannotated KRn structural subdomain.
PKZILLA-1__cDUF6	PKZILLA-1:26033-26207	174	M19	Sequence similarity to KR domains. Nearby KRc. Likely an unannotated KRn structural subdomain.
PKZILLA-1__cDUF13	PKZILLA-1:43935-44108	173	M33	Sequence similarity to FLX domains. Short, probably vestigial.
PKZILLA-1__cDUF3	PKZILLA-1:17527-17697	170	M13	Sequence similarity to KR domains. Nearby KRf. Possibly an unannotated KRn structural subdomain.
PKZILLA-1__cDUF5	PKZILLA-1:24460-24630	170	M18	Sequence similarity to KR domains. Nearby KRf. Possibly an unannotated KRn structural subdomain.
PKZILLA-1__cDUF12	PKZILLA-1:41376-41541	165	M31	Sequence similarity to KR domains. Nearby KRc. Likely an unannotated KRn structural subdomain.
PKZILLA-1__cDUF8	PKZILLA-1:31749-31903	154	M24	Weak sequence similarity to FLX4. Short, probably vestigial.
PKZILLA-1__cDUF11	PKZILLA-1:39951-40061	110	M30	Some sequence similarity hits in 12B1, unclear role.

Table S6: Analysis of InterProScan unannotated regions in PKZILLA-1 as candidate domains of unknown function (cDUFs). All contiguous unannotated regions of the PKZILLAs larger than 50 amino acid residues are shown, excepting those that seemed reasonably associated with an existing annotated domain (FLX extended C-terminal regions, i.e. eFLXs; doi:10.5281/zenodo.10120640, fig. S6). Regions were queried against other *P. parvum* 12B1 polypeptides using blastp. Source data, analysis scripts, and raw blast results are available on Zenodo (doi:10.5281/zenodo.10028178). For PKZILLA-2, see next table, and for PKZILLA-3 see Zenodo item.

cDUF ID	PKZILLA coordinates	Length	In module	Comments
PKZILLA-2__cDUF17	PKZILLA-2:27013-27222	209	M54	Sequence similarity to KR domains. Nearby KRc. Likely an unannotated KRn structural subdomain.
PKZILLA-2__cDUF4	PKZILLA-2:5942-6137	195	M39	Sequence similarity to KR domains. Possibly an unannotated KRn structural subdomain.
PKZILLA-2__cDUF9	PKZILLA-2:15752-15938	186	M47/M48	No hits to anything. (Including KSs, and KRs)
PKZILLA-2__cDUF2	PKZILLA-2:322-499	177	M34	Sequence similarity to KR domains. Nearby KRc. Likely an unannotated KRn structural subdomain.
PKZILLA-2__cDUF8	PKZILLA-2:13946-14120	174	M46	Sequence similarity to KR domains. Nearby KRc. Likely an unannotated KRn structural subdomain.
PKZILLA-2__cDUF7	PKZILLA-2:11843-11970	127	M44	Sequence similarity to KS-KR-ACP-ACP modules. Possible structural role.
PKZILLA-2__cDUF3	PKZILLA-2:2895-3016	121	M36	Sequence similarity to KS-KR-ACP-ACP modules. Possible structural role.
PKZILLA-2__cDUF12	PKZILLA-2:19745-19845	100	M50	Associated with AMT domains. Possible structural role
PKZILLA-2__cDUF14	PKZILLA-2:20741-20841	100	M50	Associated with AMT domains. Possible structural role
PKZILLA-2__cDUF10	PKZILLA-2:18744-18839	95	M50	Multiple hits in PKZILLA-2, not within annotated domains or modules. Possible structural role.
PKZILLA-2__cDUF13	PKZILLA-2:20243-20332	89	M50	Multiple hits in PKZILLA-2, possible structural role.
PKZILLA-2__cDUF15	PKZILLA-2:21239-21328	89	M50	Multiple hits in PKZILLA-2, possible structural role.
PKZILLA-2__cDUF11	PKZILLA-2:19248-19336	88	M50	Multiple hits in PKZILLA-2, possible structural role.
PKZILLA-2__cDUF16	PKZILLA-2:21737-21809	72	M50	Multiple hits in PKZILLA-2, possible structural role.
PKZILLA-2__cDUF6	PKZILLA-2:10441-10511	70	M42/M43	No hits.
PKZILLA-2__cDUF1	PKZILLA-2:0-52	52	M34	Sequence similarity to KR domains. Possibly an unannotated KRn structural subdomain. Interesting as this is the N-terminus of PKZILLA-2, might have a protein-protein interaction role.
PKZILLA-2__cDUF5	PKZILLA-2:10112-10164	52	M42	No hits.

Table S7: Analysis of InterProScan unannotated regions in PKZILLA-2 as candidate domains of unknown function (cDUFs). All contiguous unannotated regions of the PKZILLAs larger than 50 amino acid residues are shown, excepting those that seemed reasonably associated with an existing annotated domain (FLX extended C-terminal regions, i.e. eFLXs; doi:10.5281/zenodo.10120640, fig. S6). Regions were queried against other *P. parvum* 12B1 polypeptides using blastp. Source data, analysis scripts, and raw blast results are available on Zenodo (doi:10.5281/zenodo.10028178). For PKZILLA-1 see previous table and for PKZILLA-3, see Zenodo item.

module	seqid	start	end	components	KS#	ACP#	DH#	ER#	KR#	FLX#	comments
LM	PKZILLA-1	600	1242	ANL-ACP		ACP1					Loading module
M1	PKZILLA-1	1351	2591	KS-DH-KR-ACP	KS1	ACP2	DH1		KR1		
M2	PKZILLA-1	2624	4147	KS-DH-ER-KR-ACP	KS2	ACP3	DH2	ER1	KR2c		
M3	PKZILLA-1	4168	5148	KS-KR-ACP	KS3	ACP4			KR3		
M4	PKZILLA-1	5168	6140	KS-KR-ACP	KS4	ACP5			KR4		
M5	PKZILLA-1	6160	7132	KS-KR-ACP	KS5	ACP6			KR5		
M6	PKZILLA-1	7152	8677	KS-KR-FLX-ACP	KS6	ACP7			KR6	FLX1	
M7	PKZILLA-1	8700	9673	KS-KR-ACP	KS7	ACP8			KR7		
M8	PKZILLA-1	9693	10900	KS-DH-KR-ACP	KS8	ACP9	DH3		KR8		
M9	PKZILLA-1	10918	12999	KS-FLX-KR-FLX-ACP	KS9	ACP10			KR9	FLX2 FLX3	
M10	PKZILLA-1	13023	14232	KS-DH-KR-ACP	KS10	ACP11	DH4		KR10		
M11	PKZILLA-1	14250	15807	KS-FLX-KR-ACP-ACP	KS11	ACP12 ACP13			KR11	FLX4	
M12	PKZILLA-1	15819	17041	KS-DH-KR-ACP	KS12	ACP14	DH5		KR12		
M13	PKZILLA-1	17062	18379	KS-KR-ACP-ACP	KS13	ACP15 ACP16			KR13		Sat. bimodule (S2M) M13/M14
M14	PKZILLA-1	18398	19912	KS-DH-ER-KR-ACP	$KS^0$14	ACP17	DH6	ER2	KR14c0		(S2M) KR inactive via phylogeny
M15	PKZILLA-1	19934	21162	KS-DH-KR-ACP	KS15	ACP18	DH7		KR15		
M16	PKZILLA-1	21180	22740	KS-FLX-KR-ACP-ACP	KS16	ACP19 ACP20			KR16	FLX5	
M17	PKZILLA-1	22751	23973	KS-DH-KR-ACP	KS17	ACP21	DH8		KR17		
M18	PKZILLA-1	23995	25312	KS-KR-ACP-ACP	KS18	ACP22 ACP23			KR18		Sat. bimodule (S2M) M18/M19
M19	PKZILLA-1	25331	26845	KS-DH-ER-KR-ACP	$KS^0$19	ACP24	DH9	ER3	KR19c0		(S2M) KR inactive via phylogeny
M20	PKZILLA-1	26867	28095	KS-DH-KR-ACP	KS20	ACP25	DH10		KR20		
M21	PKZILLA-1	28112	29438	KS-KR-ACP-ACP	KS21	ACP26 ACP27			KR21		Pass-through bimodule (PT2M)
M22	PKZILLA-1	29450	29999	KS-ACP	$KS^0$22	ACP28					(PT2M) M21/M22
M23	PKZILLA-1	30017	31221	KS-DH-KR-ACP	KS23	ACP29	DH11		KR22		
M24	PKZILLA-1	31240	32555	KS-KR-ACP-ACP	KS24	ACP30 ACP31			KR23		Pass-through bimodule (PT2M)
M25	PKZILLA-1	32576	33116	KS-ACP	$KS^0$25	ACP32					(PT2M) M24/M25
M26	PKZILLA-1	33134	34338	KS-DH-KR-ACP	KS26	ACP33	DH12		KR24		
M27	PKZILLA-1	34357	35691	KS-KR-ACP-ACP	KS27	ACP34 ACP35			KR25		Sat. bimodule (S2M) M27/M28
M28	PKZILLA-1	35709	37227	KS-DH-KR-ER-KR-ACP	$KS^0$28	ACP36	DH13	ER4	KR26n0 KR27c0		S2M, KR27 inactive via phylogeny
M29	PKZILLA-1	37252	38466	KS-DH-KR-ACP	KS29	ACP37	DH14		KR28		
M30	PKZILLA-1	38482	40909	KS-DH-KR-MT-KR-ACP-ACP-ACP-ACP	KS30	ACP38 ACP39 ACP40 ACP41	DH15		KR29n0 KR30c		(S2M), PKZILLA-1 cDUF10, cveFLX6 contained within
M31	PKZILLA-1	40933	42203	KS-ER-KR-ACP	$KS^0$31	ACP42		ER5	KR31c0		(S2M) M30/M31
M32	PKZILLA-1	42214	43440	KS-DH-KR-ACP	KS32	ACP43	DH16		KR32		
M33	PKZILLA-1	43458	44768	KS-KR-ACP-ACP	KS33	ACP44 ACP45			KR33		Split sat. bimodule (S2M) M33/M34
M34	PKZILLA-1	44790	45210	KS-	$KS^0$34						S2M, Split module (split w/ PKZILLA-2)

Table S8: Organization of PKZILLA-1 domains into modules and the assignment of domain catalytic activity or inactivity based on active site analysis. Number, contents, and extents of modules have been modified from original bioinformatic predictions to account for non-standard or split module structures. Source data & code for bioinformatic predictions of modules are available at Zenodo (doi:10.5281/zenodo.10028239). Analogous module structures for PKZILLA-3 and non-PKZILLA polypeptides are not shown for brevity, but are available at Zenodo (doi:10.5281/zenodo.10028239). For PKZILLA-2, see next table. KR domains are annotated as KR/KRf, KRn, KRc depending on their respective classification as a full length non-split KR, a split KR N-terminal subdomain, or a split KR C-terminal subdomain, and "0" is appended to the domain name if the active site residues suggest the domain is catalytically inactive, or in case of KSs, if it is a predicted catalytically active but non-elongating domain. For further details on catalytic activity determination via active site analysis, see "Analysis of active site residues within PKZILLA PKS domains" in the Materials and Methods and the associated Zenodo item (doi:10.5281/zenodo.10028517).

module cont.	module restart	seqid	start	end	components	KS#	ACP#	DH#	ER#	KR#	comments
M34	(M1)	PKZILLA-2	52	1139	-DH-ER-KR-ACP		ACP1	DH1	ER1	KR1c0	Split module (split w/ PKZILLA-1). KR inactive via phylogeny.
M35	(M2)	PKZILLA-2	1186	2382	KS-DH-KR-ACP	KS1	ACP2	DH2		KR2	
M36	(M3)	PKZILLA-2	2400	3707	KS-KR-ACP-ACP	KS2	ACP3 ACP4			KR3	Pass-through bimodule (PT2M) M36/M37
M37	(M4)	PKZILLA-2	3735	4275	KS-ACP	KS^{0}3	ACP5				(PT2M)
M38	(M5)	PKZILLA-2	4294	5497	KS-DH-KR-ACP	KS4	ACP6	DH3		KR4	
M39	(M6)	PKZILLA-2	5519	6822	KS-KR-ACP-ACP	KS5	ACP7 ACP8			KR5	Dehydrating bimodule (DH2M) M39/M40
M40	(M7)	PKZILLA-2	6850	7654	KS-DH-ACP	KS^{0}6	ACP9	DH4			(DH2M)
M41	(M8)	PKZILLA-2	7664	9233	KS-DH-KR-ER-KR-ACP	KS7	ACP10	DH5	ER2	KR6n0 KR7c	ER2 is diverged from other ERs , ER*
M42	(M9)	PKZILLA-2	9258	10437	KS-KR-ACP-ACP-ACP	KS8	ACP11 ACP12 ACP13			KR8	Dehydrating bimodule (DH2M) M42/M43
M43	(M10)	PKZILLA-2	10519	11331	KS-DH-ACP	KS^{0}9	ACP14	DH6			(DH2M)
M44	(M11)	PKZILLA-2	11350	12655	KS-KR-ACP-ACP	KS10	ACP15 ACP16			KR9	Saturating trimodule (S3M) M44/M45/M46
M45	(M12)	PKZILLA-2	12678	13225	KS-ACP	KS^{0}11	ACP17				(S3M)
M46	(M13)	PKZILLA-2	13243	14757	KS-DH-ER-KR-ACP	KS^{0}12	ACP18	DH7	ER3	KR10c0	(S3M), KR inactive via phylogeny
M47	(M14)	PKZILLA-2	14779	15743	KS-KR-ACP	KS13	ACP19			KR11*	KR*. Initiates polyether.
M48*	(M15*)	PKZILLA-2	15938	16942	DH-KR-ACP-ACP-ACP		ACP20 ACP21 ACP22	DH8		KR12	Missing KS. Unannotated DH- upstream-gap is PKZILLA-2__cDUF9
M49	(M16)	PKZILLA-2	16958	18303	KS-DH-KR-ACP-ACP	KS14	ACP23 ACP24	DH9		KR13	KS,DH diverged vs PKZILLA others
M50	(M17)	PKZILLA-2	18323	22019	KS-AMT-AMT-AMT-AMT-AMT-AMT-ACP-ACP	KS15	ACP25 ACP26				AMT1, AMT2, …, AMT6
M51	(M18)	PKZILLA-2	22043	23279	KS-DH-KR-ACP	KS16	ACP27	DH10		KR14	
M52	(M19)	PKZILLA-2	23307	24554	KS-DH-KR-ACP	KS17	ACP28	DH11		KR15	
M53	(M20)	PKZILLA-2	24582	25829	KS-DH-KR-ACP	KS18	ACP29	DH12		KR16	
M54	(M21)	PKZILLA-2	25857	27862	KS-DH-KR-ER-KR-ACP	KS19	ACP30	DH13	ER4	KR17 KR18c0	KR17 is full length (f). KR18 inactive via phylogeny
M55	(M22)	PKZILLA-2	27918	29114	KS-DH-KR-ACP	KS20	ACP31	DH14		KR19	
M56	(M23)	PKZILLA-2	29132	30667	KS-KR-ACP-ST-TE	KS21	ACP32			KR20*	ST-TE=Curacin/ CurM-like termination didomain. KR*

Table S9: Organization of PKZILLA-2 domains into modules and the assignment of domain catalytic activity or inactivity based on active site analysis. Number, contents, and extents of modules have been modified from original bioinformatic predictions to account for non-standard or split module structures. Source data & code for bioinformatic predictions of modules are available at Zenodo (doi:10.5281/zenodo.10028239). Analogous module structures for PKZILLA-3 and non-PKZILLA polypeptides are not shown for brevity, but are available at Zenodo (doi:10.5281/zenodo.10028239). For PKZILLA-1, see previous table. KR domains are annotated as KR/KRf, KRn, KRc depending on their respective classification as a full length non-split KR, a split KR N-terminal subdomain, or a split KR C-terminal subdomain, and a 0 is appended to the domain name if the active site residues suggest the domain is catalytically inactive, or in case of KSs, if it is a predicted catalytically active but non-elongating domain. For further details on catalytic activity determination via active site analysis, see "Analysis of active site residues within PKZILLA PKS domains" in the Materials and Methods and the associated Zenodo item (doi:10.5281/zenodo.10028517)

Uniprot taxon mnemonic	informative taxonomic parent	explanation
PKZILLA	haptophyte algae	Domain arising from a PKZILLA gene from *Prymnesium parvum* strain 12B1 (haptophyte)
9ACTN	bacteria	Descended taxon of Actinomycetota
9CYAN	bacteria	Descended taxon of Cyanobacteriota
9DINO	dinoflagellate algae	Descended taxon of Dinophyceae (dinoflagellates)
ASPFN	fungi	*Aspergillus flavus*
ASPFU	fungi	*Aspergillus fumigatus*
ASPPU	fungi	*Aspergillus parasiticus*
ASPTE	fungi	*Aspergillus terreus*
ASPTN	fungi	*Aspergillus terreus* (strain NIH 2624 / FGSC A1156)
CHLRE	green algae	*Chlamydomonas reinhardtii*
DOTSN	fungi	*Dothistroma septosporum* (strain NZE10 / CBS 128990) aka Red band needle blight fungus
EMENI	fungi	*Emericella nidulans*
EMIHU	haptophyte algae	*Emiliania huxleyi* (haptophyte)
HUMAN	animals	*Homo sapiens*
MONPI	fungi	*Monascus pilosus* aka Red mold
MYCBO	bacteria	*Mycobacterium bovis* (strain ATCC BAA-935 / AF2122/97)
MYCMM	bacteria	*Mycobacterium marinum* (strain ATCC BAA-535 / M)
PENAE	fungi	*Penicillium aethiopicum* (fungi)
SACER	bacteria	*Saccharopolyspora erythraea* - erythromycin producer
STRAT	bacteria	*Streptomyces antibioticus* - oleandomycin producer
STRVZ	bacteria	*Streptomyces venezuelae* - pikromycin producer

Table S10: Mapping of uniprot taxonomy mnemonics to human readable descriptions. Key for taxonomic interpretation of fig. S16, S17, S18, S19.

seqid	module	MSA sequence context around diagnostic site (+/- 10 residues)	residue at diagnostic site	predicted stereochemical outcome	If DH present, proposed ene outcome	comment
A9GJ40	N/A	VIHSAIVLR-**D**RSLREMDEP-	D	*(R)*		seqid is Uniprot ID. Corresponds to *(R)* hydroxyl forming KR "1. Etn_KR12_D-OH" from Supplementary Figure 4 of (*32*)
A1KQR8	N/A	AIFSGMVFDF**E**NSIQQTSEA-	E	*(S)*		seqid is Uniprot ID. Corresponds to *(S)* hydroxyl forming KR "12. rhi_KR3_L-OH" from Supplementary Figure 4 of (*32*)
PKZILLA-1__KR1	M1	FWHTAGVLF-**D**ALVKKQNAV-	D	*(R)*	*(E)*-	
PKZILLA-1__KR2c	M2	VWHAAGVLA-**D**SMLPKQTAL-	D	*(R)*		
PKZILLA-1__KR3	M3	VLHAAGYAV-**D**TLSIDLVAR-	D	*(R)*		
PKZILLA-1__KR4	M4	MLHAAGASD-**K**GLLLDIVAR-	K	*(S)*		
PKZILLA-1__KR5	M5	MLHAAGVGD-**K**GLLLDIVAR-	K	*(S)*		
PKZILLA-1__KR6	M6	IFHMTEVLI-**D**KLIFLMPAR-	D	*(R)*		
PKZILLA-1__KR7	M7	VLHAAGVGD-**K**GLLLDIVAR-	K	*(S)*		
PKZILLA-1__KR8	M8	VWHAAGALA-**D**SLLPSLRAE-	D	*(R)*	*(E)*-	
PKZILLA-1__KR9	M9	VFHMTEILQ-**D**KLIFGMTSK-	D	*(R)*		
PKZILLA-1__KR10	M10	LWHAAGVLV-**D**GVLSKQTAR-	D	*(R)*	*(E)*-	
PKZILLA-1__KR11	M11	VLHAAGTGD-**K**GLLLELVSL-	K	*(S)*		
PKZILLA-1__KR12	M12	VWHAAGVLA-**D**AILHKQTAR-	D	*(R)*	*(E)*-	
PKZILLA-1__KR13	M13	ILHAAGVLR-**D**ALLRNTRAA-	D	*(R)*		
PKZILLA-1__KR14c0	M14	VWHAAGM----SESMQQHTH-	-	N/A		
PKZILLA-1__KR15	M15	VWHASGVLA-**D**GMVPKQDSR-	D	*(R)*	*(E)*-	
PKZILLA-1__KR16	M16	VLHAAGTGD-**K**GLLLELVSL-	K	*(S)*		
PKZILLA-1__KR17	M17	VWHAAGVLA-**D**AILHKQTAR-	D	*(R)*	*(E)*-	
PKZILLA-1__KR18	M18	ILHAAGVLR-**D**ALLRNTRAA-	D	*(R)*		
PKZILLA-1__KR19c0	M19	VWHAAGM----SESMQQHTH-	-	N/A		
PKZILLA-1__KR20	M20	VWHASGVLA-**D**GMVPKQDSR-	D	*(R)*	*(E)*-	
PKZILLA-1__KR21	M21	ILHAAGVLR-**D**ALLRNTRAA-	D	*(R)*		
PKZILLA-1__KR22	M23	VWHAAGVLA-**D**GMLAKQSAR-	D	*(R)*	*(E)*-	
PKZILLA-1__KR23	M24	ILHAAGVLR-**D**ALLRNTRAA-	D	*(R)*		
PKZILLA-1__KR24	M26	VWHAAGVLA-**D**GMLAKQSAR-	D	*(R)*	*(E)*-	
PKZILLA-1__KR25	M27	ILHAAGVLR-**D**ALLRNTRAA-	D	*(R)*		
PKZILLA-1__KR26n0	M28	----------**-**----------	-	N/A		
PKZILLA-1__KR27c0	M28	VWHTSSSFY-**D**AEFLQQNAL-	D	*(R)*		Note: predicted to be inactive.
PKZILLA-1__KR28	M29	VWHAAGVLA-**D**ALLPNQTAM-	D	*(R)*	*(E)*-	
PKZILLA-1__KR29n0	M30	----------**-**----------	-	N/A		
PKZILLA-1__KR30c	M30	IFHAAHRLA-**D**AVLANQKAT-	D	*(R)*		
PKZILLA-1__KR31c0	M31	VWHTASSLS-**E**ASIPTTTSAV	E	*(S)*		Note: predicted to be inactive.
PKZILLA-1__KR32	M32	LWHAAGVVS-**D**GVLAKQSAQ-	D	*(R)*	*(E)*-	
PKZILLA-1__KR33	M33	VLHAAGVLW-**D**ALLRNTRAP-	D	*(R)*		
PKZILLA-2__KR1c0	M34	VWHTMGVMS-**S**AELNQQDAL-	S	*(S)*		Note: predicted to be inactive.
PKZILLA-2__KR2	M35	LWHAAGLLS-**D**GLIPKQTAR-	D	*(R)*	*(E)*-	
PKZILLA-2__KR3	M36	VLHAAGVLR-**D**SLLRNTRAQ-	D	*(R)*		
PKZILLA-2__KR4	M38	VWHAAGVLA-**D**GMLAKQSAR-	D	*(R)*	*(E)*-	
PKZILLA-2__KR5	M39/M40	VLHAAGVLR-**D**SLLRNTRAQ-	D	*(R)*	*(E)*-	
PKZILLA-2__KR6n0	M41	----------**-**----------	-	N/A		

PKZILLA-2__KR7c	M41	VWHAAGVLA-**D**SLLPNQRAQ-	D	*(R)*		
PKZILLA-2__KR8	M42/M43	FVHASGVLL-**D**SLCRNISLM-	D	*(R)*	*(E)*-	
PKZILLA-2__KR9	M44	VLHAAGVLR-**D**SLLRNTRAQ-	D	*(R)*		
PKZILLA-2__KR10c0	M46	VWHAAGM----SEFMQQHTH-	-	N/A		
PKZILLA-2__KR11*	M47	VLHMPRAVE-**E**RVLVYLGAR-	E	*(S)*		Note: possibly novel catalysis or inactive. Is a KR*
PKZILLA-2__KR12	M48*	IWHAAGVIV-**D**ALLPKQTSA-	D	*(R)*	*(E)*-	
PKZILLA-2__KR13	M49	VWHAAGVLA-**D**AVLAKQDEH-	D	*(R)*	*(E)*-	
PKZILLA-2__KR14	M51	VWHAAGVLA-**D**AVLPNQTAA-	D	*(R)*	*(E)*-	
PKZILLA-2__KR15	M52	VWHAAGVLA-**D**AVLPKQTAA-	D	*(R)*	*(E)*-	
PKZILLA-2__KR16	M53	AWHSAGVLA-**D**AVLPKQTAA-	D	*(R)*	*(E)*-	
PKZILLA-2__KR17	M54	AWHSAGVLA-**D**AVLPKQTAA-	D	*(R)*		
PKZILLA-2__KR18c0	M54	VWHTMGVMS-**N**AELNQQDAL-	N	*(S)*		Note: predicted to be inactive.
PKZILLA-2__KR19	M55	LWHAAGLLS-**D**GLIPKQTAR-	D	*(R)*	*(E)*-	
PKZILLA-2__KR20*	M56	VLQMWSVQR-**D**VALKGLTCR-	D	*(R)*	*(E)*-	Note: possibly novel catalysis or inactive. Is a KR*

Table S11: Bioinformatic assignment of stereochemical outcome for PKZILLA-1/-2 ketoreductases (KRs). An *(R)* or *(S)* stereochemical outcome of ketoreduction at the hydroxyl-bound carbon (fig. S20) was predicted based on the reported heuristic of stereochemical outcome for *trans*-AT KRs (Supplementary Figure 4 of (*32*)), wherein an aspartate (D) at the designated site is predictive of *(R)* stereochemistry, while any other residue is predictive of *(S)* stereochemistry. If a DH domain was present in the module, an *(E)*- or *(Z)*- outcome for alkene formation was predicted based on the published heuristic (*94*) that an *(R)* hydroxyl is predictive of *(E)*- while an *(S)* hydroxyl is predictive of *(Z)*-. Source data, analysis code, and results are available on Zenodo (doi:10.5281/zenodo.10569208).

Carbon with stereocenter	Type	Empirically reported stereochemistry*	Responsible module	Mapped stereochemically responsible domain(s)	Bioinformatically predicted stereochemical outcome**	Predicted stereochemistry matches empirical?
C85	"α"-Cl	*(S)*	*n.d.* [**M2**]	N/A	*n.d.*	
C84	β-OH	*n.d.*	**M3**	PKZILLA-1__KR3	*(R)*	
C83	α-OH	*n.d.*	*n.d.* [**M3**]	N/A	*n.d.*	
C82	β-OH	*n.d.*	**M4**	PKZILLA-1__KR4	*(S)*	
C81	α-OH	*n.d.*	*n.d.* [**M5**]	N/A	*n.d.*	
C80	β-OH	*n.d.*	**M5**	PKZILLA-1__KR5	*(S)*	
C78	β-OH	*n.d.*	**M6**	PKZILLA-1__KR6	*(R)*	
C77	α-OH	*n.d.*	**M6**	PKZILLA-1__KR6 /FLX1	*n.d.*	
C76	β-OH	*n.d.*	**M7**	PKZILLA-1__KR7	*(S)*	
C72	β-OH	*(R)*	**M9**	PKZILLA-1__KR9	*(R)*	Yes
C71	α-OH	*(S)*	**M9**	PKZILLA-1__KR9 /FLX2/3	*n.d.*	
C68	β-OH	*(S)*	**M11**	PKZILLA-1__KR11	*(S)*	Yes
C67	α-OH	*(S)*	**M11**	PKZILLA-1__KR11/FLX4	*n.d.*	
C60	β-OH	*(S)*	**M16**	PKZILLA-1__KR16	*(S)*	Yes
C56	"β"-Cl	*(R)*	*n.d.* [**M19**]	N/A	*n.d.*	
C52	β-OH	*(R)*	**M21**/M22	PKZILLA-1__KR21	*(R)*	Yes
C48	β-OH	*(R)*	**M24**/M25	PKZILLA-1__KR23	*(R)*	Yes
C39	"α"-CH_3	*(R)*	**M30**	PKZILLA-2__MT1/ER5	*n.d.*	
C32	β-OH	*(S)*	**M36**/M37	PKZILLA-2__KR3	*(R)*	No
C20	β-OH	*(S)*	**M47**	PKZILLA-2__KR11*	*(S)*	Yes
C14	"β"-amine	*(R)*	**M50**	PKZILLA-2__AMT1…	*n.d.*	

Table S12: Comparison of stereochemical assignments from structural elucidations and retrobiosynthetic inferences with bioinformatically predicted stereochemical assignments. *=Stereochemistry determined from retrobiosynthetic inferences of reported prymnesin stereochemistry (Fig. 3) onto the proposed pre-prymnesin biosynthetic precursor (PPBP), with (*R*) or (*S*) stereochemistry calculated on a standardized polyketide chain elongation thioester intermediate (fig. S20). Due to an inversion of Cahn–Ingold–Prelog priority when γ,δ bond is an alkene vs saturated, or if the γ carbon has a hydroxyl, γ,δ carbons were drawn as always saturated and without hydroxyls for the purposes of stereochemical assignment. **=See previous Table. *n.d.* = not determined . N/A = not applicable.

Double bonded carbons in PA	Empirically reported (*E*)-ene or (*Z*)-ene isomer	Responsible module	Mapped responsible domain(s) for isomeric outcome on PPBP	Bioinformatically predicted isomeric outcome**	Predicted isomer matches empirical?
C21-C22	*(E)*-	**M49**	*n.d.*	*n.d.*	
C23-C24	*(E)*-	**M49**	*n.d.*	*n.d.*	
C12-C11	*(E)*-	**M51**	PKZILLA-2__KR14/DH10	(*E*)-	Yes
C10-C9	*(E)*-	**M52**	PKZILLA-2__KR15/DH11	(*E*)-	Yes
C8-C7	(alkyne)	**M53**	PKZILLA-2__KR16/DH12	(*E*)-	*n.d.*

Table S13: Comparison of (*E*)-ene vs (*Z*)-ene isomer observations on prymnesin from structural elucidations with bioinformatically predicted isomeric outcomes on PPBP. **=See Table S11. *n.d.* = not determined, due to lack of bioinformatic heuristic for prediction of isomeric outcome for vinylogous dehydration. N/A = not applicable. PA=prymnesin aglycone (see Fig. 3), PPBP=pre-prymnesin biosynthetic precursor (see Fig. 3).

	Title of Dataset or Summary for Github repository	Category	DOI or URL
1	Version v1.1 of the reference genome for Prymnesium parvum 12B1 (12B1_scaffolds_v1.1.fasta)	Genomics	https://doi.org/10.5281/zenodo.10023322
2	Version 1.1 of the Prymnesium parvum 12B1 gene annotation (12B1_v1.1.gff3)	Genomics	https://doi.org/10.5281/zenodo.10023330
3	Hotspots of PKS coding evidence within the Prymnesium parvum 12B1 v1.1 genome assembly	Genomics	https://doi.org/10.5281/zenodo.10309063
4	Kallisto v0.50.0 expression quantification of day and night phase rRNA depletion RNA-Seq data from *P. parvum* strain 12B1	Transcriptomics	https://doi.org/10.5281/zenodo.10023426
5	Detailed mass spectrometry instrument method text description, used to produce proteomic data files for PKZILLA manuscript	Proteomics	https://doi.org/10.5281/zenodo.10023360
6	SearchGUI proteomic search analysis for PKZILLAs in P. parvum 12B1	Proteomics	https://doi.org/10.5281/zenodo.10023441
7	Scripts and analysis files for categorization of PKZILLA matching proteomic peptides into protein-unique, protein-multimatch & exon-unique, exon-multimatch categories.	Proteomics	https://doi.org/10.5281/zenodo.10028959
8	A Nextflow pipeline that wraps InterProScan , including making it parallelized & doing some plotting	Supporting code	https://github.com/photocyte/interproscan_parallel
9	InterProScan domain annotation on non-PKZILLA polypeptides	PKS analysis	https://doi.org/10.5281/zenodo.10011739
10	InterProScan domain annotation of PKZILLA polypeptides	PKS analysis	https://doi.org/10.5281/zenodo.10023460
11	PKZILLA candidate domains of unknown function (cDUFs) analysis	PKS analysis	https://doi.org/10.5281/zenodo.10028178
12	Prymnesium parvum 12B1 polyketide synthase (PKS) domain and module analysis	PKS analysis	https://doi.org/10.5281/zenodo.10028239
13	Tabular analysis of polyketide synthase domain active site residues in the PKZILLAs	PKS analysis	https://doi.org/10.5281/zenodo.10028517
14	Bioinformatic assignment of PKZILLA ketoreductase (KR) stereochemical outcome based on application of a literature trans-AT KR diagnostic residue heuristic	PKS analysis	https://doi.org/10.5281/zenodo.10569208
15	Domain phylogenetics for the PKZILLAs	PKS analysis	https://doi.org/10.5281/zenodo.10152638
16	A wrapper around some simple Python scripts, to query the InterPro API with respect to fetching domains from arbitrary taxonomic groups, ranging from all life to specific strains	Supporting code	https://github.com/photocyte/InterPro_API_domain_toolkit
17	PKZILLA domain phylogenies with outgroup representatives from Uniprot	PKS analysis	https://doi.org/10.5281/zenodo.10247217
18	Non-length-normalized graphical plots of the PKZILLA domains, modules, cDUFs, and exon extents	PKS analysis	https://doi.org/10.5281/zenodo.10093617
19	Scripts, data, and analyses for extending flavoprotein (FLX) domains C-terminally to form extended FLX domains (eFLX) & performing structural predictions & alignments using AlphaFold2, RoseTTAFold, FoldSeek, and DALI	PKS analysis	https://doi.org/10.5281/zenodo.10120640

Table S14: Extended analyses, datasets, and code available on Zenodo or Github.

References:

1. G. M. Hallegraeff, D. M. Anderson, K. Davidson, F. Gianella, P. Hansen, *Fish-Killing Marine Algal Blooms: Causative Organisms, Ichthyotoxic Mechanisms, Impacts and Mitigation.* (UNESCO, Paris, France, 2023; https://dx.doi.org/10.25607/OBP-1964)*IOC Manuals and Guides*.

2. J. Sobieraj, D. Metelski, Insights into Toxic *Prymnesium parvum* Blooms as a Cause of the Ecological Disaster on the Odra River. *Toxins* **15**, 403 (2023).

3. D. M. Anderson, E. Fensin, C. J. Gobler, A. E. Hoeglund, K. A. Hubbard, D. M. Kulis, J. H. Landsberg, K. A. Lefebvre, P. Provoost, M. L. Richlen, J. L. Smith, A. R. Solow, V. L. Trainer, Marine harmful algal blooms (HABs) in the United States: History, current status and future trends. *Harmful Algae* **102**, 101975 (2021).

4. K. C. Nicolaou, M. O. Frederick, R. J. Aversa, The Continuing Saga of the Marine Polyether Biotoxins. *Angew. Chem. Int. Ed.* **47**, 7182–7225 (2008).

5. T. Igarashi, M. Satake, T. Yasumoto, Structures and Partial Stereochemical Assignments for Prymnesin-1 and Prymnesin-2: Potent Hemolytic and Ichthyotoxic Glycosides Isolated from the Red Tide Alga *Prymnesium parvum*. *J. Am. Chem. Soc.* **121**, 8499–8511 (1999).

6. R. E. Moore, G. Bartolini, Structure of palytoxin. *J. Am. Chem. Soc.* **103**, 2491–2494 (1981).

7. M. Murata, H. Naoki, T. Iwashita, S. Matsunaga, M. Sasaki, A. Yokoyama, T. Yasumoto, Structure of maitotoxin. *J. Am. Chem. Soc.* **115**, 2060–2062 (1993).

8. K. Nakanishi, The chemistry of brevetoxins: A review. *Toxicon* **23**, 473–479 (1985).

9. I. Vilotijevic, T. F. Jamison, Epoxide-Opening Cascades Promoted by Water. *Science* **317**, 1189–1192 (2007).

10. A. Nivina, K. P. Yuet, J. Hsu, C. Khosla, Evolution and Diversity of Assembly-Line Polyketide Synthases. *Chem. Rev.* **119**, 12524–12547 (2019).

11. K. Anestis, G. S. Kohli, S. Wohlrab, E. Varga, T. O. Larsen, P. J. Hansen, U. John, Polyketide synthase genes and molecular trade-offs in the ichthyotoxic species *Prymnesium parvum*. *Sci. Total Environ.* **795**, 148878 (2021).

12. F. M. V. Dolah, J. S. Morey, S. Milne, A. Ung, P. E. Anderson, M. Chinain, Transcriptomic analysis of polyketide synthases in a highly ciguatoxic dinoflagellate, *Gambierdiscus polynesiensis* and low toxicity *Gambierdiscus pacificus*, from French Polynesia. *PLOS ONE* **15**, e0231400 (2020).

13. N. Heimerl, E. Hommel, M. Westermann, D. Meichsner, M. Lohr, C. Hertweck, A. R. Grossman, M. Mittag, S. Sasso, A giant type I polyketide synthase participates in zygospore maturation in *Chlamydomonas reinhardtii*. *Plant J.* **95**, 268–281 (2018).

14. M. H. Medema, T. de Rond, B. S. Moore, Mining genomes to illuminate the specialized chemistry of life. *Nat. Rev. Genet.* **22**, 553–571 (2021).

15. M.-L. Bang, T. Centner, F. Fornoff, A. J. Geach, M. Gotthardt, M. McNabb, C. C. Witt, D. Labeit, C. C. Gregorio, H. Granzier, S. Labeit, The Complete Gene Sequence of Titin, Expression of an Unusual ≈700-kDa Titin Isoform, and Its Interaction With Obscurin Identify a Novel Z-Line to I-Band Linking System. *Circ. Res.* **89**, 1065–1072 (2001).

16. M. Sasaki, N. Takeda, H. Fuwa, R. Watanabe, M. Satake, Y. Oshima, Synthesis of the JK/LM-ring model of prymnesins, potent hemolytic and ichthyotoxic polycyclic ethers isolated from the red tide alga

Prymnesium parvum: confirmation of the relative configuration of the K/L-ring juncture. *Tetrahedron Lett.* **47**, 5687–5691 (2006).

17. T. Hashimoto, J. Hashimoto, I. Kozone, K. Amagai, T. Kawahara, S. Takahashi, H. Ikeda, K. Shin-ya, Biosynthesis of Quinolidomicin, the Largest Known Macrolide of Terrestrial Origin: Identification and Heterologous Expression of a Biosynthetic Gene Cluster over 200 kb. *Org. Lett.* **20**, 7996–7999 (2018).

18. S. Donadio, M. Staver, J. McAlpine, S. Swanson, L. Katz, Modular organization of genes required for complex polyketide biosynthesis. *Science* **252**, 675–679 (1991).

19. S. B. Binzer, D. K. Svenssen, N. Daugbjerg, C. Alves-de-Souza, E. Pinto, P. J. Hansen, T. O. Larsen, E. Varga, A-, B- and C-type prymnesins are clade specific compounds and chemotaxonomic markers in *Prymnesium parvum*. *Harmful Algae* **81**, 10–17 (2019).

20. J. H. Wisecaver, R. P. Auber, A. L. Pendleton, N. F. Watervoort, T. R. Fallon, O. L. Riedling, S. R. Manning, B. S. Moore, W. W. Driscoll, Extreme genome diversity and cryptic speciation in a harmful algal-bloom-forming eukaryote. *Curr. Biol.* **33**, 2246-2259.e8 (2023).

21. J. H. Wisecaver, J. D. Hackett, Dinoflagellate Genome Evolution. *Annu. Rev. Microbiol.* **65**, 369–387 (2011).

22. H.-H. Hong, H.-G. Lee, J. Jo, H. M. Kim, S.-M. Kim, J. Y. Park, C. B. Jeon, H.-S. Kang, M. G. Park, C. Park, K. Y. Kim, H.-H. Hong, H.-G. Lee, J. Jo, H. M. Kim, S.-M. Kim, J. Y. Park, C. B. Jeon, H.-S. Kang, M. G. Park, C. Park, K. Y. Kim, The exceptionally large genome of the harmful red tide dinoflagellate *Cochlodinium polykrikoides* Margalef (Dinophyceae): determination by flow cytometry. *Algae* **31**, 373–378 (2016).

23. National Center for Biotechnology Information (NCBI), Sequence Read Archive (SRA), *Prymnesium parvum* strain 12B Illumina reads - SRA PRJNA201451, SRR1685644. https://www.ncbi.nlm.nih.gov/sra/?term=SRR1685644.

24. Y. Dou, Y. Liu, X. Yi, L. K. Olsen, H. Zhu, Q. Gao, H. Zhou, B. Zhang, SEPepQuant enhances the detection of possible isoform regulations in shotgun proteomics. *Nat. Commun.* **14**, 5809 (2023).

25. P. Jones, D. Binns, H.-Y. Chang, M. Fraser, W. Li, C. McAnulla, H. McWilliam, J. Maslen, A. Mitchell, G. Nuka, S. Pesseat, A. F. Quinn, A. Sangrador-Vegas, M. Scheremetjew, S.-Y. Yong, R. Lopez, S. Hunter, InterProScan 5: genome-scale protein function classification. *Bioinformatics* **30**, 1236–1240 (2014).

26. F. Hemmerling, K. E. Lebe, J. Wunderlich, F. Hahn, An Unusual Fatty Acyl:Adenylate Ligase (FAAL)–Acyl Carrier Protein (ACP) Didomain in Ambruticin Biosynthesis. *ChemBioChem* **19**, 1006–1011 (2018).

27. F. Hemmerling, R. A. Meoded, A. E. Fraley, H. A. Minas, C. L. Dieterich, M. Rust, R. Ueoka, K. Jensen, E. J. N. Helfrich, C. Bergande, M. Biedermann, N. Magnus, B. Piechulla, J. Piel, Modular Halogenation, α-Hydroxylation, and Acylation by a Remarkably Versatile Polyketide Synthase. *Angew. Chem. Int. Ed.* **61**, e202116614 (2022).

28. A. J. Winter, R. N. Khanizeman, A. M. C. Barker-Mountford, A. J. Devine, L. Wang, Z. Song, J. A. Davies, P. R. Race, C. Williams, T. J. Simpson, C. L. Willis, M. P. Crump, Structure and Function of the α-Hydroxylation Bimodule of the Mupirocin Polyketide Synthase. *Angew. Chem. Int. Ed.* **62**, e202312514 (2023).

29. E. J. N. Helfrich, J. Piel, Biosynthesis of polyketides by trans-AT polyketide synthases. *Nat. Prod. Rep.* **33**, 231–316 (2016).

30. D. T. Wagner, J. Zeng, C. B. Bailey, D. C. Gay, F. Yuan, H. R. Manion, A. T. Keatinge-Clay, Structural and Functional Trends in Dehydrating Bimodules from trans-Acyltransferase Polyketide Synthases. *Structure* **25**, 1045-1055.e2 (2017).

31. J. Masschelein, P. K. Sydor, C. Hobson, R. Howe, C. Jones, D. M. Roberts, Z. Ling Yap, J. Parkhill, E. Mahenthiralingam, G. L. Challis, A dual transacylation mechanism for polyketide synthase chain release in enacyloxin antibiotic biosynthesis. *Nat. Chem.* **11**, 906–912 (2019).

32. E. J. N. Helfrich, R. Ueoka, A. Dolev, M. Rust, R. A. Meoded, A. Bhushan, G. Califano, R. Costa, M. Gugger, C. Steinbeck, P. Moreno, J. Piel, Automated structure prediction of trans-acyltransferase polyketide synthase products. *Nat. Chem. Biol.* **15**, 813–821 (2019).

33. F. Taft, M. Brünjes, T. Knobloch, H. G. Floss, A. Kirschning, Timing of the Δ10,12-Δ11,13 Double Bond Migration During Ansamitocin Biosynthesis in *Actinosynnema pretiosum*. *J. Am. Chem. Soc.* **131**, 3812–3813 (2009).

34. G. Hibi, T. Shiraishi, T. Umemura, K. Nemoto, Y. Ogura, M. Nishiyama, T. Kuzuyama, Discovery of type II polyketide synthase-like enzymes for the biosynthesis of cispentacin. *Nat. Commun.* **14**, 8065 (2023).

35. L. Gu, B. Wang, A. Kulkarni, J. J. Gehret, K. R. Lloyd, L. Gerwick, W. H. Gerwick, P. Wipf, K. Håkansson, J. L. Smith, D. H. Sherman, Polyketide Decarboxylative Chain Termination Preceded by O-Sulfonation in Curacin A Biosynthesis. *J. Am. Chem. Soc.* **131**, 16033–16035 (2009).

36. Y. Jiang, A. Kim, C. Olive, J. C. Lewis, Selective C-H Halogenation of Alkenes and Alkynes Using Flavin-Dependent Halogenases. ChemRxiv [Preprint] (2023). https://doi.org/10.26434/chemrxiv-2023-23r4l.

37. T. Hua, D. Wu, W. Ding, J. Wang, N. Shaw, Z.-J. Liu, Studies of Human 2,4-Dienoyl CoA Reductase Shed New Light on Peroxisomal β-Oxidation of Unsaturated Fatty Acids. *J. Biol. Chem.* **287**, 28956–28965 (2012).

38. Yong-Yeng Lin, Martin Risk, Sammy M. Ray, Donna Van Engen, Jon Clardy, Jerzy Golik, John C. James, Koji Nakanishi, Isolation and structure of brevetoxin B from the “red tide” dinoflagellate *Ptychodiscus brevis* (*Gymnodinium breve*). *J. Am. Chem. Soc.* **103**, 6773–6775 (1981).

39. Z.-P. Jiang, S.-H. Sun, Y. Yu, A. Mándi, J.-Y. Luo, M.-H. Yang, T. Kurtán, W.-H. Chen, L. Shen, J. Wu, Discovery of benthol A and its challenging stereochemical assignment: opening up a new window for skeletal diversity of super-carbon-chain compounds. *Chem. Sci.* **12**, 10197–10206 (2021).

40. J. Cortes, P. Schöffski, B. A. Littlefield, Multiple modes of action of eribulin mesylate: Emerging data and clinical implications. *Cancer Treat. Rev.* **70**, 190–198 (2018).

41. F. M. V. Dolah, G. S. Kohli, J. S. Morey, S. A. Murray, Both modular and single-domain Type I polyketide synthases are expressed in the brevetoxin-producing dinoflagellate, Karenia brevis (Dinophyceae). *J. Phycol.* **53**, 1325–1339 (2017).

42. J. Jian, Z. Wu, A. Silva-Núñez, X. Li, X. Zheng, B. Luo, Y. Liu, X. Fang, C. T. Workman, T. O. Larsen, P. J. Hansen, E. C. Sonnenschein, Long-read genome sequencing provides novel insights into the harmful algal bloom species *Prymnesium parvum*. *Sci. Total Environ.*, 168042 (2023).

43. R. M. Van Wagoner, M. Satake, J. L. C. Wright, Polyketide biosynthesis in dinoflagellates: what makes it different? *Nat. Prod. Rep.*, 37 (2014).

44. R. Teufel, A. Miyanaga, Q. Michaudel, F. Stull, G. Louie, J. P. Noel, P. S. Baran, B. Palfey, B. S. Moore, Flavin-mediated dual oxidation controls an enzymatic Favorskii-type rearrangement. *Nature* **503**, 552–556 (2013).

45. S. Guo, Y. Sang, C. Zheng, X.-S. Xue, Z. Tang, W. Liu, Enzymatic α-Ketothioester Decarbonylation Occurs in the Assembly Line of Barbamide for Skeleton Editing. *J. Am. Chem. Soc.* **145**, 5017–5028 (2023).

46. J. K. Brunson, S. M. K. McKinnie, J. R. Chekan, J. P. McCrow, Z. D. Miles, E. M. Bertrand, V. A. Bielinski, H. Luhavaya, M. Oborník, G. J. Smith, D. A. Hutchins, A. E. Allen, B. S. Moore, Biosynthesis of the neurotoxin domoic acid in a bloom-forming diatom. *Science* **361**, 1356–1358 (2018).

47. Y. Perez-Riverol, J. Bai, C. Bandla, D. García-Seisdedos, S. Hewapathirana, S. Kamatchinathan, D. J. Kundu, A. Prakash, A. Frericks-Zipper, M. Eisenacher, M. Walzer, S. Wang, A. Brazma, J. A. Vizcaíno, The PRIDE database resources in 2022: a hub for mass spectrometry-based proteomics evidences. *Nucleic Acids Res.* **50**, D543–D552 (2022).

48. W. W. Driscoll, N. J. Espinosa, O. T. Eldakar, J. D. Hackett, ALLELOPATHY AS AN EMERGENT, EXPLOITABLE PUBLIC GOOD IN THE BLOOM-FORMING MICROALGA *PRYMNESIUM PARVUM*. *Evolution* **67**, 1582–1590 (2013).

49. R. R. L. Guillard, P. E. Hargraves, *Stichochrysis immobilis* is a diatom, not a chrysophyte. *Phycologia* **32**, 234–236 (1993).

50. F. J. Sedlazeck, P. Rescheneder, M. Smolka, H. Fang, M. Nattestad, A. von Haeseler, M. C. Schatz, Accurate detection of complex structural variations using single-molecule sequencing. *Nat. Methods* **15**, 461–468 (2018).

51. J. T. Robinson, H. Thorvaldsdóttir, W. Winckler, M. Guttman, E. S. Lander, G. Getz, J. P. Mesirov, Integrative genomics viewer. *Nat. Biotechnol.* **29**, 24–26 (2011).

52. A. R. Quinlan, I. M. Hall, BEDTools: a flexible suite of utilities for comparing genomic features. *Bioinformatics* **26**, 841–842 (2010).

53. R. Pracana, A. Priyam, I. Levantis, R. A. Nichols, Y. Wurm, The fire ant social chromosome supergene variant Sb shows low diversity but high divergence from SB. *Mol. Ecol.* **26**, 2864–2879 (2017).

54. W. J. Kent, BLAT—The BLAST-Like Alignment Tool. *Genome Res.* **12**, 656–664 (2002).

55. O. Tange, GNU Parallel 20230522 ('Charles'), Zenodo (2023); https://doi.org/10.5281/zenodo.7958356.

56. G. Gremme, S. Steinbiss, S. Kurtz, GenomeTools: A Comprehensive Software Library for Efficient Processing of Structured Genome Annotations. *IEEE/ACM Trans. Comput. Biol. Bioinform.* **10**, 645–656 (2013).

57. P. Di Tommaso, M. Chatzou, E. W. Floden, P. P. Barja, E. Palumbo, C. Notredame, Nextflow enables reproducible computational workflows. *Nat. Biotechnol.* **35**, 316–319 (2017).

58. T. Lassmann, O. Frings, E. L. L. Sonnhammer, Kalign2: high-performance multiple alignment of protein and nucleotide sequences allowing external features. *Nucleic Acids Res.* **37**, 858–865 (2009).

59. N. P. Brown, C. Leroy, C. Sander, MView: a web-compatible database search or multiple alignment viewer. *Bioinformatics* **14**, 380–381 (1998).

60. Zymo Research, RNA Clean & Concentrator -25 Protocol. https://files.zymoresearch.com/protocols/_r1017_r1018_rna_clean_concentrator-25.pdf.

61. A. M. Bolger, M. Lohse, B. Usadel, Trimmomatic: a flexible trimmer for Illumina sequence data. *Bioinformatics*, 1–7 (2014).

62. D. Kim, J. M. Paggi, C. Park, C. Bennett, S. L. Salzberg, Graph-based genome alignment and genotyping with HISAT2 and HISAT-genotype. *Nat. Biotechnol.* **37**, 907–915 (2019).

63. M. Pertea, G. M. Pertea, C. M. Antonescu, T.-C. Chang, J. T. Mendell, S. L. Salzberg, StringTie enables improved reconstruction of a transcriptome from RNA-seq reads. *Nat. Biotechnol.* **33**, 290–295 (2015).

64. C. Camacho, G. Coulouris, V. Avagyan, N. Ma, J. Papadopoulos, K. Bealer, T. L. Madden, BLAST+: architecture and applications. *BMC Bioinformatics* **10**, 421 (2009).

65. J. M. Palmer, J. Stajich, Funannotate v1.8.1: Eukaryotic genome annotation, Zenodo (2020); https://doi.org/10.5281/zenodo.4054262.

66. G. S. C. Slater, E. Birney, Automated generation of heuristics for biological sequence comparison. *BMC Bioinformatics* **6**, 31 (2005).

67. R. Craig, R. C. Beavis, TANDEM: matching proteins with tandem mass spectra. *Bioinformatics* **20**, 1466–1467 (2004).

68. J. K. Eng, T. A. Jahan, M. R. Hoopmann, Comet: An open-source MS/MS sequence database search tool. *PROTEOMICS* **13**, 22–24 (2013).

69. H. Barsnes, M. Vaudel, SearchGUI: A Highly Adaptable Common Interface for Proteomics Search and de Novo Engines. *J. Proteome Res.* **17**, 2552–2555 (2018).

70. J. E. Elias, S. P. Gygi, "Target-Decoy Search Strategy for Mass Spectrometry-Based Proteomics" in *Proteome Bioinformatics*, S. J. Hubbard, A. R. Jones, Eds. (Humana Press, Totowa, NJ, 2010; https://doi.org/10.1007/978-1-60761-444-9_5)*Methods in Molecular Biology*^{TM}, pp. 55–71.

71. W. Shen, S. Le, Y. Li, F. Hu, SeqKit: A Cross-Platform and Ultrafast Toolkit for FASTA/Q File Manipulation. *PLOS ONE* **11**, e0163962 (2016).

72. M. Vaudel, J. M. Burkhart, R. P. Zahedi, E. Oveland, F. S. Berven, A. Sickmann, L. Martens, H. Barsnes, PeptideShaker enables reanalysis of MS-derived proteomics data sets. *Nat. Biotechnol.* **33**, 22–24 (2015).

73. D. W. Powell, C. M. Weaver, J. L. Jennings, K. J. McAfee, Y. He, P. A. Weil, A. J. Link, Cluster Analysis of Mass Spectrometry Data Reveals a Novel Component of SAGA. *Mol. Cell. Biol.* **24**, 7249–7259 (2004).

74. G. M. Kurtzer, cclerget, M. Bauer, I. Kaneshiro, D. Trudgian, D. Godlove, hpcng/singularity: Singularity, Zenodo (2021); https://doi.org/10.5281/zenodo.4667718.

75. G. M. Kurtzer, V. Sochat, M. W. Bauer, Singularity: Scientific containers for mobility of compute. *PLOS ONE* **12**, e0177459 (2017).

76. T. R. Fallon, photocyte/interproscan_parallel: v1.0.0, Zenodo (2023); https://doi.org/10.5281/zenodo.8432691.

77. V. Zulkower, S. Rosser, DNA Features Viewer: a sequence annotation formatting and plotting library for Python. *Bioinformatics* **36**, 4350–4352 (2020).

78. M. C. Kim, J. M. Winter, R. Cullum, A. J. Smith, W. Fenical, Expanding the Utility of Bioinformatic Data for the Full Stereostructural Assignments of Marinolides A and B, 24- and 26-Membered Macrolactones Produced by a Chemically Exceptional Marine-Derived Bacterium. *Mar. Drugs* **21**, 367 (2023).

79. K. D. Bauman, V. V. Shende, P. Y.-T. Chen, D. B. B. Trivella, T. A. M. Gulder, S. Vellalath, D. Romo, B. S. Moore, Enzymatic assembly of the salinosporamide γ-lactam-β-lactone anticancer warhead. *Nat. Chem. Biol.*, 1–9 (2022).

80. D. Khare, W. A. Hale, A. Tripathi, L. Gu, D. H. Sherman, W. H. Gerwick, K. Håkansson, J. L. Smith, Structural Basis for Cyclopropanation by a Unique Enoyl-Acyl Carrier Protein Reductase. *Structure* **23**, 2213–2223 (2015).

81. J. Jumper, R. Evans, A. Pritzel, T. Green, M. Figurnov, O. Ronneberger, K. Tunyasuvunakool, R. Bates, A. Žídek, A. Potapenko, A. Bridgland, C. Meyer, S. A. A. Kohl, A. J. Ballard, A. Cowie, B. Romera-Paredes, S. Nikolov, R. Jain, J. Adler, T. Back, S. Petersen, D. Reiman, E. Clancy, M. Zielinski, M. Steinegger, M. Pacholska, T. Berghammer, S. Bodenstein, D. Silver, O. Vinyals, A. W. Senior, K. Kavukcuoglu, P. Kohli, D. Hassabis, Highly accurate protein structure prediction with AlphaFold. *Nature*, 1–11 (2021).

82. M. Mirdita, K. Schütze, Y. Moriwaki, L. Heo, S. Ovchinnikov, M. Steinegger, ColabFold: making protein folding accessible to all. *Nat. Methods* **19**, 679–682 (2022).

83. M. van Kempen, S. S. Kim, C. Tumescheit, M. Mirdita, J. Lee, C. L. M. Gilchrist, J. Söding, M. Steinegger, Fast and accurate protein structure search with Foldseek. *Nat. Biotechnol.*, 1–4 (2023).

84. F. M. Ferroni, C. Tolmie, M. S. Smit, D. J. Opperman, Structural and Catalytic Characterization of a Fungal Baeyer-Villiger Monooxygenase. *PLOS ONE* **11**, e0160186 (2016).

85. C. R. Nicoll, G. Bailleul, F. Fiorentini, M. L. Mascotti, M. W. Fraaije, A. Mattevi, Ancestral-sequence reconstruction unveils the structural basis of function in mammalian FMOs. *Nat. Struct. Mol. Biol.* **27**, 14–24 (2020).

86. R. Al-Dhelaan, P. S. Russo, S. E. Padden, A. Amaya, D. W. Dong, Y.-O. You, Condensation-Incompetent Ketosynthase Inhibits trans-Acyltransferase Activity. *ACS Chem. Biol.* **14**, 304–312 (2019).

87. J. Masschelein, P. K. Sydor, C. Hobson, R. Howe, C. Jones, D. M. Roberts, Z. L. Yap, J. Parkhill, E. Mahenthiralingam, G. L. Challis, A dual transacylation mechanism for polyketide synthase chain release in enacyloxin antibiotic biosynthesis. *Nat. Chem.* **11**, 906–912 (2019).

88. S. Smith, S.-C. Tsai, The type I fatty acid and polyketide synthases: a tale of two megasynthases. *Nat. Prod. Rep.* **24**, 1041–1072 (2007).

89. J. Zheng, A. T. Keatinge-Clay, The status of type I polyketide synthase ketoreductases. *MedChemComm* **4**, 34–40 (2013).

90. T. M. McCullough, A. Dhar, D. L. Akey, J. R. Konwerski, D. H. Sherman, J. L. Smith, Structure of a modular polyketide synthase reducing region. *Structure* **31**, 1109-1120.e3 (2023).

91. C. Pockrandt, M. Alzamel, C. S. Iliopoulos, K. Reinert, GenMap: ultra-fast computation of genome mappability. *Bioinformatics* **36**, 3687–3692 (2020).

92. A. M. Kozlov, D. Darriba, T. Flouri, B. Morel, A. Stamatakis, RAxML-NG: a fast, scalable and user-friendly tool for maximum likelihood phylogenetic inference. *Bioinformatics* **35**, 4453–4455 (2019).

93. J. Huerta-Cepas, F. Serra, P. Bork, ETE 3: Reconstruction, Analysis, and Visualization of Phylogenomic Data. *Mol. Biol. Evol.* **33**, 1635–1638 (2016).

94. Z. Yin, J. S. Dickschat, Cis double bond formation in polyketide biosynthesis. *Nat. Prod. Rep.* **38**, 1445–1468 (2021).